

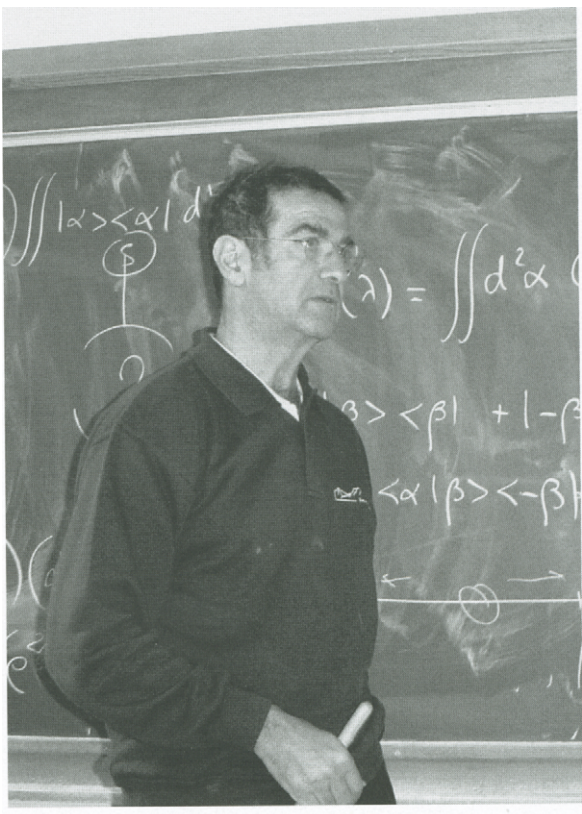
Course 2

MESOSCOPIC STATE SUPERPOSITIONS AND DECOHERENCE IN QUANTUM OPTICS

S. Haroche

*Laboratoire Kastler Brossel, Département de Physique
Ecole Normale Supérieure, 24 rue Lhomond F-75005 Paris
and Collège de France, 11 place M. Berthelot, F-75005 Paris*

*D. Estève, J.-M. Raimond and J. Dalibard, eds.
Les Houches, Session LXXIX, 2003
Quantum Entanglement and Information Processing
Intrication quantique et traitement de l'information
© 2004 Elsevier B.V. All rights reserved*



Contents

1. An overview of quantum optics	60
1.1. Field as a sum of harmonic oscillators	61
1.2. Coherent states	67
1.3. Schrödinger cats as superpositions of coherent states	70
1.4. Field representations: the Q and W functions	74
1.4.1. The Q function	74
1.4.2. The W function	76
1.5. Coupling between field and charges: modeling sources and photon detectors	78
1.5.1. Single atom coupled to field: Rabi oscillation, spontaneous emission and preparation of Fock states	79
1.5.2. Classical current coupled to field: generation of coherent states	81
1.6. Modeling a photon counting process	84
2. Beam splitters and interferences in quantum optics	86
2.1. Linear beam splitters	86
2.2. Schrödinger picture: effect of the beam splitter on some field states	88
2.3. The Mach-Zehnder interferometer	91
2.4. Homodyne detection of field quadratures	94
2.5. Beam splitters as couplers to environment: relaxation of a coherent state and of a Schrödinger cat	98
2.5.1. Relaxation of a coherent state	99
2.5.2. Relaxation of a Schrödinger cat state	101
2.6. Non-linear beam splitters	103
2.6.1. A simple model of non-linear beam splitter	103
2.6.2. Simulation of multiparticle interferometry in an ion trap experiment	109
3. Schrödinger cats in cavity QED	112
3.1. A reminder on microwave cavity QED and the Jaynes-Cummings model	113
3.2. Rabi oscillation in a mesoscopic field: collapse and revival revisited	116
3.3. Observing the Schrödinger cat by a homodyne Q function measurement	123
3.4. Dispersive cats in cavity QED	128
3.5. Testing the coherence of π -phase cats: a parity measurement	134
3.6. Non-local cats	138
4. Collapse and revivals of matter-waves: proposals for atomic Schrödinger cats	139
4.1. Ideal Bose-Einstein condensate without interactions	140
4.2. Coherent collisions in BEC: the analogy with the Kerr effect in quantum optics	144
4.2.1. Simple model of elastic binary collisions in a bi-modal condensate	144
4.2.2. Collapse and revivals of a condensate bi-modal phase state: the optical analogy	146
4.3. Proposal to prepare a Schrödinger cat state in a bi-modal condensate	150
5. Conclusion: a brief comparison with other mesoscopic state superpositions in quantum optics	153
References	155

The study of mesoscopic superpositions of states, the so-called Schrödinger cats, has become a very active field of theoretical and experimental physics. Mesoscopic superpositions play an important role in quantum information science, where systems of qubits made of atoms or photons in entangled configurations of increasing complexity are manipulated [1, 2]. These superpositions are notoriously fragile, loosing rapidly their quantum coherence. The coupling of mesoscopic systems to their environment very efficiently blurs the interference effects between their states. This phenomenon, called decoherence, has been extensively studied in various contexts [3–7]. Monitoring and controlling decoherence, as well as correcting for its effects, are among the essential goals of quantum information physics [1].

At a more fundamental level, preparing mesoscopic state superpositions and studying their decoherence is a way to test the measurement process in quantum physics [8]. In an usual quantum measurement, the microsystem is coupled to a macroscopic meter. In the absence of decoherence, this coupling would result in an entanglement between these two systems and in the generation of Schrödinger-cat-like states of the meter. These superpositions are never observed, though, because the system very quickly evolves under the effect of environment induced decoherence into a statistical mixture of states. The coupling to the environment has the effect of leaving unaltered some states, the “pointer states” [3, 9] of the meter which are correlated to the eigenstates of the measured microscopic system, while the coherences between these states is rapidly destroyed. Eluciding the mechanisms by which the robust pointer states are selected out of the huge ensemble of fragile mesoscopic superpositions is an essential aspect of decoherence theory [7, 10].

The study of mesoscopic states and their decoherence has brought closer theorists and experimentalists from disparate domains of physics. Atomic and solid state physicists, in particular, have developed a common interest in quantum information science. The Les Houches Summer School in which this course was given has been a manifestation of this common interest, with experts and students coming from atomic and condensed matter physics discussing together and benefitting from each other expertise.

These Lecture Notes provide an introduction to mesoscopic state studies in quantum optics, a field of physics which has become a testing ground for the manipulation of systems of increasing complexity. On the theoretical side, the

evolution of the atomic and photonic systems of quantum optics is often entirely calculable, making the physics understandable in terms of very simple models. On the experimental side, the sophistication of modern laser technology allows for a very delicate control of the systems under study, giving in particular the possibility to manipulate their particles one at a time, with unsurpassed precision. Schrödinger cat states of several kinds have been proposed in quantum optics [11–15], and some versions of these states realized and studied in the laboratory [16–19]. These studies have illustrated various aspects of decoherence theory and opened a ‘bottom up’ approach to the mesoscopic frontier, complementary to the ‘top down’ approach of condensed matter physics.

The goal of this Course was threefold. I intended first to present the main ideas and methods of quantum optics to an audience which was coming, in part, from a different physics community. I wanted also to show, on simple examples, how mesoscopic states could be prepared and studied using the conceptually simple methods of quantum optics. Finally, I wished to analyze simple models of decoherence and describe textbook experiments which illustrate clearly the fundamental connexion between environment induced decoherence, entanglement and complementarity. These Notes start by an overview of quantum optics (section 1), followed by a description of beam splitters and particle interference effects (section 2). Section 3 is devoted to the description of Schrödinger cats in Cavity Quantum Electrodynamics experiments. In section 4 proposals to generate and study mesoscopic state superpositions of atoms in Bose Einstein condensates are described. Finally, these Notes conclude with a brief review of other kinds of quantum optics and atomic physics experiments dealing with mesoscopic state superpositions.

1. An overview of quantum optics

This first section presents an overview of the quantum optics formalism [20–25]. We start by a reminder about the analogy between the electromagnetic field and a collection of quantized harmonic oscillators characterized by their annihilation and creation operators. We introduce the main observables of the field (energy, photon number, field quadratures). We describe some important states of the field associated to a single mode, giving a special attention to the quasi-classical coherent states and to their superpositions (Schrödinger cat states). We define then two convenient field representations in phase space, the Q and W functions, and summarize their main properties. We finally recall how to describe the coupling of the field with atoms and we show how an atomic source can generate single photons, while a classical current creates coherent states. We end the section by describing a simple model of photon counter.

1.1. Field as a sum of harmonic oscillators

We start by recalling briefly the general formalism of field quantization in Coulomb gauge, which is described in more details in [26]. The vector potential $\mathbf{A}(\mathbf{r}, t)$ of a classical electromagnetic field, or equivalently its electric field $\mathbf{E}(\mathbf{r}, t)$ or magnetic field $\mathbf{B}(\mathbf{r}, t)$, can be expanded along plane waves of polarization ϵ_j and wave vector \mathbf{k}_j according to :

$$\mathbf{A}(\mathbf{r}, t) = \sum_j A_j \left[a_j \epsilon_j e^{i\mathbf{k}_j \cdot \mathbf{r}} + a_j^* \epsilon_j^* e^{-i\mathbf{k}_j \cdot \mathbf{r}} \right], \quad (1.1)$$

$$\begin{aligned} \mathbf{E}(\mathbf{r}, t) &= -\frac{d\mathbf{A}(\mathbf{r}, t)}{dt} = i \sum_j E_j \left[a_j \epsilon_j e^{i\mathbf{k}_j \cdot \mathbf{r}} - a_j^* \epsilon_j^* e^{-i\mathbf{k}_j \cdot \mathbf{r}} \right] \\ &\quad (E_j = \omega_j A_j) \end{aligned} \quad (1.2)$$

$$\begin{aligned} \mathbf{B}(\mathbf{r}, t) &= \nabla \times \mathbf{A}(\mathbf{r}, t) \\ &= i \sum_j \left(\frac{E_j}{c} \right) \left[a_j \boldsymbol{\kappa}_j \times \epsilon_j e^{i\mathbf{k}_j \cdot \mathbf{r}} - a_j^* \boldsymbol{\kappa}_j \times \epsilon_j^* e^{-i\mathbf{k}_j \cdot \mathbf{r}} \right]. \end{aligned} \quad (1.3)$$

In these expressions, the a_j coefficients are C-number field coordinates and $\boldsymbol{\kappa}_j = \mathbf{k}_j / |\mathbf{k}_j|$ is the unit vector defining the wave vector direction. There are two modes corresponding to two orthogonal polarizations ϵ_j normal to each wave vector \mathbf{k}_j . The time evolution of the field coordinates simply writes:

$$a_j(t) = a_j(0) e^{-i\omega_j t}, \quad (1.4)$$

where $\omega_j = c|\mathbf{k}_j|$ is the angular frequency of mode j . The A_j 's and E_j 's are adjustable normalization constants. The continuous sum over the field modes is made discrete by introducing a cubic ‘quantization box’ of linear dimension L , whose infinite limit is taken at the end of calculations. The wave vector coordinates $k_{j_x}, k_{j_y}, k_{j_z}$ are integer multiples of $2\pi/L$. The sum over j in Eqs. (1.1-1.3) is thus equivalent to a continuous three dimension integral.

The field hamiltonian H is obtained by evaluating the sum over space of the energy density:

$$H = \frac{\varepsilon_0}{2} \int (\mathbf{E}^2 + c^2 \mathbf{B}^2) d^3 \mathbf{r} = \varepsilon_0 L^3 \sum_j E_j^2 \left(a_j a_j^* + a_j^* a_j \right). \quad (1.5)$$

This equation can be written as:

$$H = \sum_j \frac{\hbar \omega_j}{2} \left(a_j a_j^* + a_j^* a_j \right), \quad (1.6)$$

provided the normalization constant is taken as $E_j = \sqrt{\hbar\omega_j/2\epsilon_0 L^3}$, where \hbar is Planck's constant and ϵ_0 the vacuum permittivity. As shown below, this normalization choice makes obvious the analogy between each field mode and a mechanical harmonic oscillator. This expression of H can be finally rewritten as:

$$H = \sum_j \hbar\omega_j (X_j^2 + P_j^2) , \quad (1.7)$$

where we have introduced the real and imaginary parts of the field coordinates as:

$$a_j = \left(\sqrt{m\omega_j/2\hbar} \right) x_j + (i/\sqrt{2m\hbar\omega_j}) p_j = X_j + i P_j . \quad (1.8)$$

We recognize here the hamiltonian of a sum of independent harmonic oscillators whose normalized coordinates in phase space are X_j and P_j .

The standard quantization procedure is then straightforward [26]. As for a mechanical oscillator, the classical field coordinates are replaced by non-commuting operators (marked for the moment with 'hats'), obeying the relations:

$$[\hat{x}_j, \hat{p}_k] = i\hbar\delta_{jk} \quad (1.9)$$

$$[\hat{X}_j, \hat{P}_k] = \frac{i}{2}\delta_{jk}; \quad [\hat{a}_j, \hat{a}_k^\dagger] = \delta_{jk} \quad (1.10)$$

These 'hats' will be omitted in the following when there will be no confusion. In the Heisenberg picture, the field coordinates become time-dependent operators $\hat{a}(t)$, one for each plane wave mode of the field:

$$\hat{a}(t) = \hat{a}(0) e^{-i\omega t} \quad (1.11)$$

The electric field in each mode (\mathbf{k}, ϵ) becomes likewise a time dependent operator, linear superpositions of the field operator a and its hermitian adjunct a^\dagger (we omit the indices in the expression of the field operators, when there is no possible confusion):

$$\mathbf{E}_{\mathbf{k},\epsilon}(\mathbf{r}, t) = i\sqrt{\frac{\hbar\omega}{2\epsilon_0 L^3}} (\epsilon a(t) e^{i\mathbf{k}\cdot\mathbf{r}} - \epsilon^* a^\dagger(t) e^{-i\mathbf{k}\cdot\mathbf{r}}) , \quad (1.12)$$

while the free field Hamiltonian in each mode takes the familiar form:

$$H = \hbar\omega \left(a^\dagger a + \frac{1}{2} \right) . \quad (1.13)$$

In the Schrödinger picture these operators are given by similar expressions in which a and a^\dagger are time independent. The field's expression [Eq.(1.12)] contains

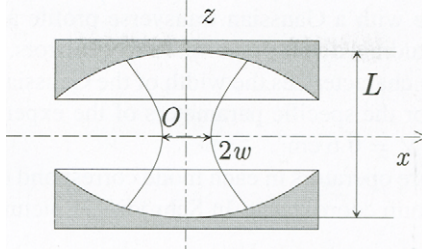


Fig. 1. Scheme of a microwave Fabry-Perot cavity. The two spherical mirrors separated by L sustain a Gaussian mode with waist w . The cavity axis normal to the mirrors is Oz . The sinusoidal standing wave pattern (with field nodes and antinodes along Oz) is not represented. Atoms propagate along Ox axis.

explicitely the expression of the vacuum field fluctuations in the quantization box of size L^3 : $E_0 = \sqrt{\hbar\omega/2\varepsilon_0 L^3}$. This quantity also represents the field per photon in the L^3 volume. This field goes to 0 when L is taken to infinity, in usual situations where the quantization box is merely a computation convenience.

Special mention must be made of Cavity Quantum Electrodynamics (CQED) [27–30] where the quantization volume V remains actually finite, with a well defined meaning: it is the physical volume of the real cavity in which the field is stored. Instead of expanding the field in plane waves, it is then more convenient to develop it along the standing wave modes of the cavity. In one of these modes, the field operator writes (Schrödinger picture):

$$\mathbf{E}(\mathbf{r}) = i E_0 (\boldsymbol{\epsilon} a f(\mathbf{r}) - \boldsymbol{\epsilon}^* a^\dagger f^*(\mathbf{r})) \quad (1.14)$$

where $f(\mathbf{r})$ is a scalar function which describes the spatial variation of the field in the mode (we consider here for simplicity that the mode polarization $\boldsymbol{\epsilon}$ is constant). The effective mode volume is then:

$$V = \int |f(\mathbf{r})|^2 d^3\mathbf{r}, \quad (1.15)$$

and the field per photon:

$$E_0 = \sqrt{\frac{\hbar\omega}{2\varepsilon_0 V}} \quad (1.16)$$

As a specific example, consider the case of a Fabry-Perot cavity made of two spherical mirrors facing each other (Figure 1). This is the geometry of the microwave CQED experiments described later in this chapter [30]. The mode is

then a standing wave with a Gaussian transverse profile and a sinusoidal field variation in the longitudinal direction normal to the mirrors, separated by the distance L . The waist w characterizes the width of the Gaussian. The mode volume is $V = \pi L w^2 / 4$. For the specific parameters of the experiment ($L = 2.7$ cm; $w = 6$ mm) we have $V = 0.6$ cm³.

The field quadrature operators in each mode correspond to the usual oscillator position and momentum coordinates. In Schrödinger picture they are expressed as:

$$X = \frac{a + a^\dagger}{2} ; \quad P = \frac{a - a^\dagger}{2i} = \frac{e^{-i\pi/2}a + e^{i\pi/2}a^\dagger}{2}. \quad (1.17)$$

More generally, we define phase quadratures as linear combinations of a and a^\dagger :

$$X_\varphi = \frac{e^{-i\varphi}a + e^{i\varphi}a^\dagger}{2}; \quad X_{\varphi+\pi/2} = \frac{e^{-i\varphi}a - e^{i\varphi}a^\dagger}{2i}. \quad (1.18)$$

They satisfy the commutation rules:

$$[X_\varphi, X_{\varphi+\pi/2}] = \frac{i}{2}, \quad (1.19)$$

which correspond to the uncertainty relations:

$$\Delta X_\varphi \Delta X_{\varphi+\pi/2} \geq \frac{1}{4}, \quad (1.20)$$

where ΔX_φ and $\Delta X_{\varphi+\pi/2}$ are conjugate phase quadrature fluctuations.

We recall below how these quadrature operators are measured in quantum optics. The eigenstate of the quadrature operator X_φ corresponding to the real and continuous eigenvalue x is defined by the eigenvalue equation:

$$X_\varphi |x\rangle_\varphi = x|x\rangle_\varphi. \quad (1.21)$$

The non-normalizable $|x\rangle_\varphi$ states obey the orthogonality and closure relationships:

$${}_\varphi \langle x | x' \rangle_\varphi = \delta(x - x'); \quad \int |x\rangle_\varphi {}_\varphi \langle x| dx = 1, \quad (1.22)$$

and the transformation from the $|x\rangle_\varphi$ basis to the conjugate basis $|x\rangle_{\varphi+\pi/2}$ is a simple Fourier transform:

$$|x\rangle_{\varphi+\pi/2} = \int dy |y\rangle_{\varphi\varphi} {}_\varphi \langle y | x \rangle_{\varphi+\pi/2} = \frac{1}{\sqrt{\pi}} \int dy e^{2ixy} |y\rangle_\varphi \quad (1.23)$$

Note the unusual factor 2 in the exponent of the Fourier transformation, due to the normalization we have chosen for the conjugate variables [factors 1/2 in Eqs.(1.17)and (1.18)].

The phase quadrature eigenstates are the natural generalization for fields of the usual position and momentum basis states of a mechanical oscillator. A more fundamental state basis widely used in quantum optics is formed by the energy eigenstates. The operator $a^\dagger a$ appearing in Eq (1.13) has a non-degenerate spectrum made of all non-negative integers. The corresponding eigenstates are the Fock states, or photon number states noted $|n\rangle$. The ground state $|0\rangle$ of the field in each mode, called the vacuum state, is the eigenstate of $a^\dagger a$ with eigenvalue 0. It obeys the equation:

$$a|0\rangle = 0 . \quad (1.24)$$

The expectation value $\langle 0 | X_\varphi | 0 \rangle$ of any phase quadrature in vacuum is zero while the quadrature fluctuations are isotropic and correspond to the minimal value compatible with Heisenberg uncertainty relations:

$$\Delta X_\varphi^{(0)} = \sqrt{\langle 0 | X_\varphi^2 | 0 \rangle} = 1/2 . \quad (1.25)$$

The probability distribution $P^{(0)}(x)$ of the field quadrature in vacuum is a Gaussian, like the distribution of the positions of a ground state mechanical oscillator:

$$P^{(0)}(x) = |\varphi \langle x | 0 \rangle|^2 = \left(\frac{2}{\pi}\right)^{1/2} e^{-2x^2} . \quad (1.26)$$

In summary, the vacuum field in each mode has isotropic Gaussian fluctuations around zero field.

The n -photon Fock state in a field mode obeys the eigenvalue equation:

$$a^\dagger a |n\rangle = n |n\rangle . \quad (1.27)$$

The action of the field operators a and a^\dagger on this state are:

$$a |n\rangle = \sqrt{n} |n-1\rangle ; \quad a^\dagger |n\rangle = \sqrt{n+1} |n+1\rangle \quad (1.28)$$

hence the name of photon annihilation and creation operators given to a and a^\dagger .

The n -photon state is generated by repeated operation of the photon creation operator on the vacuum, according to:

$$|n\rangle = \frac{a^{\dagger n}}{\sqrt{n!}} |0\rangle . \quad (1.29)$$

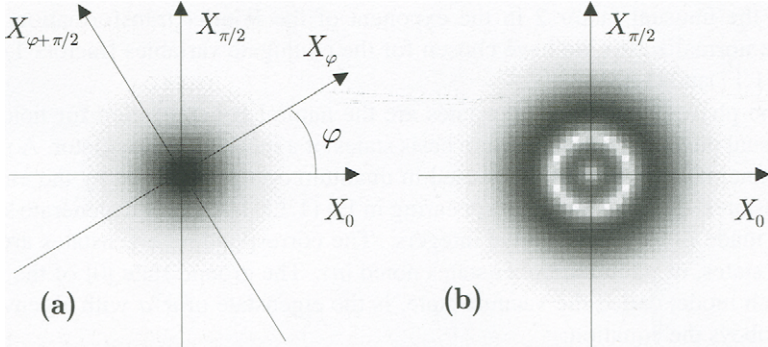


Fig. 2. The phase space of a field mode. (a) Graphical illustration of the X_0 , $X_{\pi/2}$, X_φ and $X_{\varphi+\pi/2}$ quadratures together with a representation of the vacuum state wavefunction. (b) Graphical representation of a 3-photon Fock state.

Fock states have isotropic non-minimal fluctuations of their field quadratures:

$$\langle n | X_\varphi | n \rangle = 0; \quad \Delta X_\varphi^{(n)} = \sqrt{\langle n | X_\varphi^2 | n \rangle} = \frac{1}{2} \sqrt{2n + 1}. \quad (1.30)$$

The probability distribution $P^{(n)}(x)$ of a quadrature in state $|n\rangle$ can be deduced from the analogous expression giving the square of the wave function of n quanta in a harmonic oscillator:

$$P^{(n)}(x) = |\varphi \langle x | n \rangle|^2 = \left(\frac{2}{\pi}\right)^{1/2} \frac{1}{2^n n!} e^{-2x^2} \left(H_n(x\sqrt{2})\right)^2 \quad (1.31)$$

where $H_n(x)$ is the Hermite polynomial of rank n .

A qualitative picture of Fock states is shown in Fig. 2. The phase space of a single mode is represented with the two X_0 and $X_{\pi/2}$ quadratures as reference axes. The quadrature X_φ is associated with a direction making the angle φ with the X_0 direction. An ensemble of X_φ measurements in the vacuum field yields a Gaussian distributions of points along this direction. Measurements along all possible quadrature directions gives an isotropic Gaussian cloud centered at phase space origin, as shown in Fig. 2(a). For a Fock state with $n > 0$ the quadrature distribution along any direction exhibits maxima separated by dark fringes corresponding to the zero of the Hermite polynomials. The $n = 3$ state is represented in Fig. 2(b), as an isotropic cloud of points distributed over concentric rings centered at phase space origin.

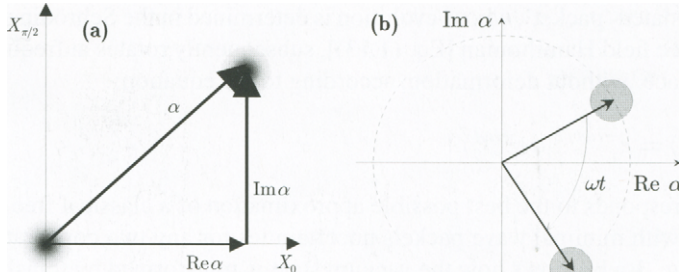


Fig. 3. Coherent state. (a) Pictorial representation of the action of the displacement operator on the vacuum state. The displacement by a complex amplitude α amounts to a displacement by $\text{Re } \alpha$ along the X_0 quadrature axis, followed by a displacement by $\text{Im } \alpha$ along the $X_{\pi/2}$ quadrature. (b) Time evolution of a coherent state.

1.2. Coherent states

Fock states contain no phase information. Quadrature field eigenstates have a well defined phase, but they are non-physical since they are non-normalizable and have an infinite mean energy. Their amplitude along one phase direction is perfectly determined, while it is totally random in the conjugate orthogonal direction (infinite squeezing). To describe situations where the phase of the field is relevant, it is thus often more convenient to expand the field neither on Fock nor on quadrature field eigenstates, but on the basis of so-called coherent states [31, 32], which are more physical and experimentally much more easily accessible. We recall briefly in this section the definition and the main properties of these states.

A coherent state of a single field mode is defined as resulting from the translation of the vacuum field in phase space. This translation is represented, in its most general form by the unitary operator:

$$D(\alpha) = e^{\alpha a^\dagger - \alpha^* a} \quad (1.32)$$

where α is an arbitrary C -number whose real and imaginary parts are the projections along the X_0 and $X_{\pi/2}$ directions respectively of the two-dimensional translation vector. Applying this translation amounts to displacing the vacuum Gaussian ‘packet’ in a given direction, without changing its shape. The translated vacuum state is the coherent state simply noted as $|\alpha\rangle$:

$$|\alpha\rangle = D(\alpha)|0\rangle . \quad (1.33)$$

The translated ‘packet’, whose evolution is determined in the Schrödinger picture by the free field Hamiltonian [Eq. (1.13)], subsequently rotates at frequency ω in phase space, without deformation, according to the equation:

$$|\Psi(t)\rangle = e^{-i\omega t/2} |\alpha e^{-i\omega t}\rangle . \quad (1.34)$$

This corresponds to the best possible approximation of a classical free oscillator motion, with minimal wave packets uncertainties for any two conjugate quadratures. Fig. 3(a,b) shows how the vacuum state is transformed by translation into a coherent state of well defined amplitude and phase and how this state freely evolves in phase space. For simplicity, the Gaussian clouds of points have been replaced in Fig. 3(b) by uncertainty circles of radius unity.

In order to make the translation operation more explicit, it is convenient to split the exponential in Eq.(1.34) in two, separating the contributions of the real and imaginary parts of α . For this, we make use of the Glauber relation [24] $e^{A+B} = e^A e^B e^{-[A,B]/2}$ (valid if $[A, B]$ commutes with A and B) and we get:

$$D(\alpha) = e^{-i\alpha_1\alpha_2} \exp(2i\alpha_2 X_0) \exp(-2i\alpha_1 X_{\pi/2}) \quad (1.35)$$

Using a mechanical oscillator analogy, the displacement $D(\alpha)$ can thus be viewed as a translation along space by an amount $\alpha_1 = \text{Re}(\alpha)$, followed by a ‘momentum kick’ of magnitude $\alpha_2 = \text{Im}(\alpha)$. This kick can be produced by the action of a delta-like impulsive force on the oscillator. The operation is completed by a global phase shift of the system’s state. Note that the order of these two translations along X_0 and $X_{\pi/2}$ can be exchanged, provided the overall phase shift is replaced by its opposite (the two translations along the conjugate directions in phase space do not commute).

Let us compute the probability amplitude for finding the value x when measuring the quadrature operator X_0 on a field in state $|\alpha\rangle$. A straightforward calculation using Eqs.(1.33) and (1.35) yields:

$$\langle x | \alpha \rangle = \left(\frac{2}{\pi} \right)^{1/4} \exp(-i\alpha_1\alpha_2) \exp(2i\alpha_2 x) \exp[-(x - \alpha_1)^2] . \quad (1.36)$$

We recognize in this expression a translation by the amount α_1 of the ground state wave packet, accompanied by a phase modulation at frequency α_2 which describes the momentum kick of the state. The probability for finding the value x for the quadrature is thus:

$$P(x) = \left(\frac{2}{\pi} \right)^{1/2} \exp[-2(x - \alpha_1)^2] \quad (1.37)$$

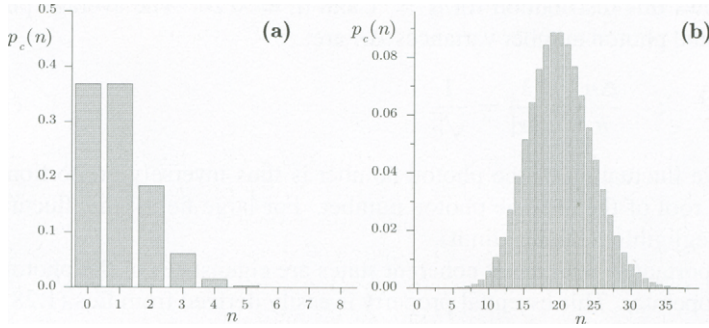


Fig. 4. Photon number statistical distributions. (a) Coherent field with $\bar{n} = 1$ photons on the average. (b) Coherent field with $\bar{n} = 20$.

If the coherent state is left to evolve freely, this probability becomes at time t :

$$P(x, t) = \left(\frac{2}{\pi} \right)^{1/2} \exp \left[-2(x - \alpha_1 \cos \omega t - \alpha_2 \sin \omega t)^2 \right]. \quad (1.38)$$

We will see below how the translation in phase space can be physically implemented when the oscillator is not a material particle, but a field in a cavity.

An alternative and useful expression of the displacement operator is obtained by using again the Glauber relation, separating this time the a and a^\dagger terms:

$$D(\alpha) = \exp [\alpha a^\dagger - \alpha^* a] = \exp \left(-\frac{|\alpha|^2}{2} \right) \exp(\alpha a^\dagger) \exp(-\alpha^* a). \quad (1.39)$$

This form corresponds to the ‘normal ordering’ in quantum optics. If we expand the exponential of operators along increasing powers, all the a^n terms are on the right and the $a^{\dagger n}$ terms on the left. The normal ordering of $D(\alpha)$ makes it straightforward to expand a coherent state along the Fock basis. The action of the $\exp(-\alpha^* a)$ operator placed on the right leaves the vacuum unchanged, since only the zero order term in the expansion along powers of a yields a non zero result. Combining Eqs.(1.33)and (1.39), one finds easily:

$$|\alpha\rangle = \sum_n C_n(\alpha) |n\rangle \quad \text{with} \quad C_n(\alpha) = \exp \left(-\frac{|\alpha|^2}{2} \right) \frac{\alpha^n}{\sqrt{n!}}. \quad (1.40)$$

The distribution of photon numbers in a coherent state obeys a Poisson statistics. Fig. 4 shows this distribution for $\alpha = 1$ and $\alpha = \sqrt{20}$. The average photon number \bar{n} and photon number variances Δn are:

$$\bar{n} = |\alpha|^2 \quad ; \quad \frac{\Delta n}{\bar{n}} = \frac{1}{|\alpha|} = \frac{1}{\sqrt{\bar{n}}} . \quad (1.41)$$

The relative fluctuation of the photon number is thus inversely proportional to the square root of the average photon number. For large fields, this fluctuation becomes negligible (classical limit).

It is important to notice that coherent states are eigenstates of the photon annihilation operator. This essential property is easily derived from Eqs.(1.28) and (1.40):

$$a |\alpha\rangle = \alpha |\alpha\rangle \quad \text{and} \quad \langle \alpha | a^\dagger = \langle \alpha | \alpha^* \quad (1.42)$$

It is also useful to recall the expression of the scalar product of two coherent states:

$$\langle \alpha | \beta \rangle = e^{-|\alpha|^2/2 - |\beta|^2/2 + \alpha^* \beta} \quad ; \quad |\langle \alpha | \beta \rangle|^2 = e^{-|\alpha - \beta|^2} , \quad (1.43)$$

which shows that the overlap of two such states decreases exponentially with their ‘distance’ in phase space. Although they are never strictly orthogonal, they become practically so when the distance of their centers is much larger than 1, the radius of the coherent state uncertainty circle. The coherent states of a field mode constitute a complete set of states in the Hilbert space of this mode. This is expressed by a closure relationship, easily derived by using the Fock state expansion of coherent states and the completeness of these Fock states:

$$\frac{1}{\pi} \int d\alpha_1 d\alpha_2 |\alpha\rangle \langle \alpha| = \mathbb{1} . \quad (1.44)$$

Note however that the coherent state basis, being made of non-orthogonal states, is over-complete. This means in particular that, although any field state can be expanded on it, this expansion is not unique.

1.3. Schrödinger cats as superpositions of coherent states

Among all the possible field states, we will give a special attention to the superpositions of two quasi-orthogonal coherent states, represented in space phase by two non-overlapping circles. These states are prototypes of Schrödinger cats [14, 15]. We will see later how they can be prepared and used to study the phenomenon of decoherence. We give here only some of their remarkable properties. As a simple example of such a cat state, let us consider a linear superposition with equal

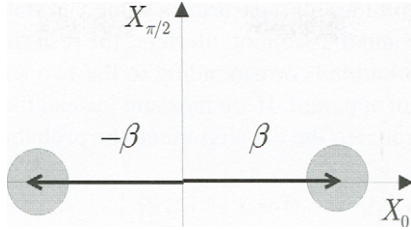


Fig. 5. Pictorial representation of a π -phase cat in phase space.

weights of two coherent states with opposite phases, represented in phase space by two circles whose centers are on the X_0 axis, symmetrical with respect to the origin (see Fig 5). This superposition, called a π -phase cat in the following, writes:

$$|\Psi_{cat}^{even}\rangle = \frac{|\beta\rangle + |-\beta\rangle}{\sqrt{2(1 + e^{-2|\beta|^2})}} \approx (1/\sqrt{2})(|\beta\rangle + |-\beta\rangle), \quad (1.45)$$

where β is the amplitude of the field (real in this case). The superscript ‘even’ in the state expression will be explained below. The denominator in the first right hand side term insures the normalization of the state, taking into account the overlap of the two $|\beta\rangle$ and $|-\beta\rangle$ coherent states. If $|\beta| \gg 1$, this overlap can be neglected and the cat state is expressed by the simpler form given by the second right-hand-side term in Eq.(1.45). The coherence between the two states is an essential feature which distinguishes it from a mere statistical mixture. This is made clear by expressing the field density operator:

$$\rho_{cat} \approx \frac{1}{2} (|\beta\rangle\langle\beta| + |-\beta\rangle\langle-\beta| + |\beta\rangle\langle-\beta| + |-\beta\rangle\langle\beta|). \quad (1.46)$$

The ‘cat state’ coherence is described by the off-diagonal part of this density operator (last two terms in the right hand side of Eq.(1.46)). This coherence is displayed by analyzing the field quadrature distribution in this state, with a proper choice of phase. Suppose first that we measure the quadrature X_0 along the direction of the cat alignment. It is straightforward that the probability distribution for this quadrature is merely the sum of two Gaussians, centered at $\pm\beta$:

$$P_0^{(cat)}(x) \approx \frac{1}{\sqrt{2\pi}} (e^{-2(x-\beta)^2} + e^{-2(x+\beta)^2}). \quad (1.47)$$

The probability amplitudes for measuring a value x in state $|+\beta\rangle$ and $|-\beta\rangle$ do not appreciably overlap and thus cannot interfere: the resulting distribution is simply the sum of the distributions corresponding to the two state components and the state coherence is not apparent. If we measure instead the quadrature $X_{\pi/2}$ along the direction orthogonal to the cat alignment, the probability distribution writes:

$$P_{\pi/2}^{(cat)}(x) \approx \frac{1}{2} |\pi/2 \langle x | \beta \rangle + \pi/2 \langle x | -\beta \rangle|^2, \quad (1.48)$$

where the index $\pi/2$ in the $\pi/2 \langle x |$ bra indicates an eigenstate of $X_{\pi/2}$, related to those of X_0 by a Fourier transform [see Eq.(1.23)]. The probability $P_{\pi/2}(x)$ is the square of the sum of two amplitudes which are both non zero. These amplitudes are easy to compute. The scalar product of $|x\rangle_{\pi/2}$ with $|\beta\rangle$ is equal to the product of $|x\rangle_0$ with $| -i\beta\rangle$, as a mere rotation in phase space indicates. Using Eq.(1.36), we immediately get:

$$\begin{aligned} \pi/2 \langle x | \beta \rangle &= {}_0 \langle x | \beta e^{-i\pi/2} \rangle = {}_0 \langle x | -i\beta \rangle \\ &= \left(\frac{2}{\pi}\right)^{1/4} \exp(-2i\beta x) \exp(-x^2) \end{aligned} \quad (1.49)$$

and:

$$P_{\pi/2}^{(cat)} \approx \left(\frac{2}{\pi}\right)^{1/2} e^{-2x^2} (1 + \cos 4\beta x). \quad (1.50)$$

The probability distribution is a Gaussian centered at $x = 0$, modulated by an interference term with fringes having a period $1/4\beta$ inversely proportional to the ‘cat size’ β . This interference term is a conspicuous signature of the coherence of the state superposition. The distribution of any phase quadrature X_φ can be obtained in the same way. The interference term exists only when φ is close to $\pi/2$. A graphical representation is very convenient to understand why it is so (Fig. 6). For a coherent state, a field quadrature takes non zero values in an interval corresponding to the projection of the state uncertainty circle on the direction of the quadrature. For a Schrödinger cat state, there are two such intervals, corresponding to the two state components. If $\beta \gg 1$ and $\varphi = 0$ [Fig. 6(a)], the two intervals are non-overlapping and there is no interference. For a φ value between 0 and $\pi/2$ [Fig. 6(b)], the two intervals are closer than for $\varphi = 0$, resulting in two still non-overlapping Gaussians without interference. It is only when φ gets very close to $\pi/2$ that the two projected intervals overlap along the direction of the quadrature, leading to a large interference term [Fig. 6(c)].

Instead of rotating the quadrature for a given ‘frozen’ cat state, let us choose a given quadrature (e.g. X_0) and consider the evolution of its probability distribution for a freely evolving cat state. This evolution amounts to a rotation in

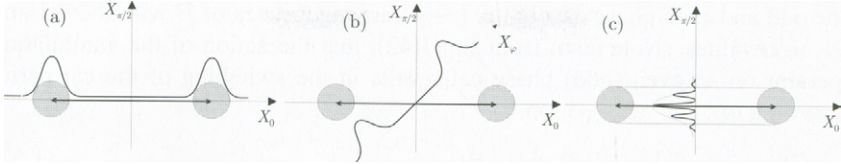


Fig. 6. Quadratures of a π phase Schrödinger cat. (a) The X_0 quadrature exhibits well separated Gaussian peaks corresponding to the cat's components. (b) For $X_{\pi/4}$, the Gaussian peaks distance is reduced. (c) For $X_{\pi/2}$ the two peaks merge and fringes show up.

the same direction of the two coherent state components which stay opposite to each other in phase space. Their projections along the (now fixed) direction of the field quadrature oscillate with opposite phases, corresponding to two wave packets periodically colliding at $x = 0$. When the two packets merge, fringes with 100 % contrast appear under the Gaussian envelope. This periodic fringe pattern is a signature of the cat state coherence. It would not exist if the field were described by an incoherent superposition of coherent states [first two terms in Eq.(1.46)]. The fringes are getting narrower when the amplitude of the field is increased. We will see later that these fringes are very fragile and efficiently washed out by decoherence.

Another aspect of the coherence of cat states made with fields of opposite phases is revealed by considering their photon number distribution. The cat state given by Eq. (1.45) develops only along even number states, since the probability for finding n photons in it is proportional to $1 + (-1)^n$. For this reason, we have added the superscript ‘even’ in its name. Similarly the Schrödinger cat state with opposite amplitudes: $|\psi^{odd}\rangle = (1/\sqrt{2})[|\beta\rangle - |- \beta\rangle]$ develops only along the odd photon number states since the probability for finding n photons in it is proportional to $1 - (-1)^n$. We will call it an “odd phase cat”. The periodicity of the photon number is related to the coherence of the state, since a statistical mixture of $|\beta\rangle$ and $|- \beta\rangle$ contains obviously all photon numbers. We can thus say that the photon number distribution, with its “dark fringes” corresponding to zero probability for odd or even photon numbers, is a signature of the even and odd cats coherence, as is the existence of dark fringes in their $X_{\pi/2}$ quadrature.

It is finally convenient for this discussion to introduce the photon number parity operator \mathcal{P} [24] which admits as eigenstates all the superpositions of even photon numbers with the eigenvalue +1 and all the superpositions of odd photon number states with the eigenvalue -1. An obvious expression for this operator is:

$$\mathcal{P} = e^{i\pi a^\dagger a}. \quad (1.51)$$

The odd and even phase cats $|\beta\rangle \pm |-\beta\rangle$ are eigenstates of \mathcal{P} with the +1 and -1 eigenvalues. Note also, from Eq.(1.42), that the action of the annihilation operator on an even (odd) phase cat results in the switching of the cat parity according to:

$$a[|\beta\rangle \pm |-\beta\rangle] = \beta[|\beta\rangle \mp |-\beta\rangle]. \quad (1.52)$$

Let us note finally the action of the parity operator on a quadrature eigenstate:

$$\mathcal{P}|x\rangle_\varphi = |-x\rangle_\varphi, \quad (1.53)$$

This is a direct consequence of the parity of the Hermite polynomials, proportional to the scalar product $\langle n|x\rangle$, which develop on even (odd) powers of x if n is even (odd). Eq.(1.53) can be taken as an alternative definition of \mathcal{P} , as the operator which reflects any quadrature eigenstate into the state with an opposite eigenvalue.

1.4. Field representations: the Q and W functions

We have extensively used pictorial phase-space representations in the description of various field states. They have remained however up to this point rather qualitative, fuzzy distributions of points or uncertainty circles. In this section, we show that the formalism of quantum optics can make these phase space pictures fully quantitative by associating to each state of the field two functions taking real values in phase space. These functions, called Q and W , are usually represented by three-dimensional plots in which the horizontal plane is the phase space and the vertical axis represents the value of the function. They give a vivid description of any single mode field state, whether it is pure or a statistical mixture. They can be deduced from one another and the knowledge of one of them is sufficient to reconstruct the field density operator. In other words, the Q or the W function contains all the quantum information there is about the field state. A full discussion of the phase space representation of fields in quantum optics can be found in [22]. We recall here only the definition of these functions and some of their important properties.

1.4.1. The Q function

Given a field state described by its density operator ρ , its Q function at the point in phase space associated to the C -number α is defined as:

$$Q(\alpha) = \frac{1}{\pi} \langle \alpha | \rho | \alpha \rangle = \frac{1}{\pi} \text{Tr} [\rho |\alpha\rangle \langle \alpha|]. \quad (1.54)$$

The Q function thus represents, for a pure case, the square of the overlap of the state with a coherent one. It is a real and positive quantity. Its normalization is

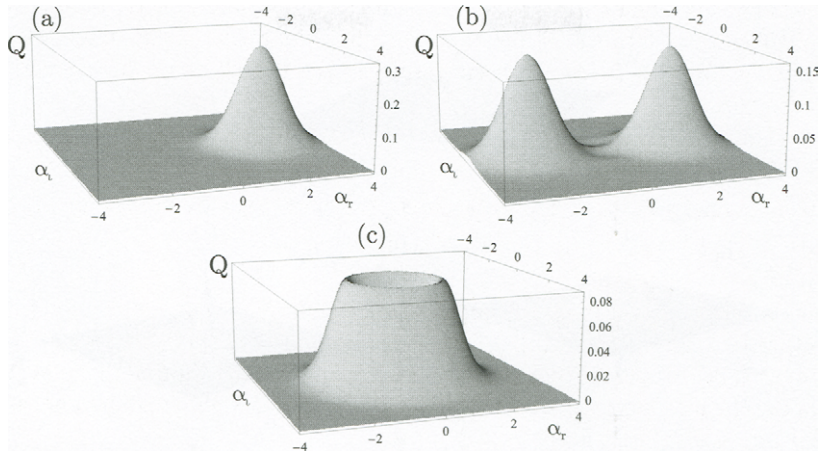


Fig. 7. Plots of Q functions. (a) 5 photons coherent state (real amplitude). (b) Schrödinger cat state, superposition of two 5 photon coherent states with opposite phases. Note the weak interference pattern near the origin. (c) Two-photon Fock state.

chosen to insure that the integral of Q over the whole phase space is equal to 1. An alternative definition of Q is given by using Eq.(1.33):

$$Q(\alpha) = \frac{1}{\pi} \text{Tr}[|0\rangle\langle 0| D(-\alpha)\rho D(\alpha)] \quad (1.55)$$

The Q function for the coordinate α is the expectation value, in the state of the field translated by $-\alpha$, of the projector on the vacuum. We will see in section 3 how this definition can be directly exploited for an experimental determination of Q in CQED.

It results directly from Eqs.(1.54) and (1.43) that the Q function of a coherent state is a Gaussian centered at the value corresponding to the complex amplitude of the state [see Fig. 7(a)]. The Q function of a Schrödinger cat of the form [Eq.(1.45)] is essentially the superposition of two Gaussians, centered at $\pm\beta$ [Fig. 7(b)]. There is a small additional interference term taking non zero values between these two Gaussians, but it is of the order of the scalar product of the two cat components, vanishingly small as soon as they are separated. The Q function is thus not appropriate to describe, in practice, the coherence of a cat state. We have finally shown in Fig. 7(c) the Q function of a $n = 2$ Fock state.

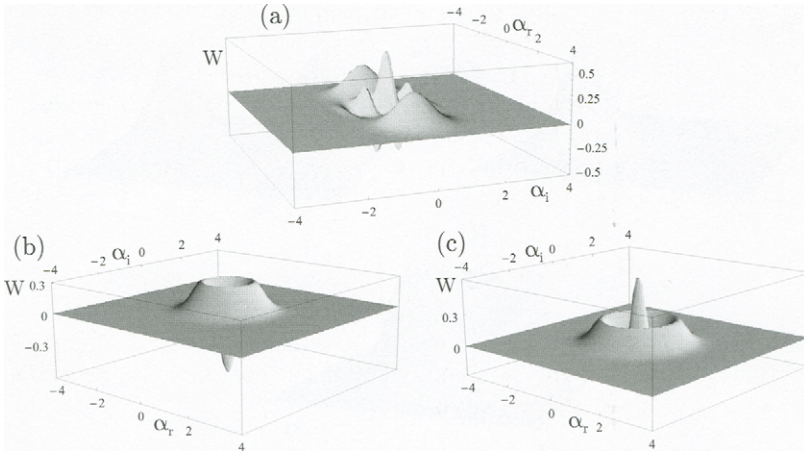


Fig. 8. Plot of W functions. (a) Schrödinger cat, superposition of two 5-photon coherent states with opposite phases. (b) One-photon Fock state. (c) Two-photon Fock state.

1.4.2. The W function

Given a field state described by its density operator ρ , its W function at the point in phase space whose C -number coordinate is $\alpha = x + ip$ is defined as:

$$W(x, p) = \frac{1}{\pi} \int dx' e^{-2ix'p} \langle x + \frac{x'}{2} | \rho | x - \frac{x'}{2} \rangle. \quad (1.56)$$

It appears as the Fourier transform of a function built on off-diagonal matrix elements of the field density operator in a quadrature representation. This expression was derived first by Wigner in 1932 [33] (hence the name W or Wigner function) in order to build a phase space distribution for a quantum particle resembling as closely as possible the probability distribution of classical statistical physics. The W function is, as Q , a real function, whose integral in phase space is equal to 1. Contrary to Q , however, it can take negative values in some domains of phase space. These negative values are, as shown below, a signature of non-classical behavior for the corresponding states.

From the definition [Eq.(1.56)] and the expressions of the coherent states in a quadrature basis [Eq.(1.36)], the W function of coherent states are easy to compute. They are, like Q , Gaussian functions centered at the value corresponding to the complex amplitude of the state, but their width is $\sqrt{2}$ times smaller. The W function of a π -phase cat state is, as its Q function, a superposition of two Gaussian peaks with, in addition, a large interference pattern between these peaks presenting oscillations, with an alternance of positive and negative ridges [Fig.

8(a)]. This pattern is a signature of the state coherence, lacking in the W function of a statistical mixture of coherent states. The W function is thus much better adapted than Q for the study of a mesoscopic state coherence. Fig. 8(b) and (c) present the W function of the $n = 1$ and $n = 2$ Fock states which also exhibit negative parts as typical non-classical features.

By inverse Fourier transform of Eq.(1.56), the matrix elements of the field density operator are expressed as:

$$\langle x + \frac{x'}{2} | \rho | x - \frac{x'}{2} \rangle = \int dp e^{2ix'p} W(x, p) , \quad (1.57)$$

which shows explicitly that the field density operator is fully determined by the knowledge of W . In particular the diagonal elements, representing the probability density of the quadrature X_0 , are given by:

$$\langle x | \rho | x \rangle = \int dp W(x, p) . \quad (1.58)$$

This equation expresses an important property that W shares with a classical probability distribution for a particle in phase space. The probability that the X_0 quadrature takes a given value x is obtained by integrating the W function for this x value, along all the possible values of the orthogonal quadrature. In the same way, the probability for finding a classical particle at one point is given by integrating its phase space probability density over its momentum and vice versa. We have chosen here to use the X_0 and $X_{\pi/2}$ axes as reference frame in phase space. Any other set of orthogonal quadratures is of course equally possible. Transforming from one to the other amounts to a rotation in phase space, with a simple linear coordinate transformation for the W function. The integration property is obviously independent upon the coordinate frame. In other words, the density probability for any quadrature is given by summing W over the orthogonal one. We have seen above that some states, such as the Schrödinger cats or the Fock states have for some quadratures values occurring with 0 probability ('dark fringes'). The existence of these destructive interferences is an indication of non-classicality. This means that the integral of the W function along the orthogonal quadrature vanishes, which is possible only if W presents alternances of positive and negative values. We thus understand that negative values of W are related to non-classicality. We will show in section 2 that the integral property of W expressed by Eq.(1.58) is at the basis of a very general method to determine the W function of a light field, involving the measurement of the fluctuations of all its quadratures (quantum tomography).

We conclude this section by giving an alternative expression of W which will also be useful in the following. To obtain it, we let the reader demonstrate the

simple translation relations:

$$|x - \frac{x'}{2}\rangle = e^{-i(x-x')p} D(x + ip) |-\frac{x'}{2}\rangle, \quad (1.59)$$

and

$$\langle x + \frac{x'}{2}| = \langle \frac{x'}{2}| D(-x - ip) e^{i(x+x')p}, \quad (1.60)$$

which follow directly from the definition of the displacement operators. Replacing $|x \pm x'/2\rangle$ in Eq.(1.57) by the expressions given by Eqs.(1.59) and (1.60), and noting that $\mathcal{P}|x'/2\rangle = |-x'/2\rangle$ [see Eq. (1.53)], we immediately get:

$$W(x, p) = \frac{2}{\pi} \text{Tr}[D(-\alpha)\rho D(\alpha)\mathcal{P}], \quad (1.61)$$

which shows that the W function for the coordinate α is the expectation value in the state translated by $-\alpha$ of the field parity operator. The derivation presented here is due to L. Davidovich (private communication). The expression (1.61) is usually derived in a more complex way [24]. We will see in section 3 how this definition can be directly exploited for an experimental determination of W in CQED.

1.5. Coupling between field and charges: modeling sources and photon detectors

We have so far considered free fields, without describing the material systems they are coupled to. The field interacts in fact with charged particles (atomic electrons, currents ...). These interactions are essential to describe the field emission (sources) and its measurement (detectors). The Hamiltonian describing the evolution of the field +charges system writes in Coulomb gauge, at the non-relativistic limit [26, 34]:

$$\begin{aligned} H_{\text{charges + field}} &= \sum_i \frac{1}{2m_i} (\mathbf{p}_i - q_i \mathbf{A}(\mathbf{r}_i))^2 + U(\mathbf{r}_1, \mathbf{r}_2, \dots, \mathbf{r}_i, \dots) \\ &\quad + \sum_j \hbar\omega_j \left(a_j^\dagger a_j + \frac{1}{2} \right). \end{aligned} \quad (1.62)$$

The $q_i, m_i, \mathbf{r}_i, \mathbf{p}_i$ are respectively the charge, mass, position and momentum of particle i (electrons and nuclei inside atoms or molecules). $U(\mathbf{r}_1, \mathbf{r}_2, \dots, \mathbf{r}_i, \dots)$ is the Coulomb potential of the charges, which depends only on their positions. The classical version of this Hamiltonian yields the dynamical equation for the

charges driven by the Lorentz force produced by the field, and the Maxwell equations describing the evolution of the fields produced by the distribution of charges and currents. This coupled evolution leads in general to a complicated dynamics. We recall here only some simple situations in which either single photon Fock states or quasi-classical coherent states of the field are generated.

1.5.1. Single atom coupled to field: Rabi oscillation, spontaneous emission and preparation of Fock states

Consider first a one-electron atom coupled to a field mode in a cavity [27–30]. The atom has two relevant energy levels e and g separated by a transition resonant or nearly resonant with the mode, so that one photon processes are dominant (we neglect the A^2 term creating or annihilating 0 or 2 photons). Eq.(1.62) then reduces to:

$$\begin{aligned} H_{\text{charges + field}} &= H_{\text{at}} + H_{\text{field}} + H_{\text{int}} \\ H_{\text{at}} &= \frac{p^2}{2m} + U(\mathbf{r}) ; \quad H_{\text{field}} = \hbar\omega \left(a^\dagger a + \frac{1}{2} \right) \\ H_{\text{int}} &= -\frac{q}{m} \frac{E}{\omega} [(\mathbf{p} \cdot \boldsymbol{\epsilon}) a f(\mathbf{r}) + (\mathbf{p} \cdot \boldsymbol{\epsilon}^*) a^\dagger f^*(\mathbf{r})] . \end{aligned} \quad (1.63)$$

This Hamiltonian consists of three terms, the free hydrogen-like atom hamiltonian H_{at} , the free field hamiltonian H_{field} and the coupling term H_{int} . Projecting explicitly on the two atomic levels e and g and making the rotating wave approximation (RWA) which amounts to neglecting far off-resonant couplings [34], we get:

$$H_{\text{int}} \approx -\frac{q}{m} \frac{E}{\omega} [f(\mathbf{r}) (\mathbf{p} \cdot \boldsymbol{\epsilon})_{eg} |e\rangle \langle g| a + f^*(\mathbf{r}) (\mathbf{p} \cdot \boldsymbol{\epsilon}^*)_{ge} |g\rangle \langle e| a^\dagger] . \quad (1.64)$$

The a term in the right hand side describes photon absorption processes accompanied by the g to e atom jump, while the a^\dagger term accounts for photon emission combined to e to g atom transitions. The RWA approximation amounts to disregarding two other off-resonant processes in which the atom and the field get excited or de excited together. To simplify this expression further, we can combine the atomic matrix elements and the field parameters into a single constant describing the strength of the atom field coupling, which is called the vacuum Rabi frequency $\Omega(\mathbf{r})$:

$$\begin{aligned} H_{\text{int}} &\approx \frac{\hbar\Omega(\mathbf{r})}{2} [|e\rangle \langle g| a + |g\rangle \langle e| a^\dagger] ; \\ \Omega(\mathbf{r}) &= -\frac{q}{m} f(\mathbf{r}) (\mathbf{p} \cdot \boldsymbol{\epsilon})_{eg} \sqrt{\frac{2}{\hbar\omega\varepsilon_0 V}} . \end{aligned} \quad (1.65)$$

The Rabi frequency is a function of the atom's position since the field strength seen by the atom depends on its location inside the mode via the $f(\mathbf{r})$ function. We will assume, without loss of generality, that $f(\mathbf{r})$, $(\mathbf{p}\cdot\boldsymbol{\epsilon})_{eg}$ and thus $\Omega(\mathbf{r})$ are real. If the atom is fixed in space, we can disregard the \mathbf{r} parameter and consider the Rabi frequency as a constant Ω . To describe an experiment in which an atom is moving across the field mode, we can also, in general, replace the spatially dependent $\Omega(\mathbf{r})$ quantity by an effective spatial average and drop the explicit \mathbf{r} dependence. The system's evolution ruled by the Hamiltonian given by Eq.(1.65) corresponds to the Rabi oscillation in which the atom and the field reversibly exchange their energy. Assume that the atom is prepared at time $t = 0$ in level e with no photon in the field. The system evolves at time t into a linear superposition of the two states $|e, 0\rangle$ and $|g, 1\rangle$ corresponding respectively to the atom in e without photon or to the atom in g with 1 photon present:

$$|\Psi(0)\rangle = |e\rangle |0\rangle \rightarrow |\Psi(t)\rangle = \cos(\Omega t/2) |e\rangle |0\rangle - i \sin(\Omega t/2) |g\rangle |1\rangle . \quad (1.66)$$

The two probability amplitudes oscillate at the Rabi frequency Ω . In general, the atom-field state is non-separable, a manifestation of entanglement. For $\Omega t = \pi$, however, there is no entanglement and a one photon Fock state is deposited in the mode.

The reversibility of the Rabi oscillation is a special feature of the single field mode situation which requires in practice that the atom must be placed into a high- Q cavity sustaining the mode, with negligible field losses. In the more general situation where the atom interacts with the field in free space, its coupling to a continuum of field modes must be considered. Focusing again on a two-level atom in the RWA approximation, we get the following atom-field Hamiltonian:

$$H'_{\text{int}} = -\frac{q}{m} \sum_j \frac{E_j}{\omega_j} (\mathbf{p}\cdot\boldsymbol{\epsilon}_j)_{eg} e^{i\mathbf{k}_j\cdot\mathbf{r}} |e\rangle \langle g| a_j + h.c.. \quad (1.67)$$

The evolution of the atom-field system ruled by this Hamiltonian has been first described by Wigner and Weisskopf [35] and analyzed since in many papers and text books. When the atom is initially excited and the field in vacuum, the situation corresponds to the well-known spontaneous emission phenomenon, which, in free space, is irreversible. Solving for the system's evolution in the interaction representation, and neglecting Lamb-shift terms irrelevant to this discussion, we get:

$$\begin{aligned} |\Psi(0)\rangle &= |e, 0\rangle \rightarrow |\Psi(t)\rangle = e^{-\Gamma t/2} |e, 0\rangle + \\ &\left(\frac{1}{i\hbar} \right) \sum_j \langle g, 1_j | H'_{\text{int}} |e, 0\rangle \frac{1 - e^{-\Gamma t/2} e^{-i(\omega_{eg} - \omega_j)t}}{i(\omega_{eg} - \omega_j - i\Gamma/2)} |g, 1_j\rangle . \end{aligned} \quad (1.68)$$

The final system's state is made of two parts, an initial state which is decaying exponentially in time and a final state consisting of an atom in the lower state with a photon distributed in a continuum of modes. The spontaneous decay is described by the natural rate Γ , simply expressed in terms of the matrix element $(\mathbf{p} \cdot \boldsymbol{\epsilon})_{eg}$ and the atomic frequency ω_{eg} . After a time $t \gg 1/\Gamma$, the field ends up in a superposition of one-photon states belonging to each possible final mode $|1_i\rangle$, (Lorentzian distribution in frequency, with a width Γ). The corresponding one-photon wave packet writes [we leave the reader compute the exact expression of the c_j 's from Eqs.(1.68) and (1.67)]:

$$|\Psi(t \gg 1/\Gamma)\rangle = \sum_j c_j a_j^+ |0\rangle . \quad (1.69)$$

This represents a one-photon packet whose wave vector angular distribution and polarization are determined by the matrix elements $(\mathbf{p} \cdot \boldsymbol{\epsilon})_{eg}$ which appear in the expression of the c_j 's.

This discussion can be generalized to more complex situations, involving a multilevel atom. For example, an atom with three levels e , g and i defining two cascading transitions, will emit, starting from e in vacuum, a pair of correlated photons whose direction of emission and polarizations depend on the matrix element of the electron momentum operator between the relevant atomic states. Such cascading transitions are useful for the preparation of entangled photons [36].

1.5.2. Classical current coupled to field: generation of coherent states

Single atom emitters, as just recalled, spontaneously generate Fock states of the field. Coherent states, on the other hand, can be produced by coupling the field to a monochromatic classical charge distribution [26]. If the charges motion is imposed (independent of field) and classical (negligible fluctuations of \mathbf{r}_i and \mathbf{p}_i), the field Hamiltonian reduces to:

$$H_{\text{field}}^{\text{classical source}} = \sum_j \hbar \omega_j \left(a_j^\dagger a_j + \frac{1}{2} \right) - \int \mathbf{A}(\mathbf{r}) \cdot \mathbf{J}(\mathbf{r}, t) d^3 \mathbf{r} . \quad (1.70)$$

in which $\mathbf{J}(\mathbf{r}, t)$ is the classical current density which can be expressed as a distribution over the particles velocities:

$$\mathbf{J}(\mathbf{r}, t) = \sum_i q_i \mathbf{v}_i(t) \delta(\mathbf{r} - \mathbf{r}_i(t)) ; \mathbf{v}_i = \frac{d\mathbf{r}_i}{dt} . \quad (1.71)$$

This classical current Hamiltonian can be derived from the expression of the classical field Lagrangian [26]. It can also be deduced from the fully quantum

hamiltonian $H_{\text{charges} + \text{field}}$ given by Eq.(1.62), letting the m_i go to infinity while keeping $\mathbf{p}_i/m_i = \mathbf{v}_i$ finite. The charges motion is then independent of \mathbf{A} . We must however retain the term linear in \mathbf{A} in the Hamiltonian to describe the action of the imposed currents on the field. The interaction term becomes:

$$H_{\text{int}}^{\text{classical}} = - \sum_i q_i \mathbf{v}_i(t) \cdot \mathbf{A}(\mathbf{r}_i(t)) , \quad (1.72)$$

which is identical to the current-field interaction term in Eq.(1.70). Consider the case of a monochromatic current defined as:

$$\mathbf{J}(\mathbf{r}, t) = \mathbf{J}_0(\mathbf{r}) e^{-i\omega t} . \quad (1.73)$$

and assume that this current is coupled to a resonant field mode in a cavity. Making again the RWA approximation, we can write the interaction as:

$$H_{\text{int}}^{\text{classical}} = - \int \mathbf{J}(\mathbf{r}, t) \cdot \mathbf{A}(\mathbf{r}) d^3 \mathbf{r} \approx - (s_0 e^{i\omega t} a + s_0^* e^{-i\omega t} a^\dagger) , \quad (1.74)$$

where

$$s_0 = \sqrt{\frac{\hbar}{8\epsilon_0 \omega V}} \int f(\mathbf{r}) (\mathbf{J}_0(\mathbf{r}) \cdot \boldsymbol{\epsilon}) d^3 \mathbf{r} \quad (1.75)$$

describes the overlap between the mode and the distribution of the source currents. Going in the interaction picture, the atom field coupling becomes:

$$\tilde{H}_{\text{int}}^{\text{classical}} = e^{i H_{\text{field}} t / \hbar} H_{\text{int}}^{\text{classical}} e^{-i H_{\text{field}} t / \hbar} = - (s_0 a + s_0^* a^\dagger) , \quad (1.76)$$

and the evolution of the field, supposed to be in vacuum at time $t = 0$, can be expressed as:

$$\begin{aligned} |\tilde{\Psi}(t)\rangle &= e^{-i \tilde{H}_{\text{int}} t / \hbar} |0\rangle = e^{i(s_0 t a + s_0^* t a^\dagger) / \hbar} |0\rangle \\ &= D(i s_0 t / \hbar) |0\rangle = |\alpha = i s_0 t / \hbar\rangle . \end{aligned} \quad (1.77)$$

The unitary atom evolution operator is then identical to a field displacement in phase space. The classical current source generates a coherent state in the mode, whose amplitude increases linearly with time (mean photon number scaling as t^2). We further note that the complex amplitude of this coherent field is given by an expression which does not contain Planck's constant:

$$|i s_0 t / \hbar| \sqrt{\frac{\hbar \omega}{2\epsilon_0 V}} = \frac{t}{4\epsilon_0 V} \int d^3 \mathbf{r} f(\mathbf{r}) (\mathbf{J}_0(\mathbf{r}) \cdot \boldsymbol{\epsilon}) . \quad (1.78)$$

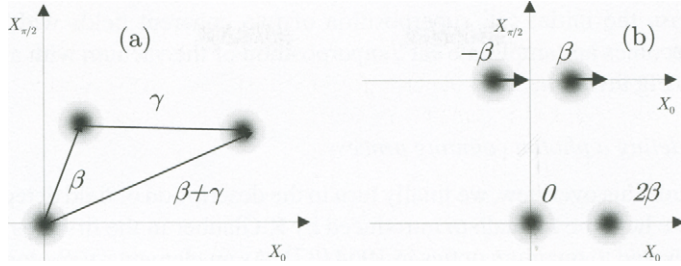


Fig. 9. Translation of field states in phase space. (a) a coherent field $|\beta\rangle$ translated by a displacement operator with the amplitude γ becomes $|\beta + \gamma\rangle$ (up to a global phase). (b) A π -phase cat $|\beta\rangle + |-\beta\rangle$ displaced by β yields an amplitude cat $|2\beta\rangle + |0\rangle$ (state normalization omitted). For the sake of clarity, the initial and final states are represented with different axis sets.

This is thus the same amplitude as the one given by a fully classical description. The field emitted by a classical imposed source is a coherent state whose amplitude is given by the classical solution of Maxwell equations. An arbitrary translation $D(\gamma)$ of the field in phase space is realized by coupling it during a given time t to a classical source with appropriate amplitude and phase ($\gamma = is_0t/\hbar$). The same analysis applies if there is already an initial field in the cavity. Coupling for a given time the cavity field to a resonant source of classical current thus provides a simple way of displacing a coherent state in phase space. Assuming that the field is initially in state $|\beta\rangle$, we get:

$$\begin{aligned} |\tilde{\Psi}(t)\rangle &= D(\gamma = is_0t/\hbar) |\beta\rangle \\ &= \exp(\gamma a^\dagger - \gamma^* a) \exp(\beta a^\dagger - \beta^* a) |0\rangle \\ &= e^{i(\beta_1\gamma_2 - \beta_2\gamma_1)} |\beta + \gamma\rangle . \end{aligned} \quad (1.79)$$

We realize in this way the translation defined by the vector represented by the C -number γ , combined with a global phase shift of the field state. This translation is schematically represented by the diagram of Fig. 9(a). A π phase cat can be translated in the same way, according to:

$$|\tilde{\Psi}(t)\rangle = \left(\frac{1}{\sqrt{2}} \right) [e^{i\beta\gamma_2} |\beta + \gamma\rangle + e^{-i\beta\gamma_2} |-\beta + \gamma\rangle] \quad (1.80)$$

and in the special case where $\beta = \gamma$ (real) we get:

$$|\tilde{\Psi}(t)\rangle = \left(\frac{1}{\sqrt{2}} \right) [|2\beta\rangle + |0\rangle] \quad (1.81)$$

In this case the initial cat, superposition of two coherent fields with opposite phases becomes an ‘amplitude cat’, superposition of the vacuum with a coherent field [see Fig 9(b)].

1.6. Modeling a photon counting process

To conclude this overview, we finally turn to the description of field detection. We summarize here the formalism introduced by R.Glauber in the first Les Houches school devoted to quantum optics in 1964 [37]. As an elementary photon counter, we consider an atom with a ground state g and a continuum of excited states e_i (corresponding to electronic states above the ionization threshold). We focus now on the photon absorption process starting with the atom in level g . The field with a given polarization ϵ is in an initial state involving a set of field modes labeled by the index j . The absorption is governed by the atom-field coupling written in the RWA approximation as:

$$H_{\text{int}}^{\text{Det}} \approx -\frac{q}{m} \mathbf{p} \cdot \mathbf{A}(\mathbf{r}) \approx -\frac{q}{m} \sum_i (\mathbf{p} \cdot \epsilon)_{ig} |e_i\rangle \langle g| \sum_j \frac{E_j}{\omega_j} a_j e^{i\mathbf{k}_j \cdot \mathbf{r}} + \text{h.c.} \quad (1.82)$$

We assume that the excited atomic continuum extends over a relatively narrow absorption band whose center defines an average transition frequency ω_0 . The field modes relevant for the absorption are the ones whose frequency ω_j are close to ω_0 , so that we can rewrite Eq.(1.82) as:

$$H_{\text{int}}^{\text{Det}} \approx -\sum_i \frac{q}{im\omega_0} (\mathbf{p} \cdot \epsilon)_{ig} |e_i\rangle \langle g| \sum_j i E_j a_j e^{i\mathbf{k}_j \cdot \mathbf{r}} + \text{h.c.} \quad (1.83)$$

We recognize in the sums over the j modes in this equations the so-called positive and negative frequency parts of the electric field operator, which respectively annihilate and create a photon:

$$E^+(\mathbf{r}) = i \sum_j E_j a_j e^{i\mathbf{k}_j \cdot \mathbf{r}} \quad ; \quad E^-(\mathbf{r}) = -i \sum_j E_j a_j^\dagger e^{-i\mathbf{k}_j \cdot \mathbf{r}}. \quad (1.84)$$

Regrouping atomic parameters in a single coupling constant κ_{ig} , we express the interaction Hamiltonian in terms of these positive and negative electric fields as:

$$H_{\text{int}}^{\text{Det}} = -\sum_i \left(\kappa_{ig} |e_i\rangle \langle g| E^+(\mathbf{r}) - \kappa_{ig}^* |g\rangle \langle e_i| E^-(\mathbf{r}) \right). \quad (1.85)$$

A last convenient transformation of this expression is obtained by going into the representation picture, changing $H_{\text{int}}^{\text{Det}}$ into

$$\tilde{H}_{\text{int}}^{\text{Det}} = e^{i(H_{\text{at}}+H_{\text{field}})t/\hbar} H_{\text{int}}^{\text{Det}} e^{i(H_{\text{at}}+H_{\text{field}})t/\hbar}. \quad (1.86)$$

The atom-field coupling then involves the electric field operators in the Heisenberg point of view, as time-dependent operators:

$$\begin{aligned}\tilde{H}_{\text{int}}^{\text{Det}} = & - \sum_i (\kappa_{ig} e^{i\omega_{ig} t} |e_i\rangle \langle g| E^+(\mathbf{r}, t) \\ & - \kappa_{ig}^* e^{-i\omega_{ig} t} |g\rangle \langle e_i| E^-(\mathbf{r}, t)).\end{aligned}\quad (1.87)$$

Assuming that at $t = 0$ the system is in state $|\tilde{\Psi}(0)\rangle = |g\rangle |\tilde{\Psi}_{\text{field}}\rangle$ we expect at first order of perturbation theory that the state at time t is:

$$\begin{aligned}|\tilde{\Psi}(t)\rangle &\approx |g\rangle |\tilde{\Psi}_{\text{field}}\rangle + \frac{1}{i\hbar} \int_0^t dt' \tilde{H}_{\text{int}}^{\text{Det}}(t') |g\rangle |\tilde{\Psi}_{\text{field}}\rangle \\ &= |g\rangle |\tilde{\Psi}_{\text{field}}\rangle - \frac{1}{i\hbar} \sum_i \kappa_{ig} |e_i\rangle \int_0^t dt' e^{i\omega_{ig} t'} E^+(\mathbf{r}, t') |\tilde{\Psi}_{\text{field}}\rangle.\end{aligned}\quad (1.88)$$

We finally get the total photo-ionization probability at time t by summing the contributions of all final states:

$$P_e(t) = \sum_i \langle \tilde{\Psi}(t) | e_i \rangle \langle e_i | \tilde{\Psi}(t) \rangle,\quad (1.89)$$

which directly yields the total atomic excitation probability:

$$\begin{aligned}P_e(t) &= \frac{1}{\hbar^2} \sum_i |\kappa_{ig}|^2 \int_0^t \int_0^t dt' dt'' e^{i\omega_{ig}(t'-t'')} \times \\ &\quad \times \langle \tilde{\Psi}_{\text{field}} | E^-(\mathbf{r}, t'') E^+(\mathbf{r}, t') | \tilde{\Psi}_{\text{field}} \rangle.\end{aligned}\quad (1.90)$$

Summing over the final atom states i is equivalent to an integration over a continuum. We assume the variation of the coupling $|\kappa_{ig}|^2$ slow enough to replace it by a constant $|\kappa_0|^2$ over the continuum width. Integration of the exponential over ω_{ig} introduces the function $2\pi\delta(t' - t'')$. Hence:

$$P_e(t) = \frac{2\pi}{\hbar^2} |\kappa_0|^2 \int_0^t dt' \langle \tilde{\Psi}_{\text{field}} | E^-(\mathbf{r}, t') E^+(\mathbf{r}, t') | \tilde{\Psi}_{\text{field}} \rangle\quad (1.91)$$

The derivative $dP_e(t)/dt$ represents the probability to detect a photo-ionization process per time unit at time t , with an atom at \mathbf{r} . It is the single photon counting rate $w_1(\mathbf{r}, t)$:

$$w_1(\mathbf{r}, t) = \frac{dP_e(t)}{dt} = \frac{2\pi}{\hbar^2} |\kappa_0|^2 \langle \tilde{\Psi}_{\text{field}} | E^-(\mathbf{r}, t) E^+(\mathbf{r}, t) | \tilde{\Psi}_{\text{field}} \rangle.\quad (1.92)$$

which is proportional to the mean value in the field state of the Hermitian operator $E^-(\mathbf{r}, t)E^+(\mathbf{r}, t)$, product of the negative and positive frequency parts of the electric field (the positive frequency part is at right). If the field is defined by its density operator ρ_{field} , the counting rate is:

$$w_1(\mathbf{r}, t) = \frac{2\pi}{\hbar^2} |\kappa_0|^2 \text{Tr} [\rho_{\text{field}} E^-(\mathbf{r}, t)E^+(\mathbf{r}, t)] . \quad (1.93)$$

We similarly define the double counting rate describing the probability to detect a photo-ionization event at \mathbf{r} , in a unit time interval around t and a photo-ionization event at \mathbf{r}' , in a unit time interval around t' :

$$w_2(\mathbf{r}, t; \mathbf{r}', t') \propto \text{Tr} [\rho_{\text{field}} E^-(\mathbf{r}, t)E^-(\mathbf{r}', t')E^+(\mathbf{r}', t')E^+(\mathbf{r}, t)] . \quad (1.94)$$

The basic formulas (1.93) and (1.94) are essential to describe field measurements in a wide variety of quantum optics experiments.

2. Beam splitters and interferences in quantum optics

We analyze in this section interference and field amplitude measurement experiments in quantum optics. This leads us to consider multi-mode fields. An essential tool to couple two modes is the linear beam splitter. We present a simple model of this device and describe how a combination of two of them makes it possible to realize text book illustrations of quantum interferences involving one or two photons. We show also that a linear beam splitter is useful to realize a homodyne detection of the field quadratures. It also provides a model of the coupling of a field with its environment, leading to a simple description of decoherence phenomena. We then consider non-linear generalizations of the beam splitter, leading directly to the realization of multi-particle interferences involving Fock states. We analyze the special features of these interferences, their extreme sensitivity to decoherence and we finally describe an ion trap experiment simulating them.

2.1. Linear beam splitters

We consider now two propagating waves (*a*) and (*b*) coupled by a beam-splitter (partly reflecting, partly transmitting plate). The two waves propagate at right angle and the beam splitter lies at the beam intersection, at 45 degrees of both beams (Fig. 10). We assume that the modes are geometrically matched and have the same polarization (orthogonal to the incidence plane). The spatial structure of mode (*b*) reflected by the beam-splitter exactly coincides with the transmitted (*a*) mode. Classically, the two field mode amplitudes are mixed by the beam

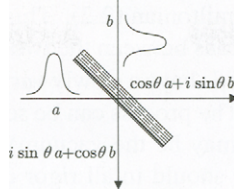


Fig. 10. Two freely propagating modes coupled by a semi-transparent beam splitter.

splitter. An impinging field in mode (a) of amplitude E_0 results in a transmitted amplitude $t_r E_0$ in mode (a) and a reflected amplitude $r_e E_0$ in mode (b), where t_r and r_e are the complex beam splitter transmission and reflexion amplitude coefficients. Fresnel reflexions laws furthermore entail that t_r/r_e is pure imaginary ($\pi/2$ phase shift between transmitted and reflected fields). We restrict ourselves to the ideal loss-less situation with $|t_r|^2 + |r_e|^2 = 1$. This makes it convenient to introduce a beam splitter mixing angle θ and to define $t_r = \cos \theta$ and $r_e = i \sin \theta$, with the i factor accounting for the Fresnel phase shift. Calling a and b the field operators of modes (a) and (b) (which commute together), it is natural to assume that the classical beam splitter action translates into a quantum transformation which affects the two modes according to the following unitary transformation:

$$U^\dagger(\theta)aU(\theta) = \cos \theta a + i \sin \theta b ; \quad U^\dagger(\theta)bU(\theta) = i \sin \theta a + \cos \theta b , \quad (2.1)$$

in which U can be viewed as the evolution operator $e^{-iHt/\hbar}$ associated to the Hamiltonian:

$$H = -\hbar g_b(ab^\dagger + a^\dagger b) , \quad (2.2)$$

acting on the field during time $t = \theta/g_b$. The connexion between Eqs.(2.1) and (2.2) can easily be made by using the well known Baker-Hausdorff relation [24]:

$$\begin{aligned} \exp(iG\theta)a \exp(-iG\theta) &= a + i\theta [G, a] + \frac{i^2\theta^2}{2!} [G, [G, a]] + \dots \\ &\quad + \frac{i^n\theta^n}{n!} [G, [G, \dots [G, a]]] + \dots , \end{aligned} \quad (2.3)$$

in which we define $G = -(ab^\dagger + a^\dagger b)$. The nested commutators in the right hand side of Eq.(2.3) are readily estimated ($[G, a] = b$; $[G, [G, a]] = a\dots$) so that all the odd-order terms in the development are proportional to b , while the even order terms are proportional to a . The coefficients of a and b coincide with the series expansion of the sine and cosine functions and we retrieve Eq.(2.1) The beam splitter thus appears as a linear device implementing between the two beams a

coupling described by the Hamiltonian (2.2). This coupling merely describes a symmetrical exchange of photons between the two modes.

In a real experiment, the fields have a slowly varying envelope and pass during a finite time τ over the plate. The process can be seen as a collision between two wave packets (one of which may be the vacuum), mixed by the beam-splitter. To describe this collision, we should in all rigor consider that each packet is a superposition of modes with wave vector \mathbf{k} (corresponding to field operators $a_{\mathbf{k}}$ distributed in frequency over an interval $c\Delta k = 1/\tau$). This point of view is mathematically cumbersome. An equivalent but much simpler model describes the fields as stationary plane waves whose coupling to the beam splitter is ‘switched on’ adiabatically during the time interval τ around 0. This amounts to considering a coupling of the form:

$$H = -\hbar g_{bs}(t)(ab^{\dagger} + a^{\dagger}b) \quad \text{with} \quad \int dt g_{bs}(t) = \theta , \quad (2.4)$$

where $g_{bs}(t)$ is a function of time of width τ whose precise shape does not matter. In order to describe the field evolution produced by the beam-splitter, we can adopt two equivalent view points: the Heisenberg picture considers that the field remains in the time-independent state $|\Psi_{\text{field}}\rangle$, while the operators evolve from their initial to their final form within time τ [transformation expressed by Eq.(2.1)]. The Schrödinger picture considers conversely that the operators are time-independent and that the system’s states evolve under the effect of U . We will adopt, depending upon the problems we have to solve, one or the other of these two equivalent perspectives.

2.2. Schrödinger picture: effect of the beam splitter on some field states

We start by describing the effect of the beam splitter on various initial field states, in the Schrödinger picture. We consider first situations where (a) is initially excited while (b) is in vacuum. The simplest case corresponds to a single photon impinging in (a). The initial state is then written as $|1, 0\rangle$ [in the following the first label in the kets refers to mode (a), the second to (b)]. With a sequence of obvious equalities, we get:

$$\begin{aligned} |1_a, 0_b\rangle \rightarrow |\Psi\rangle &= U(\theta)|1_a, 0_b\rangle = U(\theta)a^{\dagger}|0, 0\rangle = U(\theta)a^{\dagger}U^{\dagger}(\theta)|0, 0\rangle \\ &= (\cos\theta a^{\dagger} + i\sin\theta b^{\dagger})|0, 0\rangle = \cos\theta|1, 0\rangle + i\sin\theta|0, 1\rangle \end{aligned} \quad (2.5)$$

The photon is then in general coherently split between the two modes. The final energy distribution corresponds to the classical partition. Most importantly, the final state generally exhibits entanglement between the two modes. If now n

photons impinge in (a), a similar calculation yields:

$$\begin{aligned}
 |\alpha_a, 0_b\rangle \rightarrow |\Psi\rangle &= U(\theta) |\alpha_a, 0_b\rangle = U(\theta) \frac{(a^+)^n}{\sqrt{n!}} |0, 0\rangle \\
 &= \frac{1}{\sqrt{n!}} U(\theta) (a^+)^n U^\dagger(\theta) |0, 0\rangle \\
 &= \frac{1}{\sqrt{n!}} (\cos \theta a^+ + i \sin \theta b^+)^n |0, 0\rangle \\
 &= \sum_{p=0}^n \binom{n}{p}^{1/2} (\cos \theta)^{n-p} (i \sin \theta)^p |n-p, p\rangle , \quad (2.6)
 \end{aligned}$$

where $\binom{n}{p} = n!/[p!(n-p)!]$ is the binomial coefficient. The final quantum state is a coherent superposition of terms corresponding to all possible partitions of the n incoming photons between the two modes. This state is in general massively entangled. The binomial distribution is well known in statistical physics. The photon distribution between (a) and (b) is the same as the distribution of n molecules at thermal equilibrium between two compartments whose volumes are in the ratio $\tan \theta$. The average photon number in the two beams are $n_a = n \sin^2 \theta$ and $n_b = n \cos^2 \theta$. The fluctuations of these numbers correspond to the usual partition noise: $\Delta n_a = \Delta n_b = \sqrt{n} \sin \theta \cos \theta$. For a symmetrical beam splitter ($\theta = \pi/4$), half of the photon on average find their way in each beam with $\Delta n_a = \Delta n_b = \sqrt{n}/2$.

Suppose now that the initial field in (a) is in a coherent state $|\alpha\rangle$. The beam splitter then transforms it according to:

$$\begin{aligned}
 |\alpha_a, 0_b\rangle \rightarrow |\Psi\rangle &= U(\theta) |\alpha_a, 0_b\rangle = U(\theta) e^{\alpha a^\dagger - \alpha^* a} U^\dagger(\theta) |0, 0\rangle \\
 &= \exp(\alpha [\cos \theta a^\dagger + i \sin \theta b^\dagger] - \alpha^* [\cos \theta a - i \sin \theta b]) |0, 0\rangle \\
 &= |\alpha \cos \theta\rangle_a |i \alpha \sin \theta\rangle_b . \quad (2.7)
 \end{aligned}$$

This series of equalities is easily demonstrated with the help of Eq.(1.33) and (2.1) and making use of the operator identity $Uf(A)U^\dagger = f(UAU^\dagger)$, valid whenever f can be expanded in power series. The output state thus appears as a separable tensor product of coherent states in the two modes, with amplitudes having the same values as in the corresponding classical situation. The beam splitter coherent state dynamics, entirely classical even for very low average photon numbers, is thus very different from the one of Fock states. The non-entanglement of coherent states involved in linear coupling operations is a very basic feature of these states, with far reaching consequences as discussed below in the context of decoherence.

Note that, as far as the photon number distribution is concerned, a linear beam splitter acts as if it were dispatching the quanta independently in the two modes, according to the classical energy partition probability. As a result, the photon distributions are very similar for an initial Fock state or a coherent state. Note however that for a symmetrical partition, the photon number fluctuation is equal to $\sqrt{n/2}$ for an initial coherent state, i.e. $\sqrt{2}$ times larger than for an initial Fock state with the same number of photons. This is because the fluctuation of the photon number of a beam-split coherent state cumulates the initial Poisson noise of this state with the beam-splitter partition noise. Note also that this independent photon partition does not realize a separation of the Schrödinger cat type between the two modes, for which we expect the photons to be in a superposition of a state where they are all channeled in (a) with a state in which they are all channeled in (b). Such a situation corresponds to a bi-modal photon distribution in each mode, peaked at $n_a = 0, n_b = n$ and $n_a = n, n_b = 0$, very different from the partition realized by the beam splitter with its single peak at $n_a = n_b = n/2$. We will see below that the Schrödinger cat situation generally requires a different kind of non-linear beam splitting device.

A linear beam splitter can also be used to mix two excited modes. As a simple example, suppose that (a) and (b) initially contain a single photon. The output state is then:

$$\begin{aligned} |1_a, 1_b\rangle &\rightarrow |\Psi\rangle = U(\theta) |1_a, 1_b\rangle = U(\theta) a^\dagger b^\dagger U^\dagger(\theta) |0, 0\rangle \\ &= (\cos \theta a^\dagger + i \sin \theta b^\dagger)(i \sin \theta a^\dagger + \cos \theta b^\dagger) |0, 0\rangle \\ &= \frac{i \sin 2\theta}{\sqrt{2}} (|2, 0\rangle + |0, 2\rangle) + \cos 2\theta |1, 1\rangle , \end{aligned} \quad (2.8)$$

which is generally an entangled state. In the special case of a symmetrical beam-splitter, we get:

$$|1, 1\rangle \rightarrow \frac{1}{\sqrt{2}} (|2, 0\rangle + |0, 2\rangle) , \quad (2.9)$$

which is a superposition of two photons in (a) with two photons in (b). This looks like a kind of ‘Schrödinger kitten’ built on Fock states, but the situation cannot be generalized to larger photon numbers and the fact that non-linear beam splitting elements are required to prepare large Schrödinger cats remains true. The fact that the two photons are, in the symmetrical case, bunched in the same mode of the beam splitter can be seen as a consequence of the bosonic nature of photons. It is also (and not independently) a quantum interference effect. The probability amplitude for getting one photon in each mode cancels, because of the exact destructive interference between two indistinguishable quantum paths. In one of them, both photons are transmitted with a probability amplitude $t_r \times t_r =$

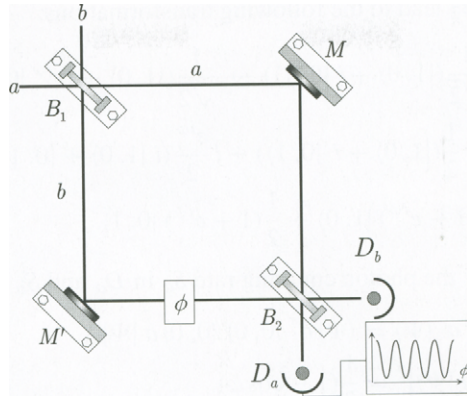


Fig. 11. Scheme of a Mach-Zehnder interferometer

1/2 whereas in the other they are both reflected with a probability amplitude $i r_e \times i r_e = -1/2$. This process and the resulting state are non-classical. The lack of photon coincidences in the two final output modes when the beam splitter is exactly balanced has been observed first by Ou and Mandel in a pioneering two-photon interference experiment [38].

This photon bunching effect occurs because the polarizations of the two photons are the same. Photons with disparate polarizations, on the other hand, behave differently. Photons with orthogonal polarization states, antisymmetric versus photon exchange for instance, emerge in an antisymmetric superposition of modes, with exactly one photon in each. This is required to preserve the overall state symmetry with respect to photon exchange. Photon entanglement and Bell state analysis of photon pairs are based on this feature, which we will not discuss further here.

2.3. The Mach-Zehnder interferometer

Beam splitters are key elements in optical interferometers. We describe here the Mach-Zehnder device for its simplicity and high symmetry. It is made of two identical 50 % beam splitters B_1 and B_2 with two folding mirrors M and M' (see Fig. 11). The photons cross the apparatus along two paths (a) and (b). A retarding plate shifts the phase in path (b) by a tunable angle φ . The field can be detected in both outputs with photon counters D_a and D_b . Consider first an experiment performed with a single photon impinging in mode (a), the initial state of the field being $|1, 0\rangle$. The successive operations on this state of B_1 , the

phase shifter and B_2 lead to the following transformations:

$$\begin{aligned} |1, 0\rangle &\rightarrow \frac{1}{\sqrt{2}}(|1, 0\rangle + i|0, 1\rangle) \rightarrow \frac{1}{\sqrt{2}}(|1, 0\rangle + ie^{i\varphi}|0, 1\rangle) \\ &\rightarrow \frac{1}{2}(|1, 0\rangle + i|0, 1\rangle) + i\frac{e^{i\varphi}}{2}(i|1, 0\rangle + |0, 1\rangle) \\ &= \frac{1}{2}(1 - e^{i\varphi})|1, 0\rangle + \frac{1}{2}(1 + e^{i\varphi})|0, 1\rangle. \end{aligned} \quad (2.10)$$

We then get simply the photon counting rate S_a in D_a and S_b in D_b as:

$$\begin{aligned} S_a &\propto \langle \Psi | a^\dagger a | \Psi \rangle = \langle \Psi | a^\dagger | 0, 0 \rangle \langle 0, 0 | a | \Psi \rangle \\ &= |\langle 00 | a | \Psi \rangle|^2 = \frac{1}{2}(1 - \cos \varphi) \\ S_b &\propto \frac{1}{2}(1 + \cos \varphi). \end{aligned} \quad (2.11)$$

Fringes with 100 % contrast are observed in both detectors, with a π -phase shift between the two. The interference occurs in the probability for detecting each photon crossing the apparatus, which is in agreement with the famous statement by Dirac that in this kind of interferometer at least, ‘photons interfere with themselves’. Note however that this statement is challenged by other quantum optics experiments, such as the Ou and Mandel one quoted above. We will come back to this point later. Even if the process described by Eq.(2.10) is intrinsically a single photon one, it has to be recorded by accumulating statistics over many photon events, repeating the same experiment for different values of the phase shift φ . Observation of such single photon interference signals have been made [39]. They are a vivid illustration of wave-particle complementarity.

Let us now consider the situation where the initial field is in an n photon Fock state. A similar analysis yields the field final state:

$$|\Psi\rangle = \frac{1}{\sqrt{n!}} \left[\frac{1}{2} \left(1 - e^{i\varphi} \right) a^\dagger + \frac{1}{2} \left(1 + e^{i\varphi} \right) b^\dagger \right]^n |0, 0\rangle, \quad (2.12)$$

which shows that we are in fact repeating n time the single photon experiment. The interferometer dispatches photons in both arms according to a binomial law with probability $p = (1 - \cos \varphi)/2$ in (a) and $q = 1 - p$ in (b). The counting rate is proportional to the mean number of photons, i.e. $n(1 - \cos \varphi)/2$ in (a) and $n(1 + \cos \varphi)/2$ in (b). The signal has the same shape as in the one photon case. To maximize the signal, it is convenient to detect the difference of the two output channels $S_b - S_a = n \cos \varphi$.

Let us also consider the case of an initial coherent state $|\alpha\rangle$ impinging in mode (a). We leave the reader to show that the final field state is then $|(\alpha/2)(1 -$

$e^{i\varphi}$), $(\alpha/2)(1 + e^{i\varphi})\rangle$, corresponding to an unentangled output in which the field in each arm is coherent, with an amplitude corresponding to the classical one. The average photon counting signal is the same as in the one or n -photon cases.

Interferometers are usually designed to measure with precision optical phase changes. It is thus relevant to discuss the fundamental limits set by quantum laws to the sensitivity η of the device. It is defined as the inverse of the smallest phase change $\delta\varphi_{min}$ which can be detected. It is equal to the slope of the fringes $d(S_b - S_a)/d\varphi = n \sin \varphi$, divided by the smallest observable variation of the signal $d(S_b - S_a)_{min} = \Delta(n_b - n_a)$. For a Fock state input, the fluctuation of the photon numbers in the output channels is simply given by the binomial partition law:

$$d(S_b - S_a)/d\varphi = n \sin \varphi ; \quad \eta = (\delta\varphi)_{min}^{-1} = \frac{d(S_b - S_a)/d\varphi}{\delta(S_b - S_a)_{min}} = \sqrt{n} . \quad (2.13)$$

The sensitivity of the interferometer is thus equal to the square root of the photon number crossing the device during the measurement time. In this case, the sensitivity is independent upon the phase setting. As the phase evolves, the fringe slope and the partition noise vary in the same way and their ratio remains constant. In particular, at dark fringe, there is no signal variation to first order, but there is no noise either.

For a coherent state input and an output detecting the difference of the (a) and (b) counting rates, a similar argument yields $\eta = \sqrt{n} \sin \varphi$. The sensitivity now depends on the phase setting and, for optimum sensitivity, one must set the interferometer at a phase corresponding to maximum fringe slope ($\varphi = \pi/2$). The sensitivity is then again equal to \sqrt{n} . This value is the so-called ‘standard quantum limit’ or ‘shot noise limit’. For a coherent state, this limit depends on the combined effects of the intrinsic photon noise of the initial field and the partition noise added by the interferometer. It is interesting to note that the same limit is obtained for a Fock state input, which has no intrinsic photon noise. We have considered here, for simplicity and symmetry, a signal based on the difference of the two output ports. In some devices, only one output detector is used. In this case, it is easy to show that a coherent state input yields a maximum sensitivity, again equal to \sqrt{n} , for a phase setting corresponding to a dark fringe. We should also note that these results can be substantially modified if mode (b), instead of being initially empty, contains a non-classical squeezed state of light [40]. The sensitivity can then be increased beyond the standard quantum limit discussed above. We will not describe it any further here. Another way to beat the standard quantum limit is to use multiparticle interferometers, as we will discuss later on.

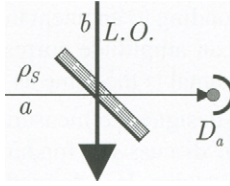


Fig. 12. Scheme of the homodyne detection of an unknown field ρ_s .

2.4. Homodyne detection of field quadratures

The experiments described so far are not sensitive to the phase of the field. Basically the same information is extracted by a Mach-Zehnder from a coherent field and from a Fock state, which has no defined phase. To get an information about the phase, one must resort to another kind of interference method which mixes the field, not with itself, but rather with another reference beam, called the local oscillator (L.O.). If this reference has the same frequency as the field to be measured, the method is referred to as ‘homodyne’ detection. The mixing is performed again with a beam-splitter according to the scheme shown in Fig.12 . We now use a highly transmitting plate ($T = t_r^2 = \cos^2 \theta \approx 1 - \theta^2$). The ‘signal’ field to be measured is described by its density operator ρ_s . The L.O. reference field, of same frequency, is a coherent state $|\beta\rangle = |\beta_0 e^{i\varphi}\rangle$. Only a small fraction of the intense L.O. signal is reflected into the output mode carrying the signal beam. The beating between the reflected L.O. beam and the transmitted signal is detected by measuring the photon counting rate w_a in the transmitted signal mode. For the sake of simplicity, we restrict ourselves to experiments in which only mode (a) is detected, the photons leaking into mode (b) being discarded. Taking into account Eqs.(1.93), (2.1) and (1.42), we obtain:

$$\begin{aligned} w_a &\propto \text{Tr} \left[\rho_s |\beta\rangle \langle \beta| (\cos \theta a^\dagger - i \sin \theta b^\dagger)(\cos \theta a + i \sin \theta b) \right] \\ &= \sin^2 \theta \langle \beta | b^\dagger b | \beta \rangle + \cos^2 \theta \text{Tr}(\rho_s a^\dagger a) \\ &\quad + i \sin \theta \cos \theta \text{Tr} \left[\rho_s |\beta\rangle \langle \beta| (a^\dagger b - ab^\dagger) \right]. \end{aligned} \quad (2.14)$$

The first term in the right hand side of this equation is a constant background representing the intensity of the reflected L.O. beam, equal to $(1 - T)\beta_0^2$. The second term corresponds to the intensity of the signal transmitted by the beam-splitter, equal to $T \langle a^\dagger a \rangle_s$, where the $\langle \rangle_s$ bracket denotes an average in the initial signal field state. The last ‘beating’ term, which is the dominant one if β_0 is large enough, contains the information about the signal field phase. It can be written

as:

$$\begin{aligned} w_{beat} &= -2\sqrt{T(1-T)}\beta_0 \frac{\langle a^\dagger e^{i\varphi} - a e^{-i\varphi} \rangle_s}{2i} \\ &= 2\sqrt{T(1-T)}\beta_0 \langle X_{\varphi+\pi/2} \rangle_s . \end{aligned} \quad (2.15)$$

We measure in this way the field quadrature which is $\pi/2$ out of phase with the L.O. By sweeping the phase of the local oscillator, we can thus measure the expectation value of any field quadrature.

In fact, the method has the potential to extract even more information. By measuring the fluctuations of the photo-detection signal, we can also obtain the probability distribution of any signal field quadrature. Repeating the measurement for a large set of quadrature phases, we get an information which can be exploited to reconstruct the field Wigner function, and hence its density operator. We have seen in section 1.4 that the probability density of a given quadrature is the integral of the W function along a line in phase space orthogonal to the direction of this quadrature. Measuring the quadrature fluctuations for all possible phases thus amounts to determining the integrals of W along all possible directions in the phase plane. A procedure known as the Radon transform can then be used to find out W from the knowledge of these integrals [41]. This Radon transform is employed in a different context in medical tomography. Here, the integrated optical density of an inhomogeneous medium irradiated by X rays is measured along different directions in a plane and the Radon inversion is used to reconstruct the density of the absorbing medium in this plane. In this way, pictures of the inner parts of the body are made. Quantum tomography is quite analogous to medical tomography. The field to be measured is mixed via a beam splitter with L.O. references of various phases and the fluctuations of the homodyne beat signal are detected. Then a Radon inversion procedure reconstructs W and hence the field density operator. The experiment has been performed for squeezed quadrature fields [42] and Fock states [43, 44]. It remains to be done for Schrödinger cat states. We will not describe in any more details quantum tomography and rather focus on some interesting properties of the quadrature fluctuations in a Schrödinger cat state.

We have seen that the quadrature of the field orthogonal to the cat state alignment presents a large interference term. The homodyne current reveals it as a modulation around its average, with an alternance of bright and dark ‘fringes’. In other words, a quantum interference signal is encoded in the fluctuations of the homodyne current, which itself results from a classical interference between the signal and the L.O. It is instructive to compute explicitly the fluctuations of this homodyne signal. It is indeed exceedingly fragile and, in a single detector scheme, very sensitive to the losses of the beam-splitter used for the homodyning

process. This device must let a small non-zero fraction of the signal leak into mode (*b*). This loss into the environment is responsible for a strong reduction of the quantum interference signal, signature of the coherence of the Schrödinger cat state. We thus get a glimpse at decoherence in a specific situation.

Let us assume that the signal field injected in mode (*a*) is prepared in an even phase-cat state $|\alpha\rangle + |-\alpha\rangle$ (α real). Since the quantum interference signal is encoded in the field quadrature $\pi/2$ out of phase with the cat components (see section 1), the L.O. state amplitude β must have the same phase as α and is also real. Adopting the Schrödinger picture, the evolution of the field in the homodyning apparatus writes:

$$\begin{aligned} |\Psi\rangle_0 &= \frac{1}{\sqrt{2}}(|\alpha\rangle + |-\alpha\rangle) |\beta\rangle \rightarrow \\ |\Psi\rangle_f &= \frac{1}{\sqrt{2}} [|\alpha \cos \theta + i\beta \sin \theta\rangle |i\alpha \sin \theta + \beta \cos \theta\rangle] \\ &\quad + \frac{1}{\sqrt{2}} [|- \alpha \cos \theta + i\beta \sin \theta\rangle |-i\alpha \sin \theta + \beta \cos \theta\rangle] \end{aligned} \quad (2.16)$$

the global final state $|\Psi_f\rangle$ is the sum of two terms, corresponding to the two components of the initial cat state. Each of these terms is the tensor product of two states, the first referring to the measured mode (*a*), the second to the undetected ‘environment’ mode (*b*). In order to analyze the fluctuations of the photo-current in mode (*a*), one must perform experiments with a large number of ‘cat’ realizations and accumulate data. The fluctuation in the number of photons detected by D_a reflects the fluctuations of the field quadrature of interest. We must thus compute the probability $P(n)$ to detect n photons in (*a*), without looking at (*b*). This is obtained by tracing over mode (*b*), obtaining the reduced density operator of the field in mode (*a*) and evaluating the probability to find n photons in this field. This standard procedure leads in a straightforward way to:

$$\begin{aligned} P_a(n) &= \frac{1}{2} \left(|\langle n | \alpha \cos \theta + i\beta \sin \theta \rangle|^2 + |\langle n | -\alpha \cos \theta + i\beta \sin \theta \rangle|^2 \right) + \\ &\quad + \text{Re} \left(\langle -\alpha \cos \theta + i\beta \sin \theta | n \rangle \langle n | \alpha \cos \theta + i\beta \sin \theta \rangle \times \right. \\ &\quad \left. \times \langle -i\alpha \sin \theta + \beta \cos \theta | i\alpha \sin \theta + \beta \cos \theta \rangle \right) \end{aligned} \quad (2.17)$$

The last term in this equation represents an n -dependent interference term in the photon number distribution. This term contains an n -independent factor [last line in Eq.(2.17)], equal to the overlap of the two final states of the field in the undetected mode (*b*). As soon as these states become distinguishable, i.e. quasi orthogonal, the interference term vanishes. This is a typical manifestation of complementarity. The fact that the environment contains an information about

the state of the field in the interferometer destroys the interference of the ‘cat’, i.e. its quantum coherence. The distance in phase space of the two field components in (b) , equal to $2\alpha \sin \theta$, is of the order of unity as soon as one photon on average has leaked into mode (b) . This is a general feature of decoherence: the mesoscopic superposition exhibits coherence as long as not a single quantum is lost in the environment. This condition is of course a drastic one, very difficult to fulfill when the mean number of quanta is large. We will encounter this condition again and again in the following.

The calculation of the photon number fluctuation in (a) is somewhat cumbersome, but straightforward. The interference amplitude term is easily determined from the general expression of coherent states scalar products [Eq. (1.43)]:

$$\begin{aligned} \langle -i\alpha \sin \theta + \beta \cos \theta | i\alpha \sin \theta + \beta \cos \theta \rangle = \\ \exp(-2\alpha^2 \sin^2 \theta) \exp(2i\alpha\beta \sin \theta \cos \theta) \end{aligned} \quad (2.18)$$

To complete the calculation, we assume that $\beta \sin \theta / \alpha \cos \theta \gg 1$ (large L.O. field), which implies that the average number of L.O. photons reflected in mode (a) is large. We can then replace the Poisson distribution of the L.O. photon number by a Gaussian approximation and we obtain:

$$\begin{aligned} |\langle n | \alpha \cos \theta + i\beta \sin \theta \rangle|^2 &= |\langle n | -\alpha \cos \theta + i\beta \sin \theta \rangle|^2 \\ &\approx |C_n(\beta \sin \theta)|^2 = e^{-\beta^2 \sin^2 \theta} \frac{(\beta \sin \theta)^{2n}}{n!} \\ &\propto \exp\left(-\frac{(n - \beta^2 \sin^2 \theta)^2}{2\beta^2 \sin^2 \theta}\right), \end{aligned} \quad (2.19)$$

$$\begin{aligned} \langle -\alpha \cos \theta + i\beta \sin \theta | n \rangle \langle n | \alpha \cos \theta + i\beta \sin \theta \rangle \\ \approx |C_n(\beta \sin \theta)|^2 \left(1 - \frac{i\alpha \cos \theta}{\beta \sin \theta}\right)^{2n} \\ \approx |C_n(\beta \sin \theta)|^2 \exp\left(-2in \frac{\alpha \cos \theta}{\beta \sin \theta}\right). \end{aligned} \quad (2.20)$$

Taking then Eqs.(2.17), (2.19) and (2.20) into account, we find:

$$\begin{aligned} P_a(n) &\propto \exp\left(-\frac{(n - \beta^2 \sin^2 \theta)^2}{2\beta^2 \sin^2 \theta}\right) \\ &\quad \left[1 + \cos 2\left(n \frac{\alpha \cos \theta}{\beta \sin \theta} - \alpha \beta \sin \theta \cos \theta\right) e^{-2\alpha^2 \sin^2 \theta}\right]. \end{aligned} \quad (2.21)$$

We finally remark that the fluctuating photon number n in mode (a) is directly related to the fluctuating quadrature of the field x by the following relation, deduced from Eq.(2.15):

$$n = \beta^2 \sin^2 \theta + 2\beta \sin \theta \cos \theta x = \beta^2(1 - T) + 2\beta\sqrt{T(1 - T)} x . \quad (2.22)$$

Substituting (2.22) into (2.21), we get the distribution of the quadrature signal as:

$$P(x) \propto e^{-2T} x^2 \left[1 + \cos(4\alpha T x) \exp\left[-2\alpha^2(1 - T)\right] \right] . \quad (2.23)$$

For $T = 1$, this expression is identical to Eq.(1.50). The fringe contrast vanishes however as soon as $\alpha\theta > 1$. This is a clear indication of the great fragility of the cat state coherence. It also shows that, when dealing with mesoscopic superpositions, we have to consider explicitly the actual way they are observed and the details of the experimental apparatus. In the version of the experiment we have described, the single detector homodyning scheme discards the information in mode (b) , which entails decoherence. This could in principle be avoided by detecting the photons in (b) too and by combining the detections in both arms (balanced homodyne detection). It remains however that any photon loss in the apparatus able to ‘give away’ the state of the field must be avoided, as we will show below in a more general way.

2.5. Beam splitters as couplers to environment: relaxation of a coherent state and of a Schrödinger cat

As we have recalled above, the linear beam splitter which couples two modes of the field via an equation of the form (2.1) is an useful model to study various fundamental effects in quantum optics. We have seen in particular that this linear device leaves coherent states immune to entanglement, preserving the classical character of these states. We show in this subsection that this immunity to entanglement survives if the coherent state is coupled not to one single mode, but to a continuum of modes initially in vacuum. This situation describes in quite general terms field damping, the mode continuum being a model for a reservoir. For example a field stored in a cavity made of mirrors facing each other is coupled to reservoir modes by the scattering of light on mirrors imperfections and this scattering process can be modeled as a linear coupling between the cavity and the reservoir modes quite similar to the coupling performed by an ensemble of beam-splitters. We will understand, with this simple model, that coherent states appear as the natural ‘pointer states’ in quantum optics. We will then consider the coupling to the same environment of a Schrödinger cat state and show that such superpositions evolve very quickly towards an incoherent mixture of their ‘pointer state’ components. This will generalize the results of section 2.4. where

we had considered not the complete Schrödinger cat density operator, but rather the evolution of one specific observable, namely one of the field quadrature fluctuations.

2.5.1. Relaxation of a coherent state

We first consider a field mode (annihilation operator a , frequency ω) coupled to a large set of other modes at frequencies ω_i described by their annihilation operators b_i . The environment modes span a wide frequency range. However the relaxation of (a) is mainly due to those modes with a frequency very close to ω (as required by energy conservation). For a qualitative approach, we thus assume a resonant coupling of (a) with each mode (b_i) through a linear hamiltonian describing a beam-splitter-like photon exchange:

$$H_i = -\hbar g_i (ab_i^\dagger + a^\dagger b_i), \quad (2.24)$$

where the g_i are coupling constants depending smoothly on i . The mode (a) contains initially a coherent state $|\alpha\rangle$. Assuming that the reservoir is at zero temperature, all modes (b_i) are initially in vacuum. The action of the coupling Hamiltonian $\sum_i H_i$ during a short time interval $\delta\tau$ (much shorter than the characteristic relaxation time, but much longer than the field period) is thus equivalent to the coupling of mode (a) to modes (b_i) by a set of beam-splitters having each an amplitude transmission $\cos\theta_i \approx 1 - (g_i\delta\tau)^2/2$ very close to 1. Since mode (a) is not appreciably depleted during time $\delta\tau$, we can sum up independently the actions of these beam splitters acting ‘in parallel’. Coupling to mode (b_i) alone transforms the initial state $|\alpha\rangle|0\rangle_i$ into $|\alpha \cos\theta_i\rangle|i\alpha \sin\theta_i\rangle_i$ [see Eq(2.7)]. Expanding the transmission and reflexion coefficients in powers of $g_i\delta\tau \ll 1$ and summing up all relevant modes, we get the global state of the field at time $\delta\tau$:

$$|\psi(\delta\tau)\rangle \approx \left| \alpha \left(1 - \sum_i \frac{g_i^2 \delta\tau^2}{2} \right) \right\rangle_a \prod_i |i\alpha g_i \delta\tau\rangle_i. \quad (2.25)$$

Mode (a) still contains a coherent state whose amplitude is slightly reduced, but which remains unentangled with the reservoir [the situation is much more complex, as discussed above, if (a) is initially in a Fock state]. The amplitude reduction corresponds to an energy transfer into the environment modes. In order to estimate the amplitude loss, we must count the number of environment modes participating in the process. During the short time interval $\delta\tau$, all modes in a frequency interval of the order of $1/\delta\tau$ around ω are appreciably coupled to (a) , as can be guessed from a simple energy-time uncertainty relation argument. The sum over i in Eq.(2.25) thus contains a number of terms of the order of $1/\delta\tau$.

Each of these terms being proportional to $\delta\tau^2$, the total amplitude decrease is, during this short time interval, quasi-linear in time. We can write:

$$|\psi(\delta\tau)\rangle \approx \left| \alpha \left(1 - \frac{\kappa}{2} \delta\tau\right) \right\rangle_a \prod_i |i\alpha g_i \delta\tau\rangle_i , \quad (2.26)$$

where κ is a constant depending upon the mode density in the environment and the distribution of the coupling constants g_i . Note that the argument developed here is quite analogous to the one used to derive qualitatively the Fermi Golden Rule in standard perturbation theory in the presence of a continuum of final states.

For describing the system's evolution during the next time interval $\delta\tau$, the initial state of the environment is a priori slightly different. Since the leaking amplitude is however diluted among a large number of modes, the process where some amplitude would leak back from the environment into (a) is very unlikely. It is thus safe, for the computation of the (a) mode evolution to assume that all modes (b_i) remain practically empty all the time (so called ‘Born approximation’ in relaxation theory). We can thus consider independently the amplitude reductions resulting from successive time intervals. At an arbitrary time t , the state of (a) is thus still coherent, with the amplitude:

$$\alpha(t) \approx \alpha \left(1 - \frac{\kappa\delta\tau}{2}\right)^{t/\delta\tau} \approx \alpha e^{-\kappa t/2} . \quad (2.27)$$

At any time, the mode (a) still contains a coherent state, unentangled with the mode reservoir. The coherent states, impervious to entanglement when they are coupled to a single beam splitter, keep this remarkable property when a large set of beam-splitters couples them to a big environment. They keep their form of coherent state throughout the evolution, merely loosing their amplitude as their energy leaks into the reservoir. They are the ‘pointer states’ of the field decoherence process.

The amplitude of the field is exponentially damped with the rate $\kappa/2$ and the field energy decays with the time constant $T_{cav} = 1/\kappa$ which can be identified with the experimental cavity damping time. In a pictorial representation, the disk representing the coherent state follows a logarithmic spiral in phase space, reaching the origin after an infinite time.

Note that the environment modes also contain at any time coherent states resulting from the accumulation of tiny coherent amplitudes along the successive time intervals. The global mode-environment state can be written as:

$$|\alpha e^{-\kappa t/2}\rangle \prod_i |\beta_i\rangle_i , \quad (2.28)$$

where the partial amplitudes β_i are such that:

$$\sum_i |\beta_i|^2 = \bar{n}(1 - e^{-t/T_{cav}}), \quad (2.29)$$

a relation resulting simply from the total energy conservation. Note that a more complete derivation of the relaxation of a coherent state can be found in [24, 26].

2.5.2. Relaxation of a Schrödinger cat state

Field states which are not coherent can always be considered as superpositions of coherent states [we can use the closure relationship (1.44) to expand them]. They generally get entangled to the environment. As a result, the field evolves from a pure state into a statistical mixture whose density matrix is obtained by tracing over the unobserved environment modes. In the process, quantum coherences are washed out. This is the decoherence phenomenon, which we have already glimpsed at by looking at a quadrature fluctuation of a Schrödinger cat state in section 2.4. We will describe now completely the decoherence of a Schrödinger cat state, by following the full evolution of its field density operator. The results obtained in subsection 2.5.1 about the relaxation of a coherent state will be very useful for this computation. We assume that we start at time $t = 0$ with a field in mode (a) , prepared in the superposition $|\Psi_{cat}\rangle = [|\alpha e^{i\phi}\rangle + |\alpha e^{-i\phi}\rangle]/\sqrt{2}$. Following the same reasoning as above, we can write after a short time $\delta\tau$ the combined state of the (a) mode and the environment as:

$$|\Psi(\delta\tau)\rangle_{(a)+(E)} = \frac{1}{\sqrt{2}} \left[\left| \alpha e^{i\phi} \left(1 - \frac{\kappa\delta\tau}{2} \right) \right\rangle \prod_i |ig_i \alpha e^{i\phi} \delta\tau\rangle_i + \left| \alpha e^{-i\phi} \left(1 - \frac{\kappa\delta\tau}{2} \right) \right\rangle \prod_i |ig_i \alpha e^{-i\phi} \delta\tau\rangle_i \right]. \quad (2.30)$$

The two products of environment states appearing in this equation will be called $|\mathcal{E}_{\pm\phi}\rangle$. These two states are correlated to the two components of the cat state in mode (a) . As soon as they are orthogonal, the field in mode (a) is maximally entangled with the environment and decoherence has occurred. It is thus important to compute the overlap of the environment states $\langle \mathcal{E}_{-\phi} | \mathcal{E}_{+\phi} \rangle$. It appears as a product over i of partial overlap integrals given by:

$$\langle ig_i \alpha e^{i\phi} \delta\tau | ig_i \alpha e^{-i\phi} \delta\tau \rangle = \exp(-2\alpha^2 g_i^2 \delta\tau^2 \sin^2 \phi) e^{-i\alpha^2 g_i^2 \delta\tau^2 \sin 2\phi}, \quad (2.31)$$

and the global state overlap in the environment thus writes:

$$\langle \mathcal{E}_{+\phi} | \mathcal{E}_{-\phi} \rangle = \exp \left[-2\alpha^2 \sin^2 \phi \left(\sum_i g_i^2 \right) \delta\tau^2 \right] e^{-i\alpha^2 \delta\tau^2 \sin 2\phi \sum_i g_i^2}$$

$$= \exp(-2\alpha^2 \sin^2 \phi \kappa \delta\tau) e^{-i\alpha^2 \sin 2\phi \kappa \delta\tau}. \quad (2.32)$$

Decoherence is completed when this global overlap vanishes. This appears clearly by computing the mode (*a*) density matrix at time $\delta\tau$, obtained by tracing over the environment:

$$\begin{aligned} \rho_{cat}(\delta\tau) &= \text{Tr}_E [|\Psi(\delta\tau)\rangle_{(a)+(E)(a)+(E)}\langle\Psi(\delta\tau)|] \\ &= \frac{1}{2}|\alpha(\delta\tau)e^{i\phi}\rangle\langle\alpha(\delta\tau)e^{i\phi}| + \frac{1}{2}|\alpha(\delta\tau)e^{-i\phi}\rangle\langle\alpha(\delta\tau)e^{-i\phi}| + \\ &\quad \frac{1}{2}\langle\mathcal{E}_{+\phi}|\mathcal{E}_{-\phi}\rangle|\alpha(\delta\tau)e^{i\phi}\rangle\langle\alpha(\delta\tau)e^{-i\phi}| + \text{h.c..} \end{aligned} \quad (2.33)$$

The coherence of the field state, given by the off diagonal contributions in the above expression, is indeed proportional to the overlap integral $\langle\mathcal{E}_{-\phi}|\mathcal{E}_{+\phi}\rangle$ and vanishes with it. This is again a manifestation of complementarity, the cat state loosing its coherence as soon as an information about the phase of the field unambiguously leaks in the environment. According to Eq.(2.32), the cat coherence disappears in a characteristic time T_D given by:

$$T_D = \frac{T_{cav}}{2\alpha^2 \sin^2 \phi} = \frac{T_{cav}}{2\bar{n} \sin^2 \phi}. \quad (2.34)$$

The denominator in this expression is directly related to the square of the ‘distance’ in phase space of the two cat components $D^2 = 4\bar{n} \sin^2 \phi$ so that we can rewrite Eq.(2.34) as:

$$T_D = 2 \frac{T_{cav}}{D^2}. \quad (2.35)$$

When there are many photons in the field, the cat state decoherence time, inversely proportional to the square of the distance between its components, is much shorter than the damping time of the field energy T_{cav} . We find again, in a quantitative way, the results obtained by the simple models considered above. Decoherence is due to leakage of information (here about the field’s phase) in environment. There is a small amount of information in each mode (i), but there are many of them and decoherence is in general very fast. The cat state evolution is especially simple when the average number of photons is large, because decoherence occurs in a very short time during which the decay of the coherent component amplitudes is negligible. Once decoherence has occurred, the subsequent evolution of the system under the effect of relaxation is trivial. The density operator has become an incoherent sum of two coherent state components relaxing independently towards vacuum with the time constant T_{cav} . The dynamics of field relaxation becomes analytically more complicated when the initial average photon number is of the order of unity, because the evolution cannot be

separated into an initial decoherence stage followed by a subsequent relaxation. The general model introduced in this subsection can however be used to obtain explicit expressions of the field density matrix evolution over an arbitrary long time [45, 46]. We will not discuss this problem any further here.

2.6. Non-linear beam splitters

We have noticed in section 2.2 that linear beam splitters channel photons one by one in their two output modes and are thus unable to produce large mesoscopic superpositions of photons. We consider now a non-linear variant of the beam splitter which can, at least in theory, realize a multiparticle channeling, sending together all the photons in one arm or the other. We first consider a simple theoretical model. We then show how this model can be implemented in a real experiment.

2.6.1. A simple model of non-linear beam splitter

We consider now a slab of non-linear material whose action on a two-mode field is described by the following non-linear coupling:

$$H_n = -\hbar g_{nl} \left[a \left(b^\dagger \right)^n + a^\dagger (b)^n \right]. \quad (2.36)$$

This Hamiltonian realizes the reversible conversion of one photon of mode (a) into n photons of mode (b) , according to the simple relations:

$$\begin{aligned} \left[a \left(b^\dagger \right)^n + a^\dagger (b)^n \right] |1_a, 0_b\rangle &= \sqrt{n!} |0_a, n_b\rangle \\ \left[a \left(b^\dagger \right)^n + a^\dagger (b)^n \right] |0_a, n_b\rangle &= \sqrt{n!} |1_a, 0_b\rangle \end{aligned} \quad (2.37)$$

To conserve energy, the process must down-convert the photons, producing in mode (b) quanta with an energy n time smaller than in mode (a) . As in section 2.1, we assume that the evolution of a field crossing this device is unitary, with an adiabatic switching on and off of the coupling g_{nl} describing in a simple way the passage of a light pulse on the plate. Making again use of the Baker-Hausdorff formula, we can easily show that the $|1, 0\rangle$ and $|0, n\rangle$ states [where the first and second label refer respectively to the photon numbers in modes (a) and (b)] are related by a unitary transformation, generalizing to the non-linear case the usual beam splitter equations:

$$\begin{aligned} \exp[i g_{nl} t (a \left(b^\dagger \right)^n + a^\dagger (b)^n)] |1, 0\rangle &= \cos \theta |1, 0\rangle + i \sin \theta |0, n\rangle \\ \exp[i g_{nl} t (a \left(b^\dagger \right)^n + a^\dagger (b)^n)] |0, n\rangle &= i \sin \theta |1, 0\rangle + \cos \theta |0, n\rangle \end{aligned} \quad (2.38)$$

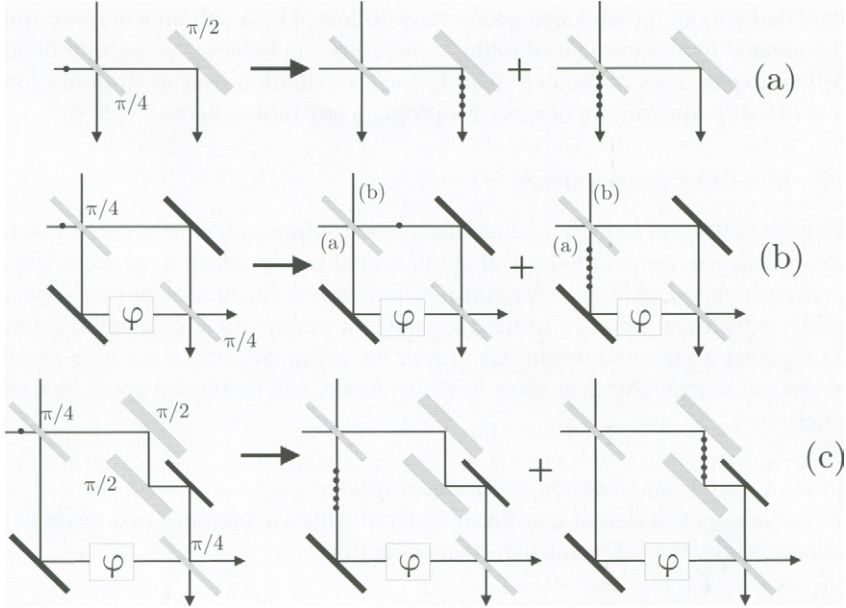


Fig. 13. Non-linear beam splitters. (a) a $(\pi/4)$ and a $(\pi/2)$ non linear beam splitter prepare a $|0, n\rangle + |n, 0\rangle$ mesoscopic superposition. (b) a Mach-Zehnder apparatus with two $\pi/4$ non linear beam splitters realizes an interference between a one-photon and an n -photon arm. (c) a variant with two additional $\pi/2$ non-linear beam splitters realizes an interference between two paths involving each n photons

The coupling angle is now defined as $\theta = g_n t / \sqrt{n!}$. Note that these equations are valid only if we restrict ourselves to initial states of the form $|1, 0\rangle$. For $\theta = \pi/4$ the plate prepares with equal weights a superposition of one photon in (a) and n photons in (b) according to:

$$|1, 0\rangle \rightarrow \frac{1}{\sqrt{2}} (|1, 0\rangle + i|0, n\rangle) . \quad (2.39)$$

whereas a plate with $\theta = \pi/2$ converts with 100% efficiency one (a) photon into n photons in (b):

$$|1, 0\rangle \rightarrow i|0, n\rangle . \quad (2.40)$$

With such devices, it is possible, at least in principle, to prepare mesoscopic superpositions of field states involving n photons all channeled in one mode or the other. Fig. 13(a) shows a simple realization using a $\theta = \pi/4$ non linear beam splitter followed by a $\theta = \pi/2$ one. The final state is in this case of the

form $|0, n\rangle + |n, 0\rangle$. It corresponds to a partition of the photons between the two modes very different from the one given by a linear beam splitter, which realizes a near equipartition as discussed in section 2.1. Instead of superposing field states belonging to the same mode, as in the phase cats described above, we are here superposing states distributing photons between two modes. The field state generated by this combination of non linear beam splitters has clearly a Schrödinger cat-like character. This cat state can be called ‘non-local’, since it exhibits an entanglement between two modes propagating in different regions of space. Each of the components can be considered as mesoscopic when $n \gg 1$, and the two components are orthogonal to each other, corresponding to two classically distinguishable states. We will see in section 3 that similar ‘breeds’ of non-local cat states can be generated in CQED by exploiting another kind of non-linear matter-field interaction.

Combining non-linear beam splitters, we can also design new kinds of multiparticle Mach-Zehnder interferometers in which many particles can follow together two different paths. These devices are intrinsically much more sensitive to phase shifts than single photon interferometers and can potentially be useful for applications. They are also, as we will see, much more sensitive to decoherence than single particle devices. We have sketched in Fig. 13(b) the principle of such an interferometer (for another scheme see [47]). As in the usual Mach-Zehnder, two $\theta = \pi/4$ non linear plates are separating and recombining the two modes, and mirrors are used to fold them. The final detection is made either in mode (*a*) (single photon channel) or in mode (*b*) (*n*-down converted photons channel). A phase shifter producing a phase shift φ per photon is introduced in the *n*-photon channel between the two beam splitters. With this device, an interference is produced between two paths, one corresponding to a single photon, the other to *n*-photons.

A variant can be easily designed in which two $\theta = \pi/2$ plates are introduced in the (*a*) mode between the two $\theta = \pi/4$ plates in order to reversibly produce and annihilate a *n*-photon state in this mode. In this way, the apparatus is a genuine *n*-particle interferometer in which *n* particles are simultaneously all present in one arm and in the other [see Fig. 13(c)]. The addition of the two $\theta = \pi/2$ plates is however not essential, since it does not change the principle of the interferometer operation. We will disregard it in the following and analyze only the system described by Fig. 13(b). The important point is that we have no way of knowing whether the *n*-photon exiting in mode (*b*) have been produced in the first non-linear beam splitter or in the second one. This ambiguity leads to an *n*-particle interference. A simple analysis similar to the one carried above in the linear Mach-Zehnder case shows that the final state of the field now writes:

$$|\Psi_f\rangle = \frac{1}{2}(1 - e^{in\varphi})|1, 0\rangle + \frac{i}{2}(1 + e^{in\varphi})|0, n\rangle , \quad (2.41)$$

and the mean photon number detected in (a) and in (b) writes:

$$S_a = \frac{1 - \cos n\varphi}{2} ; \quad S_b = n \frac{1 + \cos n\varphi}{2} . \quad (2.42)$$

Both signals exhibit now an interference pattern with a 100% fringe contrast, but with an interfrange separation n -time smaller than in the corresponding linear device. It is important to note that for such a multiparticle interferometer, Dirac's statement about 'each photon interfering with itself' does not apply. Clearly, the fringes result here from a quantum interference process involving globally the n particles which can follow two paths associated to orthogonal states. This kind of interference was unknown in Dirac's time and only linear processes were considered. Even then, though, Dirac's statement was in trouble. As we have seen above in section 2.2, a linear beam splitter on which single photon impinge in the two input ports can give rise to interference phenomena which cannot be explained in term of single photon effects [38].

The multiphoton interferometer yielding narrower fringes, it is natural to wonder whether it has a larger sensitivity to phase changes than its linear counterpart. To find it out, we have to compute the derivative of the fringe signal with respect to φ and its fluctuation. We restrict our calculation to mode (b) [the (a) output yielding the same result]. The photon number fluctuation is given by:

$$\begin{aligned} \Delta S_b &= \left(\langle \Psi_f | (b^\dagger b)^2 | \Psi_f \rangle - \langle \Psi_f | b^\dagger b | \Psi_f \rangle^2 \right)^{1/2} \\ &= \left(\frac{n^2}{2} (1 + \cos n\varphi) - \frac{n^2}{4} (1 + \cos n\varphi)^2 \right)^{1/2} = \frac{n}{2} \sin n\varphi . \end{aligned} \quad (2.43)$$

It is \sqrt{n} time larger than for a linear device with the same number of photons. The slope of the signal, proportional to n^2 is however n time larger. As a result, the sensitivity η is \sqrt{n} time larger than for an usual interferometer, becoming n instead of \sqrt{n} . The exact computation:

$$\eta = (\delta\varphi_{\min})^{-1} = \frac{(\delta S_b / \delta\varphi)}{\Delta S_b} = \frac{(n^2/2) \sin n\varphi}{(n/2) \sin n\varphi} = n , \quad (2.44)$$

yields, as for the linear device with a Fock state input, a sensitivity independent upon the phase setting.

The increased sensitivity of multiparticle interferometers makes them very attractive for high resolution measurements in spectroscopy or metrology. This advantage has however to be balanced with the difficulty in designing them and with the fact that these devices are intrinsically much more sensitive to decoherence. This point is illustrated by the simple decoherence model sketched in Fig. 14. A loss mechanism is introduced in mode (b) by inserting on the beam path a

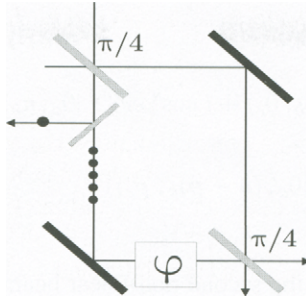


Fig. 14. Decoherence in a non-linear interferometer. Losses are modeled by a high transmission linear beam-splitter inserted in the n photon arm of the interferometer.

linear beam splitter with a small reflection coefficient ϵ . This couples the mode containing n photons with an initially empty environment mode (e) (whose annihilation operator will be called c_e). The probability to loose one of the n photons in this environment is $\sim n\epsilon^2$. We will show that as soon as this probability becomes of the order of 1, the interferometer fringe contrast collapses. In other words, as already noticed for a Schrödinger cat coupled to a reservoir, the coherence of the n -photon state superposition is lost as soon as one particle, potentially able to give an information about the path followed by the system, is leaking in the environment.

Let us follow, in the Schrödinger point of view, the state of the field as it progresses across the interferometer. We now have to keep track of the three (a), (b) and (e) modes. The three successive labels in each ket refer to the photon numbers in these modes. The first non-linear beam splitter corresponds to the transformation:

$$|1_a, 0_b; 0_e\rangle \rightarrow \left(\frac{1}{\sqrt{2}}\right) (|1_a, 0_b; 0_e\rangle + i |0_a, n_b; 0_e\rangle). \quad (2.45)$$

The coupling to the environment then changes the global field state into:

$$\begin{aligned} &\rightarrow \left(\frac{1}{\sqrt{2}}\right) (|1_a, 0_b; 0_e\rangle + i \cos^n \epsilon |0_a, n_b; 0_e\rangle + \\ &+ \sum_{p=1}^n c_p |0_a, (n-p)_b; p_e\rangle), \end{aligned} \quad (2.46)$$

where the c_p are coefficients given by the binomial law which we do not need to write explicitly. We then take into account the effect of the phase shifter in

mode (b):

$$\rightarrow \left(\frac{1}{\sqrt{2}} \right) (|1_a, 0_b; 0_e\rangle + i \cos^n \varepsilon e^{in\varphi} |0_a, n_b; 0_e\rangle + \sum_{p=1}^n c_p e^{i(n-p)\varphi} |0_a, (n-p)_b; p_e\rangle) , \quad (2.47)$$

and, finally, the action of the second non-linear beam splitter mixing again the (a) and (b) modes:

$$\rightarrow \left| \Psi_f^{(S+E)} \right\rangle = \left(\frac{1}{2} \right) [(|1_a, 0_b; 0_e\rangle + i |0_a, n_b; 0_e\rangle) + i \cos^n \varepsilon e^{in\varphi} (i |1_a, 0_b; 0_e\rangle + |0_a, n_b; 0_e\rangle)] + \left(\frac{1}{\sqrt{2}} \right) \sum_{p=1}^n c_p e^{i(n-p)\varphi} |0_a, (n-p)_b; p_e\rangle . \quad (2.48)$$

To obtain this final expression, which is an exact one within the assumptions of our model, we have to remark that the non-linear process coupling the (a) and (b) modes has no action on a field state in which the (b) mode contains less than n photons. The expression obtained for the field can be used to compute the photon counting rate in mode (b) and we get:

$$\begin{aligned} S_b &= \left\langle \Psi_f^{(S+E)} \right| b^\dagger b \left| \Psi_f^{(S+E)} \right\rangle_f \\ &= \frac{n}{4} \left| 1 + \cos^n \varepsilon e^{in\varphi} \right|^2 + \frac{1}{2} \sum_{p=1}^n |c_p|^2 (n-p) \\ &= \frac{n}{4} [1 + \cos^{2n} \varepsilon + 2 \cos^n \varepsilon \cos(n\varphi)] + \frac{n}{2} (\cos^2 \varepsilon - \cos^{2n} \varepsilon) . \end{aligned} \quad (2.49)$$

The sum over p in the second line of Eq.(2.49) is easily performed by using a sum rules satisfied by the c_p binomial coefficients. We leave the reader figure out how one goes from the second to the third line in this equation. The φ dependent term in the final formula given by Eq.(2.49) contains the interference signal. Its amplitude is proportional to $\cos^n \varepsilon$ which, for small ε is equivalent to $\exp(-n\varepsilon^2/2)$. The fringe contrast thus decreases exponentially with the size n of the multiparticle system and becomes negligibly small when $n\varepsilon^2 > 1$, i.e. when more than one photon on average has been lost in the environment.

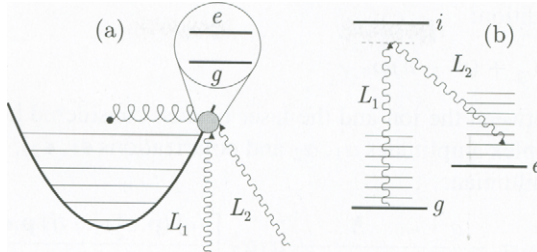


Fig. 15. Principle of an ion trap non-linear beam splitter experiment. (a) Ion in an harmonic potential, showing the quantized motional levels and the ion's internal structure. Lasers L_1 and L_2 induce Raman transitions between the internal and vibration states. (b) Energy levels diagram.

2.6.2. Simulation of multiparticle interferometry in an ion trap experiment

Realizing non-linear beam splitters of the kind just described would be very difficult. It would require in particular a medium exhibiting strong non-linearity induced by a single photon, a situation which is encountered so far only in CQED, albeit in a quite different context. We will come back to CQED experiments in section 3. We conclude this section by describing an experiment in which the multiphoton interferometry is simulated in a system where photons are replaced by phonons [48]. The physics of a non-linear Mach-Zehnder apparatus can indeed be mimicked with a single ion in a trap [49], whose evolution is described by equations quite similar to the one we have encountered above in section 2.6.1. The ion is excited by two laser beams inducing a Raman transition between two of its internal energy levels. At the same time, the momentum exchange between the laser beams and the ion results in an excitation of vibration quanta of the ion oscillation in the trap. The coupling of the ion with the laser realizes the dynamics of a non-linear beam splitter of the kind described above, in which the excitation of a single photon in mode (a) is replaced by the internal excitation of the ion and the n photons in mode (b) become n phonons of the ion vibration.

The system we are considering is sketched in Fig. 15(a), with its energy levels shown in Fig. 15(b). We call e and g the two relevant energy levels of the ion (two hyperfine ground states separated by the energy $\hbar\omega_{eg}$), n the vibration quanta of its external motion in a trap potential, which we assimilate to a one-dimension harmonic oscillator vibrating along Ox (angular frequency ω_p). Two laser beams (frequencies ω_1 and ω_2 , wave vectors projections along Ox : k_1 and k_2) induce a Raman process involving a virtual transition to an excited level i of the ion. The process is tuned to be resonant with a transition which simultaneously changes the internal state of the ion and its vibrational excitation, the laser frequencies

obeying the condition:

$$\omega_1 - \omega_2 = \omega_{eg} + (n' - n)\omega_p . \quad (2.50)$$

The coupling between the ion and the laser beams, considered here as classical fields (with complex amplitudes α_1, α_2 and polarizations ϵ_1, ϵ_2), is described by an effective hamiltonian:

$$H_{\text{Raman}}(t) = -\frac{q^2}{m^2} \frac{\hbar}{2\varepsilon_0 V \sqrt{\omega_1 \omega_2}} \alpha_1 \alpha_2^* \left[\frac{\langle e | (\mathbf{p} \cdot \epsilon_2^*) | i \rangle \langle i | (\mathbf{p} \cdot \epsilon_1) | g \rangle}{\hbar(\omega_{ig} - \omega_1)} \right] \times \\ \times |e\rangle \langle g| e^{-i(\omega_1 - \omega_2)t} e^{i(k_1 - k_2)x} + h.c. , \quad (2.51)$$

where ω_{ig} is the frequency of the transition between levels i and g . The diadic operators $|e\rangle \langle g|$ ($|g\rangle \langle e|$) in this equation are atomic excitation (deexcitation) operators describing jumps of the ion from e to g or back, quite analogous to the a and a^\dagger operators describing the jumps of the (a) mode of the field from the 0 to 1 photon state and back in the non-linear-beam splitter model. The $\exp i(k_1 - k_2)x$ term in Eq.(2.51) describes the phase dependence of the fields seen by the ion at position x . This position is an operator, superposition of the b and b^\dagger ion vibration quanta annihilation and creation operators. Expanding the exponentials in powers introduces operators of the form b^n and $b^{\dagger n}$, quite similar to the expressions appearing in Eq.(2.36). More precisely, we start by writing the exponential in Eq.(2.51) as:

$$e^{i(k_1 - k_2)x} = \exp i \sqrt{\frac{\hbar}{2M\omega_p}} \Delta k (b + b^\dagger) = \exp[i\eta_L(b + b^\dagger)] , \quad (2.52)$$

where $\Delta k = k_1 - k_2$, M is the mass of the ion and where we have introduced the dimensionless Lamb-Dicke parameter:

$$\eta_L = \left(\frac{\hbar \Delta k^2}{2M\omega_p} \right)^{1/2} = \left(\frac{E_{\text{recoil}}}{\hbar\omega_p} \right)^{1/2} \quad (2.53)$$

This quantity appears naturally when discussing the momentum exchange between an atom and light, especially in ion trap experiments (see [49] and the lecture notes by R. Blatt and D. Wineland in this volume). It can be defined as the square root of the ratio of the Raman-induced ion recoil energy by the vibration quantum. We will assume here that the Lamb-Dicke parameter is very small compared to unity, which allows us to expand in series the right hand side of Eq.(2.52) and retain the lowest non-vanishing term. We thus get:

$$H_{\text{Raman}}(t) = \frac{\hbar\Omega_R}{2} e^{-\eta_L^2/2} e^{-i(\omega_1 - \omega_2)t} |e\rangle \langle g| \sum_{p,q} \frac{(i\eta_L)^{p+q} (b^\dagger)^p b^q}{p!q!}$$

$$+h.c.. \quad (2.54)$$

In order to simplify this expression we have included the laser amplitudes, atom laser detunings and atomic matrix elements appearing explicitly in Eq.(2.52) into a single parameter Ω_R which we will call the Raman Rabi frequency. When the resonance condition (2.50) is fulfilled for an integer value $\Delta n = n' - n$, the leading contributions in H_{Raman} are such that $p - q = \Delta n$. We can thus have either $p = \Delta n, q = 0$ or $p = \Delta n + 1, q = 1$ etc. The first term is dominant (lowest order in η_L). Thus, for this resonance and in interaction picture:

$$\tilde{H}_{\text{Raman}} \approx \frac{\hbar\Omega_R}{2} (i\eta_L)^{\Delta n} |e\rangle\langle g| (b^\dagger)^{\Delta n} + h.c.. \quad (2.55)$$

This hamiltonian looks like (2.36) in which one replaces the annihilation operator of one photon in mode (a) by the operator changing $|g\rangle$ into $|e\rangle$. These states thus play respectively the roles of the states $|1\rangle_a$ and $|0\rangle_a$ in the multi-particle Mach-Zehnder model [the analogy between a and a^\dagger on one hand and the atomic operators $|e\rangle\langle g|$ and $|g\rangle\langle e|$ on the other hand holds only if there is no more than one photon in mode (a)]. The phonon operators b and b^\dagger play on the other hand the role of the photon operators in mode (b). In other words, the ion undergoing the Raman process ‘emulates’ the n -photon interferometer. By applying Raman pulses of convenient durations, one can simulate the successive non-linear beam splitter operations.

This experiment has been realized by Liebfried *et al.*, using a Be ion [48]. We summarize here its main steps. First, the ion is prepared in level g and in its vibration ground state (in a state equivalent to $|1_a, 0_b\rangle$). One then applies a Raman pulse simulating an n -photon $\pi/4$ non-linear beam splitter. This is achieved by choosing the laser resonance condition to realize the situations $\Delta n = 1, 2$ or 3 and by adjusting the pulse duration. An ion state equivalent to $(|1, 0\rangle + i|0, n\rangle)/\sqrt{2}$ is thus prepared. The n -phonon state (equivalent to $|0, n\rangle$) is then phase-shifted by changing by $\delta\omega_p$ the ion vibration frequency during a time t . This is performed by applying a bias electric field to the trap electrodes. A phase shift $\varphi = \delta\omega_p t$ per phonon is achieved in this way.

Finally, a second Raman pulse simulating a second $\pi/4$ n -photon non-linear beam splitter is applied and the ion in state g is detected by recording its fluorescence. A detection laser is switched on, bringing the ion from g into an excited state j from which a photon is emitted in transition back to g . This photon is detected. The cycle of excitation-detection is repeated a large number of times on the closed $g \rightarrow j$ transition, resulting in a large number of photons being collected when the ion is in level g only. This detection process is selective (e is not seen). It simulates the detection in mode (a) of the n -photon Mach-Zehnder. The experiment is repeated as φ is varied and fringes versus φ are obtained. Fig.

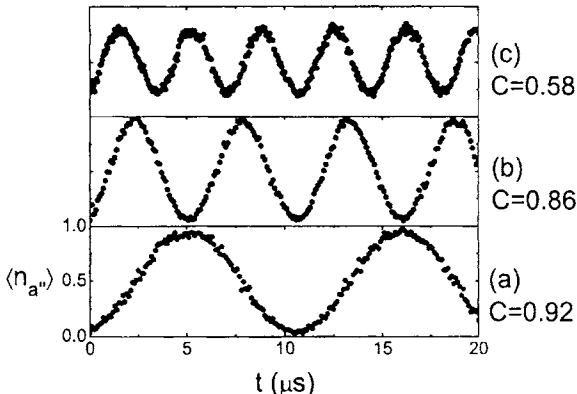


Fig. 16. Trapped ion implementation of a non-linear interferometer. Fringes obtained when varying the interferometer phase φ for $n = 1, 2, 3$ (from bottom to top). The fringes contrast values are indicated on the right. From [48].

16 shows the experimental recordings for $n = 1, 2$ and 3 . The narrowing of the fringe spacing, proportional to $1/n$ is clearly observed, as well as reduction of the fringe contrast, an illustration of the strong sensitivity to decoherence of multi-particle interference effects.

3. Schrödinger cats in cavity QED

We have seen in the previous section that a basic ingredient for the generation of a multiparticle mesoscopic state superposition is the existence of a strong non-linearity in the system. Another example of mesoscopic state superposition induced by non-linearity is provided by cavity quantum electrodynamics (CQED) [29]. Here, the strong non-linear interaction of a single atom with a cavity field made of tens of photons results in the generation of cat states, entangled with the atom [30]. These cat states have been observed in experiments and their decoherence has been studied [16, 19]. We describe in this section the theory of these experiments and discuss their relationship with the well known collapse and revival effect of the Rabi oscillation [50]. The graininess of the photon field plays an essential role in the generation of the field mesoscopic superpositions, all these effects vanishing at the classical limit where the photon number goes to infinity (the atom-field interaction remaining finite). We will see also that the concepts of quantum interference and complementarity play a very important role to analyze the physics of these Schrödinger cat systems.

3.1. A reminder on microwave cavity QED and the Jaynes-Cummings model

In CQED, single atoms interact with one mode of the field in a high Q resonator. Dissipation is kept to a minimum, so that the coherent features of the atom-field interaction manifest themselves most conspicuously. In microwave CQED with superconducting cavities [30], the photon storage time is by far the longest relevant time in the experiment, so that many atoms, crossing successively the cavity, interact with the same field, imprinting in and extracting information from it. A detailed description of CQED techniques is beyond the scope of this course. Our goal is only to show how these techniques make it possible to generate mesoscopic superpositions of field states and study their evolution. In this introductory sub-section, we briefly recall the formalism and the notations which will be useful for the description of our system and the analysis of the experiments.

Basically, microwave CQED implements as closely as possible the Jaynes-Cummings (J-C) model of quantum optics [51], consisting in a two-level atom interacting with a single field mode. The atoms cross the cavity with a well defined velocity, which allows us to control the atom-field interaction time. They are prepared in a state belonging to a subspace made of two levels e and g . In practice, the experiments are performed with a Rubidium atomic beam and the levels of interest are two circular Rydberg states of high principal quantum number (equal to 51 and 50 respectively). The transition between these levels, at frequency $\omega_0/2\pi = 51$ GHz, is resonant or nearly resonant with a mode of the cavity (frequency ω), made of two superconducting mirrors facing each other. We call a and a^\dagger the annihilation and creation operators of one photon in the mode. We will not describe here how the atomic states are prepared and detected and how the cavity is made and tuned [see [30] and lecture notes by M. Brune in this Volume].

If we neglect the atom and field relaxation processes, the ‘atom + cavity’ field evolution is ruled by the interaction Hamiltonian given by Eq.(1.65). Adding the field and the atom’s energy terms, we can write the total atom-field Hamiltonian as:

$$H_{JC} = \hbar\omega(a^\dagger a + 1/2) + \frac{\hbar\omega_0}{2}(|e\rangle\langle e| - |g\rangle\langle g|) + \frac{\hbar\Omega}{2}(a^\dagger|g\rangle\langle e| + a|e\rangle\langle g|), \quad (3.1)$$

where Ω is the vacuum Rabi frequency, which we have already introduced in section 1.5. This coupling constant depends on the position of the atom. We assume it to be a constant, for sake of simplicity (see remark about this in section 1.5.1 above).

The eigenstates of the ‘field + atom’ Hamiltonian, when the interaction is neglected, are the tensor products $|e, n\rangle, |g, n\rangle$ describing the atom in e or g with a defined photon number n in cavity. The interaction H_{int} couples these states

2 by 2, inside uncoupled two-level manifolds S_n (spanned by the kets $|e, n\rangle$, $|g, n+1\rangle$). The eigenstates and eigenenergies of the J-C Hamiltonian are thus given by the exact diagonalization of two-level systems. Using a standard procedure, it is convenient to introduce the Pauli matrices notation and write the projection of H_{JC} inside the S_n manifold (calling P_n the projector on S_n) as:

$$\begin{aligned} \frac{1}{\hbar} P_n H_{JC} P_n &= (n+1)\omega + \frac{1}{2} \begin{pmatrix} \omega_0 - \omega & \Omega\sqrt{n+1} \\ \Omega\sqrt{n+1} & -(\omega_0 - \omega) \end{pmatrix} \\ &= (n+1)\omega + \frac{1}{2} \left[(\omega_0 - \omega) \sigma_z + \Omega\sqrt{n+1} \sigma_x \right]. \end{aligned} \quad (3.2)$$

It is then handy to define an n -dependent coupling angle θ_n by the relation:

$$\theta_n = \arctan \left(\frac{\Omega\sqrt{n+1}}{\omega_0 - \omega} \right) \quad (0 \leq \theta_n < \pi). \quad (3.3)$$

With this notation, simple expressions for the atom-field eigenstates are obtained:

$$\begin{aligned} |+, n\rangle &= \cos \frac{\theta_n}{2} |e, n\rangle + \sin \frac{\theta_n}{2} |g, n+1\rangle \quad ; \\ |-, n\rangle &= \sin \frac{\theta_n}{2} |e, n\rangle - \cos \frac{\theta_n}{2} |g, n+1\rangle, \end{aligned} \quad (3.4)$$

the corresponding energies being:

$$\frac{1}{\hbar} E_{\pm, n} = (n+1)\omega \pm \frac{1}{2} \sqrt{(\omega_0 - \omega)^2 + \Omega^2(n+1)}. \quad (3.5)$$

Exact resonance ($\omega_0 = \omega$) corresponds to $\theta_n = \pi/2$. Eqs.(3.4) and (3.5) then become:

$$|+, n\rangle = \frac{1}{\sqrt{2}}(|e, n\rangle + |g, n+1\rangle) \quad ; \quad |-, n\rangle = \frac{1}{\sqrt{2}}(|e, n\rangle - |g, n+1\rangle), \quad (3.6)$$

$$\frac{1}{\hbar} E_{\pm, n} = (n+1)\omega \pm \frac{1}{2} \Omega \sqrt{(n+1)}. \quad (3.7)$$

The eigenstates of the atom-field system ('dressed states' [34, 52]) are very convenient to compute the atom field evolution. We have already seen in section 1 that an atom, initially in e and resonantly coupled to the vacuum field $|0\rangle$ undergoes a reversible Rabi oscillation. A similar effect occurs if the field is initially in an n Fock state. It is then convenient to expand the initial $|e, n\rangle$ atom-field state

on the dressed levels, by inverting Eq.(3.6). We then get in a straightforward way:

$$\begin{aligned} |\Psi(0)\rangle &= |e, n\rangle = \frac{1}{\sqrt{2}}(|+, n\rangle + |-, n\rangle) \rightarrow \\ |\Psi(t)\rangle &= \frac{1}{\sqrt{2}}e^{-i(n+1)\omega t}(e^{-i\Omega\sqrt{n+1}t/2}|+, n\rangle + e^{i\Omega\sqrt{n+1}t/2}|-, n\rangle). \end{aligned} \quad (3.8)$$

and the probability for finding the atom at time t in level e :

$$P_e(t) = |\langle e, n | \Psi(t)\rangle|^2 = \cos^2 \frac{\Omega\sqrt{n+1}}{2}t. \quad (3.9)$$

The Rabi oscillation induced by an n -photon field occurs at a frequency $\sqrt{n+1}$ time larger than in vacuum. A Fock state being difficult to prepare, the phenomenon is usually observed with a coherent field, superposition of Fock states. We must then weight the different oscillation terms, whose frequency is n -dependent, by the probability to have n photons in the field, given by a Poisson law. We find:

$$P_e(t) = \sum_n |C_n|^2 |\langle e, n | \Psi(t)\rangle|^2 = e^{-\bar{n}} \sum_n \frac{\bar{n}^n}{n!} \frac{1 + \cos(\Omega\sqrt{n+1}t)}{2}. \quad (3.10)$$

The classical limit of this expression is obtained by taking $\bar{n} \rightarrow \infty$ and $\Omega \rightarrow 0$ with $\Omega\sqrt{\bar{n}} = \Omega_{cl}$ remaining finite. We then get a steady Rabi oscillation at frequency Ω_{cl} (classical limit). As soon as the photon number is finite however the distribution of n values leads to a spread of Rabi frequencies and to a collapse of the oscillation. We qualitatively estimate the collapse time $T_{collapse}$ by expressing that the phase variation of the oscillation over the width $\sqrt{\bar{n}}$ of the Poisson law is of the order of 2π :

$$\Omega \frac{d(\sqrt{n+1})}{dn} \Bigg|_{n=\bar{n}} \times \sqrt{\bar{n}} T_{collapse} = \pi \rightarrow T_{collapse} = \frac{2\pi}{\Omega}. \quad (3.11)$$

The Rabi oscillation in a coherent field with a finite photon number thus collapses after a time $T_{collapse}$ whose order of magnitude is the Rabi oscillation period in vacuum. This period is typically $20 \mu s$ in our CQED experiments. This is however only part of the story and the atom-field evolution involves much more physics. The above calculation does not tell us what happens to the system at longer times. Furthermore, we have so far focused on the atom's state and we have disregarded the field evolution and its correlations to the atom. We are now turning our attention to these important features.

3.2. Rabi oscillation in a mesoscopic field: collapse and revival revisited

The exact evolution equation for the ‘atom + coherent field’ system is obtained by adding the contributions of the various n states in the expansion of the coherent state. Starting at time $t = 0$ from the $|e, \alpha\rangle$ state representing an initially excited atom and a coherent field of complex amplitude α , we get at time t :

$$\begin{aligned} |\Psi(0)\rangle &= |e, \alpha\rangle = \frac{1}{\sqrt{2}} \sum_n C_n (|+, n\rangle + |-, n\rangle) \rightarrow \\ |\Psi(t)\rangle &= \frac{1}{\sqrt{2}} \sum_n C_n \times \\ &\quad \times e^{-i(n+1)\omega t} (e^{-i\Omega\sqrt{n+1}t/2} |+, n\rangle + e^{i\Omega\sqrt{n+1}t/2} |-, n\rangle) \\ &= \frac{1}{2} \sum_n C_n e^{-i(n+1)\omega t} \left\{ e^{-i\Omega\sqrt{n+1}t/2} (|e, n\rangle + |g, n+1\rangle) + \right. \\ &\quad \left. + e^{i\Omega\sqrt{n+1}t/2} (|e, n\rangle - |g, n+1\rangle) \right\}. \end{aligned} \quad (3.12)$$

where the C_n are Poisson coefficients given by Eq.(1.40). If we replace in this equation $|g, n+1\rangle$ by $|g, n\rangle$ (disregarding the difference between $\sqrt{n+1}$ and \sqrt{n}) and if we neglect the variation of the Rabi frequency $\Omega\sqrt{n+1}$ over the width of the photon number distribution, we obtain the classical limit in which the atom and field states are factorized:

$$|\Psi(t)\rangle \approx \left(e^{-i\Omega_{cl}t/2} \frac{|e\rangle + |g\rangle}{\sqrt{2}} + e^{i\Omega_{cl}t/2} \frac{|e\rangle - |g\rangle}{\sqrt{2}} \right) |\alpha\rangle. \quad (3.13)$$

At this limit, the field is unaffected by the coupling. The atom on the other hand is in a linear superposition of the two ‘dipole states’ $(|e\rangle \pm |g\rangle)/\sqrt{2}$. Each term of this superposition has a probability amplitude which evolves at frequency $\pm\Omega_{cl}$ and the Rabi oscillation thus appears as a quantum interference effect between these two amplitudes. This interference can be observed because the two ‘paths’ (atom in $|e\rangle + |g\rangle$ or in $|e\rangle - |g\rangle$) are fully indistinguishable.

When the coherent field is mesoscopic, i.e. contains a large but finite average number of photons \bar{n} , the effects neglected in the classical limit must be taken into account. The atom and the field are then no longer factorized. Their entanglement evolves as a function of time, appearing and disappearing quasi-periodically. Since the evolution equation has an exact solution, we could of course compute it and analyze the atom-field state in its full complexity. This approach is not very transparent however and we prefer to present here an approximate solution which has the merit of displaying the physics of the problem in a simple way. We follow closely the calculation derived in [53–55]. We notice

first that the difference between $\sqrt{n+1}$ and \sqrt{n} has its most important effect in the rapidly evolving phase factors, but can be neglected in the expression of the slowly varying C_n coefficients. To evaluate correctly the phase factors, we make the following replacement, which takes into account the graininess of the photon number:

$$\sqrt{n+1} \approx \sqrt{n} + \frac{1}{2\sqrt{n}} \approx \sqrt{n} + \frac{1}{2\bar{n}} . \quad (3.14)$$

We then get the following expression for the atom-field state:

$$\begin{aligned} |\Psi(t)\rangle &\approx \frac{1}{2} \sum_n C_n e^{-i(n+1)\omega t} e^{-i\Omega\sqrt{n}t/2} |n\rangle (e^{-i\frac{\Omega t}{4\sqrt{n}}} |e\rangle + e^{i\omega t} |g\rangle) \\ &+ \frac{1}{2} \sum_n C_n e^{-i(n+1)\omega t} e^{i\Omega\sqrt{n}t/2} |n\rangle (e^{i\frac{\Omega t}{4\sqrt{n}}} |e\rangle - e^{i\omega t} |g\rangle) . \end{aligned} \quad (3.15)$$

In this formula, the Rabi frequency $\Omega\sqrt{n}$ is still a function of n . We approximate it by its expansion in powers of $n - \bar{n}$, limiting the development to its second order:

$$\sqrt{n} \approx \frac{\sqrt{\bar{n}}}{2} + \frac{n}{2\sqrt{\bar{n}}} - \frac{1}{8\bar{n}^{3/2}} (n - \bar{n})^2 \dots \quad (3.16)$$

We then get after a straightforward calculation:

$$\begin{aligned} |\Psi(t)\rangle &\approx \frac{1}{2} e^{-i\Omega\sqrt{\bar{n}}t/4} \sum_n C_n e^{-i(n+1)\omega t} e^{-i\frac{\Omega nt}{4\sqrt{\bar{n}}}} e^{i\frac{\Omega(n-\bar{n})^2 t}{16\bar{n}^{3/2}}} |n\rangle \\ &\times (e^{-i\frac{\Omega t}{4\sqrt{\bar{n}}}} |e\rangle + e^{i\omega t} |g\rangle) + \\ &+ \frac{1}{2} e^{i\Omega\sqrt{\bar{n}}t/4} \sum_n C_n e^{-i(n+1)\omega t} e^{i\frac{\Omega nt}{4\sqrt{\bar{n}}}} e^{-i\frac{\Omega(n-\bar{n})^2 t}{16\bar{n}^{3/2}}} |n\rangle \\ &\times (e^{i\frac{\Omega t}{4\sqrt{\bar{n}}}} |e\rangle - e^{i\omega t} |g\rangle) \end{aligned} \quad (3.17)$$

Each of the two terms in the above expression is a product of an atomic by a field state. We recognize in the field states (sums over n) the expressions of coherent-like states whose phase is spread by a second order phase diffusion term [described by the $\exp(\pm\Omega(n - \bar{n})^2 t / 16\bar{n}^{3/2})$ terms]. It is easy to show that this phase spreading occurs in a characteristic time T_{spread} of the order of $\pi\bar{n}/\Omega$. Restricting ourselves to time much shorter than this limit, we will first neglect

this phase spreading. A simple manipulation then yields:

$$\begin{aligned} |\Psi(t)\rangle \approx & \frac{1}{2} e^{-i\Omega\sqrt{\bar{n}}t/4} e^{-i\omega t/2} \left| \alpha e^{-i(\omega+\Omega/4\sqrt{\bar{n}})t} \right\rangle \times \\ & \times (e^{-i\Omega t/4\sqrt{\bar{n}}} e^{-i\omega t/2} |e\rangle + e^{i\omega t/2} |g\rangle) + \\ & + \frac{1}{2} e^{i\Omega\sqrt{\bar{n}}t/4} e^{-i\omega t/2} \left| \alpha e^{-i(\omega-\Omega/4\sqrt{\bar{n}})t} \right\rangle \times \\ & \times (e^{i\Omega t/4\sqrt{\bar{n}}} e^{-i\omega t/2} |e\rangle - e^{i\omega t/2} |g\rangle). \end{aligned} \quad (3.18)$$

We finally adopt the interaction picture, in order to get rid of the obvious free atom and field evolution terms. We write the atom-field state in a compact form which displays immediately the entanglement features of the system:

$$|\tilde{\Psi}(t)\rangle \approx \frac{1}{\sqrt{2}} \left[|\Psi_{at}^+(t)\rangle \otimes |\Psi_f^+(t)\rangle + |\Psi_{at}^-(t)\rangle \otimes |\Psi_f^-(t)\rangle \right]. \quad (3.19)$$

The global atom-field state is thus expressed in terms of four normalized atom and field states given by the relations:

$$|\Psi_{at}^\pm(t)\rangle = \frac{1}{\sqrt{2}} e^{\mp i\Omega\sqrt{\bar{n}}t/2} \left[(e^{\mp i\Omega t/4\sqrt{\bar{n}}} |e\rangle \pm |g\rangle) \right], \quad (3.20)$$

$$|\Psi_f^\pm(t)\rangle = e^{\pm i\Omega\sqrt{\bar{n}}t/4} \left| \alpha e^{\mp i\Omega t/4\sqrt{\bar{n}}} \right\rangle. \quad (3.21)$$

Eq.(3.19) describes a bipartite state whose degree of entanglement varies with time. The two atomic states $|\Psi_{at}^\pm\rangle$ are ‘dipole states’ superpositions, characterized by a phase difference between e and g evolving at frequency $\pm\Omega/\sqrt{\bar{n}}$. The two field states $|\Psi_f^\pm\rangle$ are coherent states whose complex amplitude phases also evolve at the same frequencies, in opposite directions in phase space. In the global wave function [Eq.(3.19)], the atom and field components in each term of the superposition stay locked in phase. The system’s evolution is thus described by two very different frequencies. The global phases of the atom and field states rotates ‘fast’ at the Rabi frequency $\pm\Omega\sqrt{\bar{n}}$, while the ‘internal’ phases of the atom dipole and field coherent state rotate slowly at the \bar{n} time smaller frequency $\pm\Omega/\sqrt{\bar{n}}$. At the classical limit ($\bar{n} \rightarrow \infty$), the former frequency remains finite while the latter goes to zero. We then retrieve the result given by Eq.(3.13). Let us recall that Eq.(3.19) is approximate and can be used only for $t \ll \pi\bar{n}/\Omega$. It is also valid for \bar{n} not too small (mesoscopic regime). More exact expressions of the entangled atom-field system, valid for longer times, are given by Eqs. (3.12), (3.15) and (3.17).

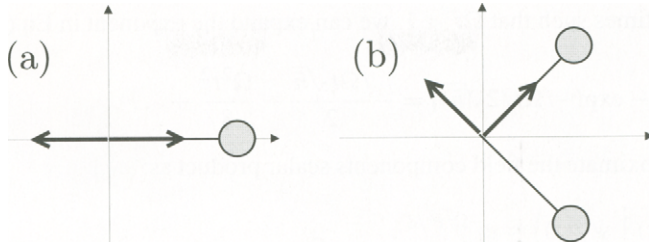


Fig. 17. Pictorial representation of the atomic and field state evolution in the phase plane. (a) initial situation. (b) at a later time, the atom and the field get entangled.

It is instructive to view the system's evolution in a pictorial way (Fig. 17). To exhibit clearly the correlated phase evolutions of the atom and field components, we describe the two level atom as a pseudo-spin evolving in the equatorial plane of a Bloch sphere and we make this plane coincide with the phase space plane of the field quadratures. The atomic states are represented as pseudo-spin vectors and the field coherent states are pictured as circles. At time $t = 0$, the initial $|e\rangle$ state appears as a superposition of the $|e\rangle + |g\rangle$ and $|e\rangle - |g\rangle$ states represented by two opposite Bloch vectors while the field state is a circle whose center lies on the X_0 quadrature axis [Fig. 17(a)]. As time evolves, the two dipole Bloch vectors start to rotate in opposite directions, while the field splits into two components which stay respectively in phase and π out of phase with the corresponding atomic dipole vectors [Fig. 17(b)]. This simple picture shows that the two subsystems get entangled as soon as the uncertainty circles associated to the field components cease to overlap. It also shows that the field evolves into a Schrödinger cat-like state, superposition of two coherent fields with opposite phases. The entanglement and the generation of the cat states occur within a time of the order of the slow phase drift period, $\sqrt{\bar{n}}/\Omega$. This time goes to infinity at the classical limit. The atom-field entanglement and the generation of Schrödinger cats of the field are thus quantum effects, directly linked to the graininess of the field state in the mesoscopic regime.

The overlap integral of the two field components is readily computed, using Eq.(1.43):

$$\begin{aligned} \langle \Psi_f^-(t) | \Psi_f^+(t) \rangle &= e^{i\Omega\sqrt{\bar{n}}t/2} \left\langle \alpha e^{i\Omega t/4\sqrt{\bar{n}}} | \alpha e^{-i\Omega t/4\sqrt{\bar{n}}} \right\rangle \\ &= e^{i\Omega\sqrt{\bar{n}}t/2} e^{-\bar{n}[1-\exp(-i\Omega t/2\sqrt{\bar{n}})]}. \end{aligned} \quad (3.22)$$

At short times such that $\Omega t < 1$, we can expand the exponent in Eq.(3.22) as:

$$-\bar{n}[1 - \exp(-i\Omega t/2\sqrt{\bar{n}})] = -\frac{i\Omega t\sqrt{\bar{n}}}{2} - \frac{\Omega^2 t^2}{8} + \dots , \quad (3.23)$$

and approximate the field components scalar product as:

$$\langle \Psi_f^-(t) | \Psi_f^+(t) \rangle \approx e^{-\Omega^2 t^2/8} . \quad (3.24)$$

The overlap between the two field states decays as a Gaussian function of time, over a time scale of the order of the vacuum Rabi period $1/\Omega$. This is indeed the time it takes for the dephasing between the two components to reach a value $1/\sqrt{\bar{n}}$, of the order of the phase uncertainty of the coherent field. The decay of the field components overlap is directly related to the collapse of the atomic Rabi oscillation. The field scalar product is indeed involved in the expression of the atomic reduced density operator which writes, at short times:

$$\begin{aligned} \tilde{\rho}_{at}(t) &= \text{Tr}_{\text{field}}(|\tilde{\Psi}(t)\rangle\langle\tilde{\Psi}(t)|) \approx \\ &\frac{1}{2} |\Psi_{at}^+(t)\rangle\langle\Psi_{at}^+(t)| + \frac{1}{2} |\Psi_{at}^-(t)\rangle\langle\Psi_{at}^-(t)| + \\ &\frac{1}{2} (\ |\Psi_{at}^+(t)\rangle\langle\Psi_{at}^-(t)| + |\Psi_{at}^-(t)\rangle\langle\Psi_{at}^+(t)|) e^{-\Omega^2 t^2/8} . \end{aligned} \quad (3.25)$$

This operator, expressed in the basis of the atomic dipole states, thus loses its off-diagonal elements as soon as the field components are separated. The atomic coherence is directly related to the contrast of the Rabi oscillation signal which can be written as:

$$\begin{aligned} P_e(t) &\approx \langle e | \tilde{\rho}_{at}(t) | e \rangle \approx \frac{1}{2} |\langle e | \Psi_{at}^+(t) \rangle|^2 + \frac{1}{2} |\langle e | \Psi_{at}^-(t) \rangle|^2 + \\ &+ \text{Re } \langle e | \Psi_{at}^+(t) \rangle \langle \Psi_{at}^-(t) | e \rangle e^{-\Omega^2 t^2/8} \end{aligned} \quad (3.26)$$

The collapse of the Rabi oscillation appears as a complementarity effect. The atomic interference is washed out when the field components (to which these dipole states are locked) carry an information about these states. This happens as soon as these field components become distinguishable, i.e. quasi orthogonal. Combining Eqs.(3.26) and (3.20), we get an analytical expression for the Rabi oscillation signal which confirms in quantitative terms the qualitative description given above :

$$P_e(t) \approx \frac{1}{2} [1 + e^{-\Omega^2 t^2/8} \cos(\Omega\sqrt{\bar{n}}t)] \quad (3.27)$$

When the Rabi oscillation has collapsed, the atom-field system presents entanglement. Its state is indeed a superposition with equal weights involving nearly orthogonal field states. A Schrödinger cat state of the field is created, generally entangled to the atom. A field state, de-correlated from the atom can be obtained by measuring the atom's state. Detecting the atom in e or g projects the field in a superposition of the two quasi orthogonal components. Defining $\Phi = \Omega t / 4\sqrt{n}$ and using Eq.(3.19), we get the expression of the field after detection of the atom in e :

$$\left| \tilde{\Psi}_{\text{field}}(t) \right\rangle_{\text{atom in } e} = \frac{1}{\sqrt{2}} \left[e^{-i(\bar{n}+1)\Phi} \left| \alpha e^{-i\Phi} \right\rangle + e^{i(\bar{n}+1)\Phi} \left| \alpha e^{i\Phi} \right\rangle \right]. \quad (3.28)$$

The state of the ‘cat’ is then conditioned to the measurement of the atom (a different cat state is prepared if atom is detected g). In fact, measuring the atom is not always required to prepare a field cat state, separate from the atom. When the phase of the field components has rotated by $\pi/2$, a π -phase cat with two components having opposite phases is produced, which is at this time not entangled with the atom:

$$\begin{aligned} \left| \tilde{\Psi}(t = 2\pi\sqrt{n}/\Omega) \right\rangle &\approx \frac{1}{2} \left[e^{-i\pi\bar{n}/2} \left| \alpha e^{-i\pi/2} \right\rangle - e^{i\pi\bar{n}/2} \left| \alpha e^{+i\pi/2} \right\rangle \right] \\ &\otimes \left[e^{-i\pi/2} |e\rangle + |g\rangle \right] \end{aligned} \quad (3.29)$$

The disentanglement occurs at this specific time because the two atomic dipole states, initially π -out of phase, have evolved into the same e, g superposition, thus resulting in a factorization of the atom-field wave function.

Let us now consider still longer atom-field interaction times. After a time $T_{\text{revival}} = 4\pi/\Omega\sqrt{n}$, such that the fields components have rotated by π , the two field components are again overlapping, with a common phase opposite to the initial one. The atomic dipole states are then again orthogonal, their initial phases being exchanged. The coherence of the reduced density operator is then restored and the Rabi oscillation revives, hence the name given to this specific time. This revival effect, predicted long ago, appears here, as does the collapse phenomenon, as a manifestation of complementarity. At the revival time, the field does not contain any information about the dipole state in which the atom is and the interference between the corresponding atomic probability amplitudes reappears.

The above analysis is only qualitative, since it relies on an approximate expression of the atom-field state. It is also possible to compute exactly the Rabi oscillation signal given by Eq.(3.10) for a finite average photon number. Fig. 18 shows the result of this exact calculation, for $\bar{n} = 15$ photons. The collapse and revival are clearly visible. According to the simplified model, the Rabi oscillations should reappear with a 100% contrast. The numerical calculation shows that

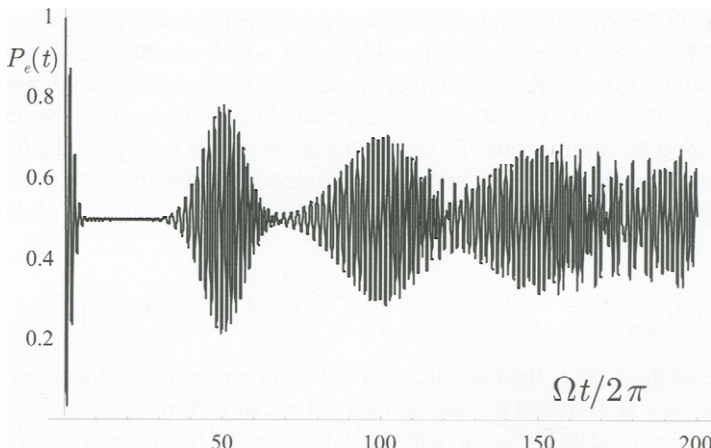


Fig. 18. Rabi oscillation collapse and revivals: computed probability $P_e(t)$ for finding the atom in state $|e\rangle$ versus the interaction time t in units of $2\pi/\Omega$. The cavity contains initially an $\bar{n} = 15$ photons coherent field.

the revival has rather a contrast of about 50%. The simple model also predicts a succession of identical revivals, as the two field components merge together periodically. The exact numerical calculation shows instead that the successive revivals have a decreasing amplitude and an increasing time duration, resulting in a smearing out of the collapse and revival features after two or three revivals. The differences between the exact results and the simple model predictions are due to the drastic approximation made by neglecting terms of second order in Eq.(3.17). Even if the complete phase diffusion of the field takes a long time of the order of \bar{n}/Ω the phase spreading after a time $\sqrt{\bar{n}}/\Omega$ is of the order of $\pi/\sqrt{\bar{n}}$ which is precisely of the order of the fluctuation of the initial coherent field phase. In other words, the phase of the field spreads by a factor of the order of 2 between time 0 and $4\pi\sqrt{\bar{n}}/\Omega$. Not surprisingly, a calculation neglecting this spreading effect is only qualitative.

Rabi oscillation collapses and revivals have been observed in experiments performed with very small coherent field (photon numbers of the order unity) [56]. Similar collapse and revival phenomena have been observed with Rydberg atoms in thermal or micromaser fields [57]. They have also been seen in studies in which two internal levels of a trapped ions are coupled via a Jaynes-Cummings-type Hamiltonian to a few vibration quanta of the trap potential [58]. One should note that the present analysis, with its specific approximations valid for mesoscopic fields containing tens of photons, does not describe quantitatively these

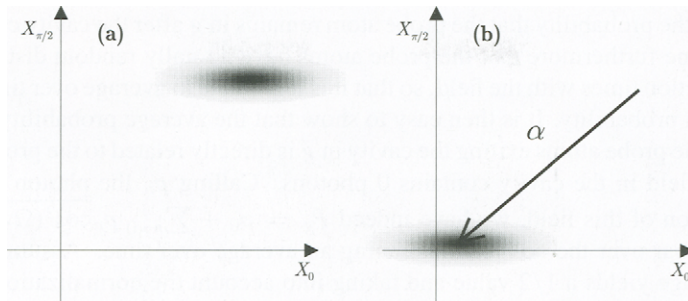


Fig. 19. Principle of homodyne detection. (a) original field. (b) translated field.

experiments. Mesoscopic collapses and revivals have not yet been observed, because the expected revival time, proportional to \sqrt{n} , is too long. We mention below a related experiment in which Rabi oscillation revivals are induced at an earlier time.

3.3. Observing the Schrödinger cat by a homodyne Q function measurement

The generation of a Schrödinger cat in the Rabi oscillation experiment manifests itself by a phase splitting effect. In order to observe the phase distribution of the field resonantly interacting with the atom, we need to implement a homodyne technique adapted to microwave CQED [19]. In an usual homodyne detection, one would employ a beam splitter to mix the signal with a reference field and a quadratic photo-detector to measure the resulting beating (see section 2). This cannot be done in microwave CQED because the field stored in the cavity cannot be perturbed by a beam splitter or an usual detector. We have developed a variant of homodyning in which a reference coherent field is added to the field to be measured by coupling the cavity to a classical source, the resulting field being detected by an absorbing ‘probe’ atom crossing subsequently the cavity. This method amounts in effect to a direct measurement of the Q function of the field in the cavity.

The principle of the method is sketched in Fig. 19. We assume that the cavity stores a field described by an operator density ρ_f , qualitatively represented by a shaded area in phase space [Fig. 19(a)]. In order to measure this field, we couple the cavity to a classical pulse of microwave of convenient phase and duration. This amounts to a translation in phase space (see section 1), the initial field being changed into the one described by the density operator $D(\alpha)\rho_f D^{-1}(\alpha)$ [Fig. 19(b)]. In order to measure this field, we then send across the cavity a probe atom, prepared in the lower level g and, by repeating the experiment many times, we

measure the probability that the probe atom remains in g after the cavity crossing. We assume furthermore that the probe atoms have a totally random distribution of interaction times with the field, so that it is legitimate to average over time their transition probability. It is then easy to show that the average probability P_g for finding the probe atoms exiting the cavity in g is directly related to the probability that the field in the cavity contains 0 photons. Calling p_n the photon number distribution of this field, we have indeed $P_g = p_0 + \bar{\sum}_{n>0} p_n \cos^2(\Omega\sqrt{n}t/2)$, with the bar over the \cos^2 term meaning an average over time. Assuming that this average yields a $1/2$ value and taking into account the normalization of the p_n 's ($\sum_{n>1} p_n = 1 - p_0$), we thus get $P_g = (1 + p_0)/2$ and $p_0 = 2P_g - 1$. We finally note that p_0 is simply the diagonal matrix element in vacuum of the translated field density operator, which we can write as:

$$p_0 = 2P_g - 1 = \langle 0 | D(-\alpha) \rho_f D(\alpha) | 0 \rangle , \quad (3.30)$$

and we conclude that measuring P_g directly yields the initial field Q function (see Section 1) at the point in phase space represented by α [compare Eq.(3.30) with (1.55)]. By sweeping this parameter and resuming the same procedure, we sample the $Q(\alpha)$ function of the initial field in the cavity. We have just described an ideal situation. Realizing a velocity distribution of probe atoms corresponding to a completely random atom-cavity interaction time is not easy. In practice, we are using probe atoms with a broad Maxwellian velocity distribution. The interaction time, inversely proportional to the velocity, does not have a flat distribution. This results in a sum over n of the p_n 's in the expression of P_g which does not exactly reduces to $1 - p_0$. The probe atom signal remains however a fair approximation of $Q(\alpha)$ and yields information about the phase distribution of the field.

We have implemented this method for investigating the ‘cat states’ produced by the interaction of a single resonant atom with the cavity field [19]. The procedure involves the following successive steps. We first inject a coherent field $|\beta\rangle$ in the cavity, with well defined phase and average photon number (determined by an independent calibration experiment based on the measurement of the light shift induced by this field on an auxiliary atom). Immediately after this field has been injected, we send a resonant atom in level e which undergoes a Rabi oscillation in the field. The interaction time of this atom with the field is adjusted to one of two preset values (32 and 52 μ s) by selecting the atom’s velocity. The resulting field is then measured by the method outlined above. A reference coherent field with amplitude α is injected and a probe atom in g is subsequently sent across the cavity, this atom being finally detected by a state selective detector. Since we know the amplitude of the field to be measured (equal to the initial amplitude of the coherent field β , diminished by the natural cavity decay during

the experimental sequence), the reference field is adjusted to the same amplitude and we vary only its phase ϕ . We finally extract from the data the probability P_g and plot it versus ϕ thus exhibiting the phase splitting effect produced by the Rabi oscillation. More experimental details can be found in [19].

Fig. 20(a) shows the $P_g(\phi)$ function for the two selected interaction times. The signals are plotted versus ϕ for different mean photon numbers \bar{n} in the range 15 to 36. The splitting by a single atom of the field into two symmetrical components with different phases is clearly visible. For a given interaction time, the splitting decreases with field amplitude and for a given \bar{n} the separation increases with time. Fig. 20(b) summarizes the results by plotting the phases of the two components as a function of the dimensionless parameter $\Phi = \Omega t / 4\sqrt{\bar{n}}$. The dotted lines correspond to the phases predicted by the simple model discussed above. The solid line results from a numerical simulation solving the exact field equation of motion and taking into account cavity damping. The agreement between the experimental points and the solid line is very good. The maximum phase splitting observed, for $\bar{n} = 15$ photons and an interaction time of $52 \mu s$ is 90 degrees.

We have also checked the correlation between the atomic state and the field phase by selectively preparing $|\Psi_{at}^+\rangle$ or $|\Psi_{at}^-\rangle$ at the beginning of the interaction [19], within a time short enough so that the slow drift of the atom and field phases can be neglected. To prepare $|\Psi_{at}^+\rangle$, the atom, initially in g , first performs a $\pi/2$ Rabi pulse according to the transformation:

$$|g\rangle \rightarrow \frac{1}{\sqrt{2}}[e^{-i\pi/4}|\Psi_{at}^+(0)\rangle - e^{i\pi/4}|\Psi_{at}^-(0)\rangle]. \quad (3.31)$$

The atom is then detuned by Stark effect with respect to the cavity, during a time much shorter than the Rabi period. A pulse of electric field is applied between the cavity mirrors, whose effect is to shift by $\pi/2$ the relative phase of the e and g states [30]. The sequence of Rabi and Stark pulses transforms the initial g state, superposition of the interfering $|\Psi_{at}^+(0)\rangle$ and $|\Psi_{at}^-(0)\rangle$ states into $|\Psi_{at}^+(0)\rangle$ alone. The system ends up in the slowly evolving quasi-stationary state described by the first term in the right hand side of Eq.(3.19). The atom and the field subsequently drift in phase in only one direction. We observe that the Rabi oscillation is frozen from then on. A homodyne measurement of the field phase after the atom exits from C reveals, as expected, only a single phase shifted component (open circles in Fig. 21). Similarly, one prepares $|\Psi_{at}^-(0)\rangle$ by applying the same Rabi and Stark switching pulse sequence starting from level e . This state couples to the other component of the field as revealed by the subsequent homodyne detection (solid squares in Fig. 21). This experiment clearly demonstrates correlations between the atomic and field state phases.

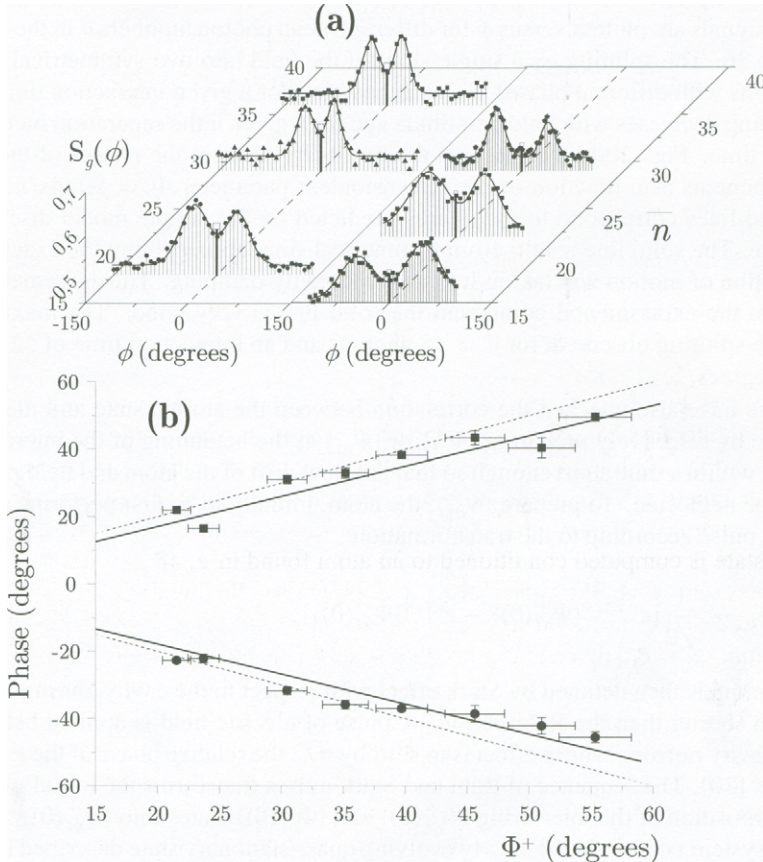


Fig. 20. (a) Field phase distribution for \bar{n} values in the range 15 to 36. The interaction time is $32 \mu s$ (left) or $53 \mu s$ (right). The points are experimental and the curves are fits on a sum of Gaussians. (b) Phases of the two field components versus $\Phi = \Omega t / 4\sqrt{\bar{n}}$. Dotted and solid lines are theoretical (see text). Adapted from [19].

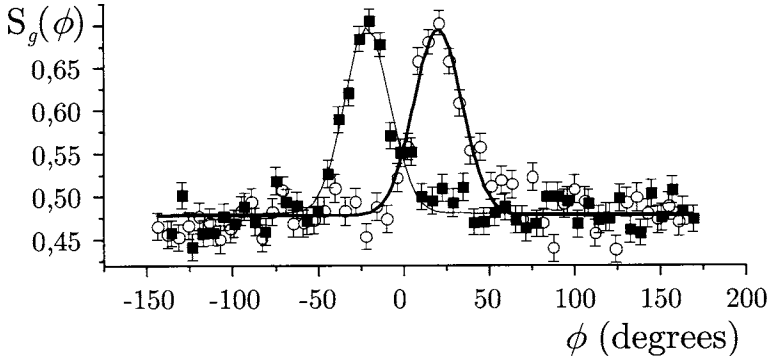


Fig. 21. Field phase distributions following preparation of atomic states $|\phi_a^\pm(0)\rangle$ by combination of Rabi and Stark pulses ($\bar{n} = 27$; interaction time $32 \mu\text{s}$). Open circles: preparation of $|\phi_a^+(0)\rangle$. Solid squares: preparation of $|\phi_a^-(0)\rangle$. Solid lines are Gaussian fits. From [19].

We now turn to the analysis of the mesoscopic state coherence. Let us first stress that the experimental parameters are consistent with a survival of this coherence. Fig. 22 shows, for $\bar{n} = 36$ and an interaction time of $32 \mu\text{s}$, the expected Wigner function $W(\beta_x + i\beta_y)$ of the field in the cavity. It results from the explicit numerical simulation including the actual experimental parameters. The field state is computed conditioned to an atom found in g , $48 \mu\text{s}$ after its crossing the cavity axis. We have chosen to compute the W function, and not the Q one, because the former is expected to contain a conspicuous interference term describing the coherence of the cat state whereas the later is largely insensitive to the coherence (see Section 1). We see indeed that this W function clearly exhibits the two separate field components and the interferences which are a clear signature of a mesoscopic quantum coherence. The square of the distance in phase space between the two components, $D^2 = 4\bar{n} \sin^2(\Omega t / 4\sqrt{\bar{n}})$ is a measure of the mesoscopic character of this superposition. In the range of \bar{n} values we have explored, D^2 is nearly constant versus \bar{n} , equal to 20 for the short interaction time ($32 \mu\text{s}$) and to 40 for the long one ($52 \mu\text{s}$). The theoretical decoherence time of the Schrödinger cat state superposition is $2T_{cav}/D^2$ [Eq.(2.35)]. With our cavity decay time $T_{cav} = 1 \text{ ms}$, we thus expect a decoherence time of $85 \mu\text{s}$ for the cat prepared within $32 \mu\text{s}$, which indicates that the field retains its macroscopic coherence over the duration of the experimental sequence, as confirmed by its Wigner function.

We should note however that the above discussion is based on theoretical arguments. The experimental determination of the field Wigner function in this experiment remains to be done. In the mean time, we have performed another

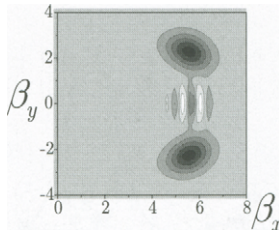


Fig. 22. Computed cavity field Wigner function $W(\beta_x + i\beta_y)$ for $\bar{n} = 36$ and a $32 \mu s$ interaction time. Adapted from [19].

simpler coherence test, based on the observation of the Rabi oscillation revival phenomenon. We have already mentioned that we cannot wait long enough for the revival to occur spontaneously. We can however induce the phenomenon at an earlier time and the observation of the reappearing Rabi oscillation is a clear indication of the cat state coherence survival over that time. After collapse of the Rabi oscillation, we apply to the atom, at time T , a Stark pulse switching the signs of the quantum amplitudes associated to e and g . This procedure implements a scheme for decoherence tests in CQED proposed in [59]. According to Eq.(3.19), the Stark pulse suddenly exchanges the atomic states correlated to the $|\Psi_f^+(t)\rangle$ and $|\Psi_f^-(t)\rangle$ field components. The atom-field coupling resumes afterwards, reversing the sign of the rotation of the two field components. At time $2T$, the two fields are back in phase and the Rabi oscillation revives, revealing the coherent nature of the atom-cavity state. This induced revival, reminiscent of a spin echo, is under investigation at the present time and will be published after these notes are completed. We describe in the next section another experiment revealing a ‘cat’ state coherence, performed in a related dispersive CQED experiment.

3.4. Dispersive cats in cavity QED

The coupling of a resonant two-level atom with a field mode in a mesoscopic coherent state singles out two atomic ‘dipole states’ $|\Phi_{at}^\pm\rangle$, equal weight superpositions of e and g , whose phase evolves slowly during the interaction (at the classical limit, this phase is stationary). These atomic dipole states can be seen as eigenstates of the interaction, corresponding to two different atomic indices seen by the field interacting with the atom in the cavity. The atom, initially in level e , is prepared in a superposition of these two eigenstates of the refractive index and the field thus evolves into a superposition of two components with different phases. This interpretation can be extended to the case when the atom and the field are off-resonant (dispersive coupling) with a detuning δ between the atom

and the field mode. In this case, the interpretation in term of refractive index is even more appropriate since an off-resonant atom does not exchange any energy with the field and thus really behaves as a piece of transparent dielectric medium as far as its coupling to the field is concerned. We now show that Schrödinger cat states of the field can be generated by exploiting this dispersive interaction and we recall briefly the experiments we have performed with these states.

When the atom-field coupling is not resonant, an exact diagonalization of the Hamiltonian is still possible [Eqs.(3.4) and (3.5)]. It is however more transparent physically to do a perturbative treatment [27, 28]. We assume $\delta = \omega_0 - \omega > 0$, with mixing angles $\theta_n \ll 1$ (the case $\delta < 0$ and $\theta_n \approx \pi$ is treated similarly, with minor obvious changes in the equations). We develop the eigenstates and eigenenergies in power of $\Omega\sqrt{n+1}/\delta$. Eqs.(3.4) and (3.5) yield (to first order for states and to second order for energies):

$$\begin{aligned} |+, n\rangle &\approx |e, n\rangle + \frac{\Omega\sqrt{n+1}}{2\delta} |g, n+1\rangle \\ |-, n\rangle &\approx -|g, n+1\rangle + \frac{\Omega\sqrt{n+1}}{2\delta} |e, n\rangle \\ \frac{1}{\hbar} E_{+,n} &= (n + \frac{1}{2})\omega + \frac{\omega_0}{2} + \frac{\Omega^2(n+1)}{4\delta} \\ \frac{1}{\hbar} E_{-,n} &= (n + \frac{3}{2})\omega - \frac{\omega_0}{2} - \frac{\Omega^2(n+1)}{4\delta}. \end{aligned} \quad (3.32)$$

The energy development is valid if the parameter $\Omega^2(n+1)/\delta^2$ is much smaller than 1. We will assume the condition:

$$\frac{\Omega\sqrt{n+1}}{\delta} \leq \frac{1}{3}. \quad (3.33)$$

We see on Eq.(3.32) that the eigenstates of the atom-field system $|+, n\rangle$ and $|-, n\rangle$ ('dressed states') are very close to the uncoupled states $|e, n\rangle$ and $|g, n+1\rangle$ which are slightly 'contaminated' (to first order for the states and to second order for the energies) by the atom-field coupling. The energies of these levels are shifted to second order by an amount linear in n (light shift effect).

Assume now that we couple an atom in level e with a coherent field $|\alpha\rangle$ and let the two systems interact for a time t . Expanding the coherent state on a Fock state basis and taking into account that $|e, n\rangle$ is very close to the $|+, n\rangle$ dressed state, we get:

$$|\Psi_{e,\alpha}(0)\rangle = |e\rangle |\alpha\rangle = \sum_n C_n |e, n\rangle \Rightarrow$$

$$|\Psi_{e,\alpha}(t)\rangle \approx \sum_n C_n e^{-i(n+1/2)\omega t} e^{-i\omega_0 t/2} e^{-i\Omega^2(n+1)t/4\delta} |e, n\rangle, \quad (3.34)$$

which, in interaction picture yields:

$$|\tilde{\Psi}_{e,\alpha}(t)\rangle \approx \sum_n C_n e^{-i\Omega^2(n+1)t/4\delta} |e, n\rangle = e^{-i\Omega^2 t/4\delta} |e\rangle \otimes |\alpha e^{-i\Omega^2 t/4\delta}\rangle. \quad (3.35)$$

Similarly, for an atom initially in level g we obtain:

$$|\tilde{\Psi}_{g,\alpha}(t)\rangle \approx \sum_n C_n e^{+i\Omega^2 n t/4\delta} |g, n\rangle = |g\rangle \otimes |\alpha e^{+i\Omega^2 t/4\delta}\rangle \quad (3.36)$$

The cavity field remains in a coherent state, phase shifted by an angle $\pm\chi = \pm\Omega^2 t/4\delta$ depending upon whether the atom is in level e or g . This effect is interpreted by attributing to the atom an index N_i which, at low field intensity, writes:

$$N_i = 1 \pm \frac{\Omega^2}{4\delta\omega_c}, \quad (3.37)$$

with the + and - signs corresponding respectively to an atom in e or g . With the parameters of our microwave CQED experiment ($\Omega = 2\pi \times 50$ kHz, $\omega = 2\pi \times 51$ GHz and $\delta = 3\Omega$) we find $|N_i - 1| = 10^{-7}$, which is a huge value for a single atom effect. Note that this index is linear for extremely low fields only and saturates for average photon numbers of the order of $(\delta/\Omega)^2$. Note also, in addition to the classical phase shift of the coherent state, the global quantum phase shift of the system's state when the atom is in level e . This is a cavity Lamb shift effect (dephasing associated to an excited state in presence of cavity vacuum).

In order to observe directly the phase shifts induced on a coherent field by a non-resonant atom, we have performed the experiment in the same way as for the resonant case, by employing the homodyne method adapted to CQED (results not yet published). The signals are very similar to the ones shown in Fig. 20. The only difference lies in the preparation of the atomic initial states, which must be eigenstates of the refractive index. These are linear combinations of e and g in the resonant case whereas they are simply the e and g states in the non-resonant situation. It is thus easier to prepare these states in the non-resonant case and we observe the two field components, with a positive or a negative phase depending on whether the atom is in e or in g .

By preparing the atom in a superposition of e and g one can also entangle the atom and field systems and prepare superposition states of the field of the Schrödinger cat type. Here again, the experiment is very similar to the one performed in the resonant case. Whereas in the resonant situation the initial atomic

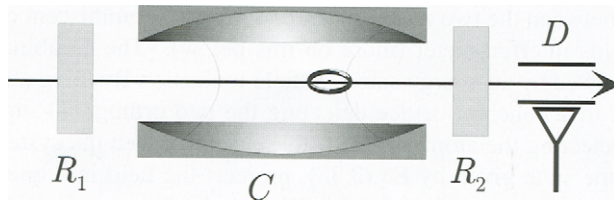


Fig. 23. Scheme of the dispersive Schrödinger cat experimental set-up

state e was already in a superposition of the eigen-atomic dipoles states, we must now achieve this preparation by an explicit manipulation, preparing first the atom in e , then submitting it to a $\pi/2$ pulse of classical radiation R_1 , using an auxiliary low- Q field mode acting on the atom before it enters the cavity. With a proper choice of the phase of the R_1 pulse, the atom-field system can evolve according to:

$$|e\rangle |\alpha\rangle \rightarrow \frac{1}{\sqrt{2}}(|e\rangle + e^{-i\chi} |g\rangle) |\alpha\rangle \rightarrow \frac{e^{-i\chi}}{\sqrt{2}}[|e\rangle |\alpha e^{-i\chi}\rangle + |g\rangle |\alpha e^{i\chi}\rangle], \quad (3.38)$$

where the first arrow represents the effect of the classical pulse and the second the one of the atom-cavity field coupling. The phase of the classical pulse R_1 can be adjusted to induce a quantum phase difference between e and g precisely equal to $-\chi$, which compensates for the Lamb shift of the e state and insures that the two components of the field correlated to e and g have quantum amplitudes with the same phase. This condition is not essential, but it simplifies the expressions of the Schrödinger cat states, by making them genuine even and odd parity states when $\chi = \pi/2$ (see below). In the experiments we have performed so far, the classical dephasing 2χ between the two field components was typically of the order of 50 to 100 degrees for fields containing on average a few photons. Note that the non-resonant phase splitting is always smaller than the one observed in resonant case for the same number of photons and interaction time [the angle χ computed under the condition (3.33) is smaller than $\Omega t/4\sqrt{n}$].

In the entangled state given by Eq.(3.38), the phase of the field acts as a meter pointing to the atomic energy. Detecting the atom in e or in g would result in a collapse of the state into one of the two components and the ambiguity of the cat state would be lost. In order to maintain the quantum ambiguity, we must mix again the two states e and g after the atom exits the cavity and perform the atomic detection only after. This second mixing occurs in a classical microwave zone R_2 identical to R_1 . By a proper choice of phase, this second pulse can induce the transitions $|e\rangle \rightarrow [|e\rangle + |g\rangle]/\sqrt{2}$; $|g\rangle \rightarrow [|g\rangle - |e\rangle]/\sqrt{2}$. The set-up used for this experiment is sketched in Fig. 23. It shows the cavity mode

sandwiched between the two zones R_1 and R_2 , a set up reminiscent of a Ramsey separated fields interferometer (more on this below). The combination of the R_2 pulse followed by an energy selective field ionization Rydberg atom detector is equivalent to a coherent device detecting the two orthogonal superpositions $|g\rangle \pm |e\rangle$. Detecting the atom in one of these states, when the system has been prepared in the state given by Eq.(3.38), projects the field into one of the two Schrödinger cat states $|\alpha e^{-i\chi}\rangle \pm |\alpha e^{i\chi}\rangle$. Here again, there is a complete analogy with the similar experiments in the resonant case.

The dispersive cat experiment [16] has been performed before the resonant ones [19]. At the time the dispersive experiment was made, the direct homodyne method adapted to CQED was not yet designed and the phase splitting of the cat was observed indirectly, via an effect quite similar to the collapse of the Rabi oscillation. We have detected the Ramsey fringes of the atom subjected to the two R_1 and R_2 pulses sandwiching the cavity [16]. By sweeping the frequency of these pulses around the atomic resonance, we have observed a modulation of the probability to detect the atom in e or in g . These so-called Ramsey fringes are a manifestation of a quantum interference. As long as we have no way of knowing whether the atom (initially prepared in e and finally detected in g) has undergone the transition in R_1 or in R_2 , we must associate a probability amplitude to each of these possibilities and the transition probability contains an interference term between them, responsible for the fringe signal. There is a strong analogy between a Ramsey interferometer and the Mach-Zehnder studied in Section 2, the beam splitters being replaced by the mixing pulses. To underscore this analogy, Fig. 24(a) represents a diagram showing the two paths followed in Hilbert space by the two-level atom as it crosses the apparatus. The upper horizontal line represents level e and the lower level g . The topological analogy with a spatial interferometer is striking (compare with Fig. 11).

Let us focus now on the effect of the coherent field in the cavity placed between the Ramsey zones. This field acts, as seen above, as a meter pointing towards the atomic energy. As soon as the two components of the field cease to overlap, this meter could tell us unambiguously whether the atom crosses the interferometer in e or in g and the Ramsey interference should vanish. This is again complementarity in action, an effect fully similar to the Rabi oscillation collapse analyzed above. The Ramsey interference between the states e and g merely replaces the Rabi oscillation corresponding to the interference between the dipole states $|e\rangle + |g\rangle$ and $|e\rangle - |g\rangle$. To observe this effect, we have recorded the Ramsey fringes for a coherent field containing on average $\bar{n} = 9$ photons and for various detunings δ . Since the cat states dephasing is inversely proportional to δ , the overlap between the two field components increases as δ is decreased [from top to bottom in Fig. 24(b)]. The Ramsey fringe contrast accordingly decreases. The fringe amplitude directly measures the scalar product of the two

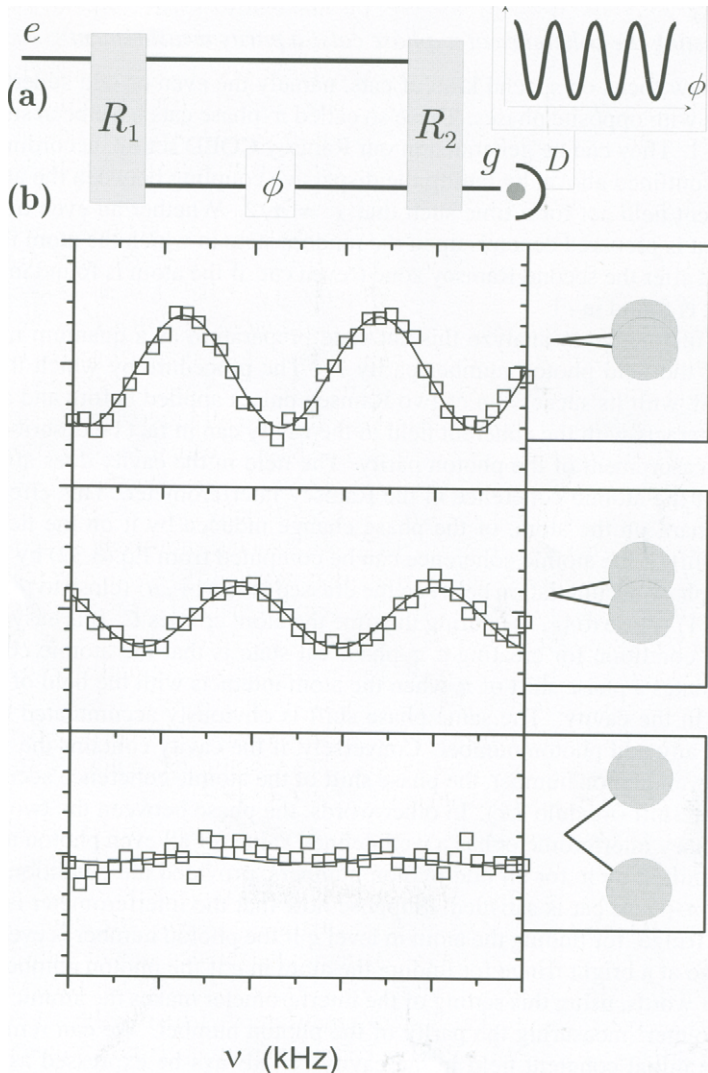


Fig. 24. (a) Scheme of a Ramsey interference process showing the two paths followed by the atom in level e or g . (b) Collapse of Ramsey fringes when the cavity C between R_1 and R_2 initially contains a coherent field with an amplitude $|\alpha| = \sqrt{9.5} = 3.1$, The atom-cavity detuning is $\delta/2\pi = 712$, 347 and 104 kHz respectively, from top to bottom. Points are experimental and curves are sinusoidal fits. Insets show the phase space representation of the final field components in C . Adapted from [16].

field component states.

3.5. Testing the coherence of π -phase cats: a parity measurement

Let us now focus on special kind of cats, namely the even or odd superposition of fields with opposite phases. These so called π -phase cats have been studied in Section 1. They can be generated in our Ramsey CQED set up, according to the method outlined above, by letting the dispersive coupling between the atom and a coherent field act for a time such that $\chi = \pi/2$. Whether an even or an odd phase cat is prepared depends upon the random state in which the atom is finally detected after the second Ramsey zone ('even cat' if the atom is found in g , 'odd cat' if it is found in e)

It is instructive to analyze this cat state preparation as a quantum measurement of the field photon number parity \mathcal{P} . The procedure by which the cat is prepared, with its succession of two Ramsey pulses applied before and after the atom interacts with the coherent field in the cavity can in fact be described as an ideal measurement of the photon parity. The field in the cavity does affects the phase of the atomic coherence in the Ramsey interferometer. This effect is the counterpart, on the atom, of the phase change induced by it on the field. The phase shift of the atomic coherence can be computed from Eq.(3.32) by estimating the phase accumulation between the dressed levels $|+, n\rangle$ (close to $|e, n\rangle$) and $|-, n-1\rangle$ (close to $|g, n\rangle$) during the time the atom crosses C . It is easy to show that the condition for creating a π -phase cat state is that the atomic coherence accumulates a phase shift of π when the atom interacts with the field of a single photon in the cavity. The same phase shift is obviously accumulated (modulo 2π) for any odd photon number. Conversely, if the cavity contains the vacuum, or any even photon number, the phase shift of the atomic coherence accumulates no phase shift (modulo 2π). In other words, the phase between the two arms of the Ramsey interferometer has a well defined value for all even photon numbers, and is shifted by π for all odd photon numbers, provided the condition for creating a π -phase cat is satisfied. Suppose now that the interferometer is set at a 'bright fringe' for finding the atom in level g if the photon number is even. It is then also at a bright fringe for finding the atom in e if the photon number is odd. In other words, using this setting of the interferometer makes the atomic state act as a 'pointer' measuring the parity of the photon number. We can remark now that the initial coherent field in the cavity can always be expressed as a linear superposition of even and odd cat states according to:

$$|\beta\rangle = \frac{1}{2}[|\beta\rangle + |-\beta\rangle] + \frac{1}{2}[|\beta\rangle - |-\beta\rangle]. \quad (3.39)$$

This analysis leads us to interpret the cat generation, when the atom has interacted with the field and has been detected, as a collapse resulting from an

information acquisition about the field. The atom, combined with the Ramsey interferometer, is a measuring device for the photon parity. Since the state to be measured is an equal weight superposition of two eigenstates with different parity eigenvalues, the outcome of the measurement is random, and after it the field is found in the corresponding eigenstate, i.e. in the even cat state $[|\beta\rangle + |-\beta\rangle]/\sqrt{2}$ if the atom is found in g , in the odd cat state $[|\beta\rangle - |-\beta\rangle]/\sqrt{2}$ if the atom is found in e . This description of the experiment is fully equivalent to the one given above, in terms of phase shifts of opposite signs experienced by the two field components interacting with the atom.

These parity considerations shed an interesting light on some already discussed properties of the π -phase cats. We have shown in Section 2 that the coherence of the cat state is destroyed as soon as a single photon is lost in the environment. According to Eq.(1.52) a photon annihilation process switches the parity of a π phase cat state. When the parity of the superposition is changed, the sign of the interference term in the cat quadrature signal, signature of the state coherence, is also changed. In fact, we do not know for sure when a photon is lost if we do not look at the environment. We can only know the probability for a photon to be lost. As soon as this probability is 50%, we can say that the system is in a statistical mixture of even and odd cat states. The interference term is then canceled. We retrieve in this way the conclusions reached earlier about the fragility of this state.

If we could observe the environment and detect the photons lost into it one by one, we could ‘see’ the cat state undergo quantum jumps between even and odd states, remaining in a coherent superposition whose phase would evolve under a stochastic process. This approach is the one adopted in the Monte Carlo calculations in quantum optics [60], in which single stochastic trajectories of a quantum system are followed and the density matrix reconstructed by summing over these trajectories. To say that the coherence of a cat state is lost is merely a statement about the fact that we are renouncing to follow the evolution of the environment.

In fact, observing the quantum jumps of the field under the effect of decoherence does not even require a direct detection of the environment. It is enough to measure the photon number parity operator, according to the atomic interferometric method described above. A succession of atoms is sent across the apparatus experiencing the Ramsey pulses and interacting in between with the cavity field. Depending on the cat state parity, these probe atoms will be detected in g or in e . Any parity jump will be revealed by a sudden change of the detected atomic level. Such an experiment, not yet performed, would be a direct way to witness the field quantum jumps and to follow the decoherence process as it happens in real time. The continuous observation of the field’s parity could also be used to control the decoherence process, as proposed in [61]. As soon as a change of parity has been observed, one could send across the cavity a single resonant atom

whose interaction time would be adjusted so that it would emit one photon in it with near unity probability. This would approximately restore the field parity to the value it had before the parity jump. The experiment would be a very delicate one, requiring two kinds of atom-field interaction, a non-resonant dispersive one for the atoms probing the parity and a resonant one for the ‘correcting’ atoms. Such a procedure is only one example of the ingenious error correction codes proposed in quantum information to fight the effects of decoherence [1].

The parity analysis clearly explains the correlations between the successive atoms interacting with a π phase cat cavity field. In absence of decoherence, the detection of the first atom, which fixes the cat parity, forces the outcome of the measurement for the second atom (and all the other ones) to be the same. In other words, there is a 100% correlation between the measurement results for two atoms interacting successively with the cavity field. This is a mere statement of the fundamental postulate of quantum physics about measurement. If decoherence has occurred between the two atoms, on the other hand, this correlation is destroyed. Studying the loss of correlation as a function of the delay between the preparing atom and a probe atom thus constitutes a simple way to analyze decoherence. The experiment would consist in repeating many times the sequence, sending a pair of preparing and probe atoms with increasing delays and reconstructing by a statistical analysis the conditional probability for finding the second atom in the same state as the first one. This probability should evolve from 1 to 1/2 as the delay between the two atoms is increased and the decoherence time could be obtained from this experiment. Such an ideal correlation measurement has not yet been performed on a π -phase cat state. A decoherence experiment along the same line has however been realized on cat state with phase splittings of ~ 100 degrees and ~ 50 degrees between the field components, for average photon numbers between 3 and 5 [16]. The two-atom correlation signal is then not as simple to understand as in the π -phase cat, but the calculation shows that a two atom-correlation signal can again be constructed, which is maximal at zero delay between the two atoms and decreases towards zero as decoherence progresses in the time interval between them. This correlation signal has actually been observed in the experiment, showing a very good agreement with the theoretical predictions. The dependence of the decoherence rate on the separation between the two cat components has also been demonstrated, the process becoming faster as this separation is increased, in good agreements with the results of Section 2.

A last interesting property of the photon number parity operator is worth noticing. As mentioned in section 1, the Wigner function W of a field state is directly obtained by translating this field in phase space and then measuring the average parity \mathcal{P} of the resulting field. This result has lead to an ingenious proposal for the measurement of W in CQED [62]. Given a field in a cavity sandwiched be-

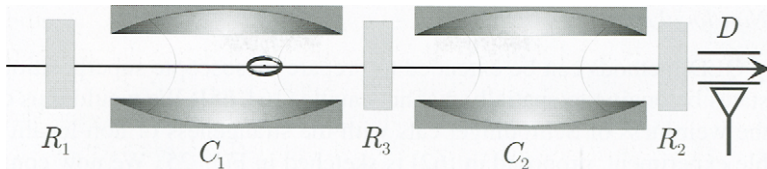


Fig. 25. Scheme of a non-local Schrödinger cat experiment

tween two Ramsey zones, displace it by a given amount α and send a probe atom across the set-up to measure the field parity according to the method described above. In general the displaced field will not be in a parity eigenstate and the outcome of the measurement will be random. Repeat the experiment many time with the same settings and reconstruct in this way the expectation value of the parity in the displaced field. You obtain, according to Eq.(1.61), the value of $W(\alpha)$. Then change α and repeat the procedure. You sample in this way W at all points in phase space and get the whole W function.

This method is much more direct than the standard quantum optics technique for determining W , which consists in measuring all the quadrature field fluctuations and reconstructing the Wigner function by the inverse Radon transform (see section 2). The parity measurement method has not yet been applied to a cat state, but we have demonstrated it for a one-photon Fock state prepared in the cavity and shown that the Wigner function of this state presents negative values, a clear sign of non-classical behavior [63]. Studying in this way the Wigner function of a π -phase cat and recording the fast decoherence induced decay of its interference term is an important goal of our CQED experimental program.

Let us finally relate this CQED W measurement method to the procedure to determine the Q function described above. In both cases, the field to be measured needs to be translated in phase space by an amount corresponding to the coordinate for which the value of the function is sought. Once the displacement made, we need to measure either the expectation value of the projection operator in vacuum [for the Q function, see Eq.(1.55)], or the photon parity operator [for W , see Eq.(1.61)]. These measurements are both performed by statistical methods, accumulating data on probe atoms sent across the cavity. For the Q function, the absorption of resonant probe atoms needs to be detected, whereas for the W function a Ramsey interferometry measurement needs to be performed on non-resonant atoms.

3.6. Non-local cats

Cavity QED methods can be extended to prepare mesoscopic superpositions of field states belonging to spatially distinct cavities [64, 65]. We would thus combine the weirdness of Schrödinger cats with the strangeness of non-locality. A possible experiment, proposed in [62] is sketched in Fig. 25. We now consider two identical cavities C_1 and C_2 , successively crossed by an atomic beam. As in the single cavity version, classical $\pi/2$ pulses are applied to the atom in R_1 before C_1 and in R_2 after C_2 , prior to detection. A π classical pulse can also be applied to the atoms between C_1 and C_2 in R_3 , giving the possibility to exchange the atomic states e and g between the two cavities. The same coherent field β is initially injected in both cavities by coupling them via a T -shaped wave guide to a classical source. Each atom crossing successively the two cavities carries information between them, resulting in an entanglement between field states localized at different positions.

In a first version of the experiment, the R_3 pulse is switched off. The two cavity then experience the same atom-field interaction as in the single cavity case discussed above. The final atom's detection results in the preparation of states of the form:

$$\frac{1}{\sqrt{2}}[|\beta e^{i\chi}, \beta e^{i\chi}\rangle \pm |\beta e^{-i\chi}, \beta e^{-i\chi}\rangle], \quad (3.40)$$

which are clearly entangled. The coherence of these states and the difference with classical mixtures can be tested, as discussed above, by sending probe atoms across the set-up and performing atom correlation experiments. Alternatively, the R_3 pulse can be activated. In this case, the fields in the two cavity experience phase shifts of opposite signs, resulting in the generation of states of the form:

$$\frac{1}{\sqrt{2}}[|\beta e^{i\chi}, \beta e^{-i\chi}\rangle \pm |\beta e^{-i\chi}, \beta e^{i\chi}\rangle], \quad (3.41)$$

which are again non-local entangled states. It is also possible, in a final experimental stage, to inject in both cavities a second coherent field of same amplitude as the first, with a phase adjusted to cancel one of the two field components. The resulting field is then:

$$\frac{1}{\sqrt{2}}[|0, 0\rangle \pm | - 2i \sin \chi \beta, -2i \sin \chi \beta\rangle], \quad (3.42)$$

in the case where R_3 is inactive and:

$$\frac{1}{\sqrt{2}}[|0, -2i \sin \chi \beta\rangle \pm | - 2i \sin \chi \beta, 0\rangle], \quad (3.43)$$

when the switching R_3 is performed. The non-local phase cats are then transformed into ‘amplitude cats’. The states described by Eq.(3.43) are particularly interesting. They are coherent superpositions of a state in which the first cavity contains a coherent field while the second is empty with the state representing the reverse situation. In other words, all the photon of the field are found together in one cavity or in the other, with equal probability and a full quantum coherence between the two states. This is the situation we have already encountered in section 2 when describing the $|0, n\rangle + |n, 0\rangle$ state produced by a combination of non-linear beam-splitters. In CQED, it is the non-linear interaction of the field with a single atom which makes this coherent and collective channeling of photons possible. It realizes a situation very different from the ones usually produced by linear beam-splitters in quantum optics. Various tests of the non-local properties of these phase or amplitude non-local cats are possible, including the study of novel kinds of Bell’s inequalities [66]. We will not discuss them any further here.

4. Collapse and revivals of matter-waves: proposals for atomic Schrödinger cats

The manipulation of cold atom matter waves in Bose Einstein condensates (BEC) has recently opened the new field of ‘atomic quantum optics’ in which the coherence properties of matter can be studied and exploited in a way similar to what is done in quantum optics with photons [67]. Whereas non-linearities must be induced in quantum optics by the introduction of an external non-linear medium, they are ‘given for free’ in BEC atom optics, since the atoms, contrary to photons, naturally interact with each other, introducing spontaneous non-linear Kerr-like effects in the propagation of matter waves. Collapse and revival effects related to the ones of quantum optics are expected in atom optics and Schrödinger cat states of matter could be generated using methods which are direct generalizations of optical processes. In this section, we compare non linear quantum optics with Bose-Einstein condensate matter-wave physics and describe how Schrödinger cat states made of atoms could be produced and studied. Analogies and differences with CQED physics will be stressed. Other discussions about collapse and revivals and Schrödinger cat state generation in BEC can be found in [68–73].

The techniques used to prepare atomic Bose-Einstein condensates, which involve laser and evaporative cooling will not be described here. We will neither discuss the numerous beautiful experiments which have demonstrated over the last nine years the remarkable coherence properties of this new state of matter (see for example the Les Houches lectures by Y. Castin [74]). Our goal is just

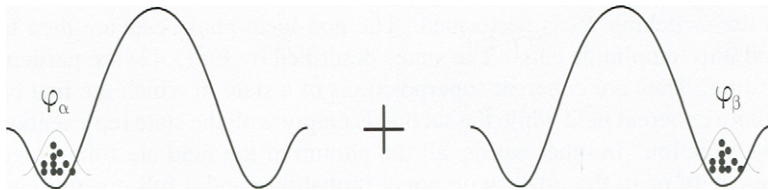


Fig. 26. A non-local cat made of N bosons shared between two potential wells: the particles are in a superposition of a state where they are all in the left well with a state where they are all in the right well.

to describe the principle of matter-wave mesoscopic state superposition experiments in an ideal situation. We will thus assume that a small sample of bosonic atoms (from a few to a few tens) is prepared in the ground state of a potential well. All atoms are supposed to be in the condensed phase (zero temperature limit of BEC) and we wish to exploit the collective properties of this gas of weakly interacting bosons in order to generate and study mesoscopic states. The typical situation we have in mind is sketched in Fig. 26. We would like to prepare the N -identical atoms in a double potential well in a superposition of a state in which they are all in the left well with the similar state in which they are all in the right one. The left and right single particle wave functions (ϕ_α and ϕ_β respectively) are non overlapping and the inter-well barrier is high enough, making tunneling negligible. This is a non-classical situation, reminiscent of the one we have considered in sections 2 and 3 with photons [see Eq.(3.43)]. Although this experiment has not been yet performed, we will show that it can be realistically envisioned, at least for relatively small atom numbers. Before describing the interatomic collisions processes which can be exploited to prepare these states, we will start by recalling the formalism adapted to the description of this system, first in the simplified case of non-interacting bosons.

4.1. Ideal Bose-Einstein condensate without interactions

Consider a system of N bosons (without internal structure for simplicity) in a trap. We call $|\phi_\mu\rangle$ (energy ϵ_μ) the basis of single particle energy eigenstates (depending on the trap potential). We adopt the formalism of second quantization. We call a_μ , a_μ^\dagger the annihilation and creation operators of one boson in state $|\phi_\mu\rangle$. They satisfy the canonical commutation rules of the operators for independent harmonic oscillators. We also call $|0\rangle$ the ‘particle vacuum’. The system’s state in which n_1 particles are in $|\phi_1\rangle$, ..., n_μ particles in $|\phi_\mu\rangle$ is:

$$|n_1 : \phi_1; n_2 : \phi_2; \dots; n_\mu : \phi_\mu; \dots\rangle =$$

$$\frac{1}{\sqrt{n_1!n_2!\dots n_\mu!\dots}}(a_1^{\dagger(n_1)}a_2^{\dagger(n_2)}\dots a_\mu^{\dagger(n_\mu)}\dots)|0\rangle , \quad (4.1)$$

while the energy operator of the system is:

$$H = \sum_{\mu} a_{\mu}^{\dagger} a_{\mu} \varepsilon_{\mu} . \quad (4.2)$$

The analogy with a light field whose photons belong to an ensemble of modes is evident. To each one-particle operator

$$V = \sum_{\mu, \nu} |\phi_{\mu}\rangle \langle \phi_{\mu}| V |\phi_{\nu}\rangle \langle \phi_{\nu}| , \quad (4.3)$$

corresponds the second quantization version:

$$\mathcal{V} = \sum_{\mu, \nu} a_{\nu} a_{\mu}^{\dagger} v_{\mu \nu} a_{\nu} \quad (v_{\mu \nu} = \langle \phi_{\mu} | V | \phi_{\nu} \rangle) . \quad (4.4)$$

The operator \mathcal{V} describes, in second quantization, the observable $\sum_{i=1,N} V(i)$, sum of one-particle operators. Let us now describe in this formalism a superposition of states. N particles in state $\lambda_a |\phi_a\rangle + \lambda_b |\phi_b\rangle$ are, in second quantization, described by:

$$|N : \lambda_{\alpha} \phi_{\alpha} + \lambda_{\beta} \phi_{\beta}\rangle = \frac{1}{\sqrt{N!}} (\lambda_{\alpha} a_{\alpha}^{\dagger} + \lambda_{\beta} a_{\beta}^{\dagger})^N |0\rangle . \quad (4.5)$$

Note the analogy with N photons in a state superposition of two modes. A particularly interesting superposition situation corresponds to a localized particle. In usual formalism it is described by

$$|\mathbf{r}\rangle = \sum_{\mu} |\phi_{\mu}\rangle \langle \phi_{\mu}| \mathbf{r} \rangle = \sum_{\mu} \phi_{\mu}^{*}(\mathbf{r}) |\phi_{\mu}\rangle . \quad (4.6)$$

In second quantization, this state becomes:

$$|1 : \mathbf{r}\rangle = \sum_{\mu} \varphi_{\mu}^{*}(\mathbf{r}) a_{\mu}^{\dagger} |0\rangle , \quad (4.7)$$

which naturally introduces the field operator $\Psi^{+}(\mathbf{r})$ creating a particle at point \mathbf{r} :

$$\Psi^{+}(\mathbf{r}) = \sum_{\mu} \varphi_{\mu}^{*}(\mathbf{r}) a_{\mu}^{\dagger} , \quad (4.8)$$

and the adjoint field annihilation operator:

$$\Psi(\mathbf{r}) = \sum_{\mu} \varphi_{\mu}(\mathbf{r}) a_{\mu}. \quad (4.9)$$

These operators satisfy the commutation relation of boson fields:

$$[\Psi(\mathbf{r}_1), \Psi^+(\mathbf{r}_2)] = \delta(\mathbf{r}_1 - \mathbf{r}_2), \quad (4.10)$$

and they can be combined to define the second quantization particle density operator:

$$n_D(\mathbf{r}) = \Psi^+(\mathbf{r})\Psi(\mathbf{r}). \quad (4.11)$$

which is the second quantization version of the projector operator $|\mathbf{r}\rangle\langle\mathbf{r}|$. Note the analogy between the annihilation and creation field operators and the positive and negative frequency parts of the electric field operator in quantum optics. The particle density at point \mathbf{r} , equal to the mean value in the system's state of the operator $\Psi^+(\mathbf{r})\Psi^-(\mathbf{r})$ is the analog of the photon counting rate, proportional to the expectation value of the product of the negative and positive frequency parts of the field.

We consider now an ideal ‘bimodal’ condensate at $T = 0$ K evolving in a double potential with two minima separated by a height-adjustable barrier. The ground states of the two wells, when tunneling is negligible, are called $|\phi_{\alpha}\rangle$ and $|\phi_{\beta}\rangle$. By lowering the barrier for a given time, one can mix the two states in a controlled way. The situation is very similar to the evolution of a field in a two-mode system under the effect of a linear beam-splitter. We assume that the system is initially prepared in one of the wells, the barrier between the two wells being high enough to make tunneling impossible. The atoms are then all described by the localized wave function ϕ_{α} . We then suddenly lower the barrier to allow for tunneling. The tunneling Hamiltonian can be written as:

$$H_J = -\hbar J(a_{\alpha}^{\dagger}a_{\beta} + a_{\alpha}a_{\beta}^{\dagger}), \quad (4.12)$$

where J is a frequency measuring the tunneling rate (which we assume here without loss of generality real). The condensate starts to oscillate between the two wells, its state at time t being:

$$|N : \cos(Jt)\phi_{\alpha} + i \sin(Jt)\phi_{\beta}\rangle = \frac{1}{\sqrt{N!}} (\cos(Jt)a_{\alpha}^{\dagger} + i \sin(Jt)a_{\beta}^{\dagger})^N |0\rangle. \quad (4.13)$$

The evolution is similar to the one produced by a beam-splitter in quantum optics. The case $Jt = \pi/4$ corresponds to a symmetrical beam-splitter. Oscillation between the two wells is also analogous to the Josephson effect in a junction

between two superconductors. Any bimodal distribution of the particles between the two wells can be obtained, freezing the system by raising suddenly the barrier at the appropriate time. We should note that the state prepared in this way is a non-entangled product state. The N particles are all in the same one-particle state, a coherent superposition of ϕ_α and ϕ_β . The state (4.13) belongs to a class of bi-modal states taking the general form:

$$\begin{aligned} |N; \theta, \phi\rangle &= \frac{1}{\sqrt{N!}} (\cos \theta a_\alpha^\dagger + \sin \theta e^{i\phi} a_\beta^\dagger)^N |0\rangle \\ &= \sum_p \binom{N}{p}^{1/2} \cos^{N-p} \theta \sin^p \theta e^{ip\phi} |N-p\rangle_\alpha |p\rangle_\beta , \end{aligned} \quad (4.14)$$

which we will call ‘phase states’ for a reason which will become clear below. These states are defined by three parameters, the atom number N , the mixing angle θ , and the phase angle ϕ . In Eq.(4.14), the $\binom{N}{p}$ symbol is the binomial coefficient already introduced in the beam-splitter theory. The phase state (4.14) corresponds to a binomial distribution of particles in the two modes, with a well defined quantum phase ϕ between the two modes. The particle mean numbers and the variance of their difference are given by:

$$N_\alpha = N \cos^2 \theta ; \quad N_\beta = N \sin^2 \theta ; \quad \Delta(N_\alpha - N_\beta) = \sqrt{N} \sin 2\theta . \quad (4.15)$$

The fluctuation $\Delta(N_\alpha - N_\beta)$ is maximum, equal to \sqrt{N} , for a symmetrical condensate ($\theta = \pi/4$) and zero for a mono-condensate ($\theta = 0$ or $\pi/2$). Let us consider now a symmetrical state. The coherence between Fock states with different particle numbers writes:

$$\begin{aligned} \langle N - p_1; p_1 | N; \pi/4, \phi \rangle \langle N; \pi/4, \phi | N - p_2, p_2 \rangle \\ = \frac{1}{2^N} \binom{N}{p_1}^{1/2} \binom{N}{p_2}^{1/2} e^{i(p_1 - p_2)\phi} . \end{aligned} \quad (4.16)$$

If the phase is unperfectly known [defined by a probability law $P(\phi)$], the system is described by its density operator:

$$\rho = \int_0^{2\pi} d\phi |N; \pi/4, \phi\rangle P(\phi) \langle N; \pi/4, \phi| , \quad (4.17)$$

and the coherence between states with particle numbers p_1 and p_2 in state $|\phi_\beta\rangle$ becomes:

$$\langle N - p_1, p_1 | \rho | N - p_2, p_2 \rangle = \frac{1}{2^N} \binom{N}{p_1}^{1/2} \binom{N}{p_2}^{1/2} \times$$

$$\times \int_0^{2\pi} d\phi P(\phi) e^{i(p_1-p_2)\phi}. \quad (4.18)$$

This equation exhibits a conjugation relation between the phase and the difference of the number of particles in two Fock states related to each other by a non-zero matrix element of ρ . When $P(\phi)$ is a δ function, ρ has non-diagonal elements on a width $p_1 - p_2$ of order \sqrt{N} . The wider $P(\phi)$ is, the narrower the non-diagonal distribution of ρ becomes. At the limit where $P(\phi) = 1/2\pi$ (undetermined phase), ρ is diagonal in $p_1 - p_2$. It is then equivalently described as an incoherent sum of diagonal operators $|N-p, p\rangle\langle N-p, p|$, each representing a projector associated to two condensates with perfectly fixed atom numbers. This complementarity relation between the phase fluctuation $\Delta\phi$ and the width ΔN of the coherent partition of the particle numbers between the two wells is again quite reminiscent of quantum optics. Likewise, by summing projectors on coherent states with different phases, one constructs a field density operator which approaches an incoherent superposition of Fock states when the phase distribution is uniformly distributed.

4.2. Coherent collisions in BEC: the analogy with the Kerr effect in quantum optics

4.2.1. Simple model of elastic binary collisions in a bi-modal condensate

We have so far neglected the interactions between atoms in the condensate. In fact, the atoms undergo binary elastic collisions which affect the dynamical behavior of the matter waves. Two atoms located at points \mathbf{r}_1 and \mathbf{r}_2 interact according to a potential $W(\mathbf{r}_1 - \mathbf{r}_2)$ which, at the low energy limit, can be considered as spherically symmetrical ('S-wave scattering'). To a good approximation, the potential can be described as an isotropic contact term:

$$W(\mathbf{r}_1 - \mathbf{r}_2) \approx \frac{4\pi\hbar^2 a_s}{M} \delta(\mathbf{r}_1 - \mathbf{r}_2), \quad (4.19)$$

where M is the atom mass and a_s the so-called scattering length, a parameter which appears naturally in the quantum description of the collision processes at very low energy [74]. This length can be tuned by applying a magnetic field on the atoms, most efficiently near certain field values corresponding to the so-called Feschbach resonances [75]. The collision probability amplitude depends on the energy level structure of the binary atom system and is strongly affected by the presence of level crossings which are conditioned by the magnetic field. Typically, for collisions between alkali atoms, a_s is of the order of 1 to 10 nm with a sign either positive (repulsive force between atoms) or negative (attractive

force). We consider here the repulsive case. The mean value of the interaction energy for a simple condensate of N atoms in state $|\phi_\alpha\rangle$ is:

$$\langle W \rangle = N(N-1) \frac{2\pi\hbar^2 a_s}{M} \int d^3\mathbf{r} |\phi_\alpha(\mathbf{r})|^4. \quad (4.20)$$

It appears as the expectation value in the condensate state of the collision Hamiltonian:

$$W = \frac{1}{2}\hbar g_c \hat{N}_\alpha (\hat{N}_\alpha - 1), \quad (4.21)$$

with the coupling g_c defined as:

$$g_c = \frac{4\pi\hbar a_s}{M} \int d^3\mathbf{r} |\phi_\alpha(\mathbf{r})|^4. \quad (4.22)$$

This hamitonian is proportional to the number $N(N-1)/2$ of atom pairs in the condensate, a result which can be understood by a simple book-keeping argument. For a double condensate, we must evaluate separately the collisions between atoms in each mode and the intermode collisions. Assuming to simplify that the interactions are the same in each subsystem and negligible between them (which is obviously the case if the two modes are spatially separated as in Fig. 26), we get:

$$W = W_\alpha + W_\beta = \frac{1}{2}\hbar g_c \hat{N}_\alpha (\hat{N}_\alpha - 1) + \frac{1}{2}\hbar g_c \hat{N}_\beta (\hat{N}_\beta - 1); \quad (4.23)$$

We should stress the extreme simplicity of this model which accounts well for the effects of collisions in the condensate. They are described by a single parameter, the tunable scattering length a_s . The situation is much simpler than in a classical gas where collisions are a source of randomness and irreversibility. In a zero-temperature degenerate condensate, the bosons after a collision process must stay in the same quantum state as before. The collisions constantly reshuffle the particles in the same state, without generating any disorder.

The interactions described by Eqs.(4.21,4.23) are reminiscent of a Kerr Hamiltonian in optics [76]. The non-linear interaction of a light wave with a transparent medium contains terms proportional to the square of the light intensity of the form $\gamma(a^\dagger a)^2$, where γ is a non-linear susceptibility. Its main effect is to make the refractive index of the medium intensity-dependent. These Kerr non linearities give rise to a phase spreading of light beams propagating in the medium over long distances (for example along optical fibers). It could, at least in theory, also lead to phase revival effects and to the generation of Schrödinger cat states of light. This cat generation method has been suggested in the 1980s as a promising way to study mesoscopic field superpositions, but experiments have not been

successful, due in part to too strong losses in the non-linear medium. The advent of BEC physics, which naturally introduces a Kerr like coupling of matter waves, has lead to a revival of these early proposals which we will now briefly present.

4.2.2. Collapse and revivals of a condensate bi-modal phase state: the optical analogy

We study now the effect of the atomic collisions on the phase of a bimodal condensate initially prepared in a symmetric phase state. We follow here closely the analysis developed in [44]. We assume that the tunnelling between the two modes is negligible (high inter-well barrier). It is convenient to expand the initial phase state along the Fock states. We change the notations and define N_α as $(N/2) + \delta N$ and N_β as $(N/2) - \delta N$. The quantity δN appears as a particle number fluctuation of the order of $\pm\sqrt{N}$. The initial state (time $t = 0$) thus writes:

$$\begin{aligned} |\psi(0)\rangle &= |N; \theta = \pi/4, \phi\rangle \\ &= \sum_{N_\alpha=0}^N \frac{e^{iN\phi/2}}{2^{N/2}} \sqrt{\frac{N!}{N_\alpha!N_\beta!}} e^{-i(N_\alpha-N_\beta)\phi/2} |N_\alpha, N_\beta\rangle. \end{aligned} \quad (4.24)$$

For large N 's, we can develop the factorials (using Stirling formula) and we get the Gaussian approximation:

$$|\psi(0)\rangle \approx \left(\frac{2}{\pi N}\right)^{1/4} \sum_{\delta N} e^{-\delta N^2/N} e^{-i\delta N\phi} \left| \frac{N}{2} + \delta N, \frac{N}{2} - \delta N \right\rangle. \quad (4.25)$$

The sum in this expression, in principle over δN between $-N/2$ and $+N/2$, is in practice restricted to $-\sqrt{N} < \delta N < \sqrt{N}$.

A simple calculation shows that a Fock state with given δN is an eigenstate of the Hamiltonian W , with the eigen energy:

$$\langle W \rangle = \hbar g_c \frac{N}{2} \left(\frac{N}{2} - 1 \right) + \hbar g_c \delta N^2. \quad (4.26)$$

This collisional energy varies quadratically with δN . The minimum energy state corresponds to the best possible equipartition of the particles between the two modes $\delta N = 0$ if N is even, $\delta N = \pm 1$ if N is odd. Let us now study the effect of these collisions on the evolution of a bimodal phase state of the form (4.25). We apply to each Fock component its collisional dephasing, proportional to time and to its collisional energy (4.26). Up to a global phase factor, we get:

$$|\psi(t)\rangle \approx \left(\frac{2}{\pi N}\right)^{1/4} \sum_{\delta N} e^{-\delta N^2/N} e^{-i\delta N[\phi+(\omega_\alpha - \omega_\beta)t]} \times$$

$$\times e^{-ig_c\delta N^2 t} \left| \frac{N}{2} + \delta N, \frac{N}{2} - \delta N \right\rangle, \quad (4.27)$$

where $\hbar\omega_\alpha$ and $\hbar\omega_\beta$ are the chemical potentials of the two condensate components. The phases in the Fock state expansion present a term linear in δN corresponding to the time evolution of a non-interacting gas and a Kerr-like term quadratic in δN describing the effect of the collisions. The phase coherence of this state is revealed by computing the expectation value of the interference term $\langle a_\beta^\dagger a_\alpha \rangle$ in it:

$$\langle a_\beta^\dagger a_\alpha \rangle = \left(\frac{N}{2\pi} \right)^{1/2} \sum_{\delta N} e^{-2\delta N^2/N} e^{-i[\phi+(\omega_\alpha-\omega_\beta)t]} e^{-ig_c(2\delta N+1)t}. \quad (4.28)$$

The phase spreading of the last exponential in Eq.(4.28) results in a collapse of this expectation value. The collapse is complete when the phase has fanned out over a full 2π angle over the distribution of δN , whose width is of the order of $2\sqrt{N}$. This occurs within a time T_{collapse} :

$$T_{\text{collapse}} \approx \frac{\pi}{g_c \sqrt{N}}, \quad (4.29)$$

inversely proportional to the collision strength g_c and to the square root of the particle number. This effect is quite analogous to the spreading of the Gaussian wave packet of a free particle in a one dimension propagation problem, the phase ϕ and the fluctuation of the number of bosons δN being replaced by the particle's position and momentum respectively. There is however a big difference between the condensate phase's and the particle position's spreadings. In the latter case the sum over momentum is a continuous integral, whereas, in the condensate situation, the sum over δN is discrete, expressing the graininess of the matter wave. While the free particle wave function spreading is an irreversible process, the phase condensate collapse is reversible. All the phases in Eq.(4.28) are refocused to the same value (modulo 2π) after a time T_{revival} :

$$T_{\text{revival}} = \frac{\pi}{g_c}, \quad (4.30)$$

as well as at all multiples of this time. At these precise moments, the coherence between the two modes of the condensates is fully restored to its initial value. The first revival time is \sqrt{N} times larger than the collapse time, and is independent of the number of particles. It depends only upon the non-linearity g_c introduced by the collisions.

We have limited this discussion, for simplicity, to bi-modal condensates, e.g. prepared in two separated potential wells. It can be generalized to a multiple-well

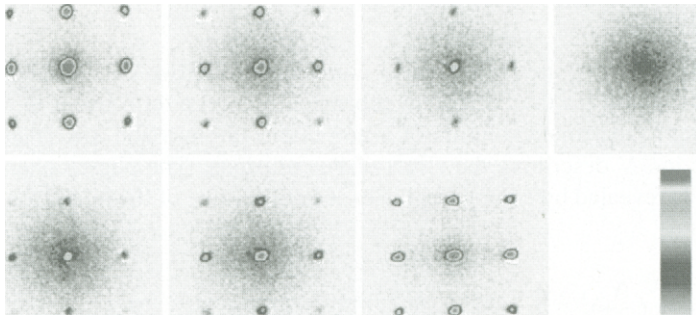


Fig. 27. Signal showing the matter wave collapse and revival in an optical lattice. The successive frames are snapshots of the expanded condensate, corresponding to increasing durations of the intra-well collision process (see text). The time increases from left to right and from top to bottom. At short times, the condensate has a well defined phase, resulting in a Bragg like pattern for the expanded atomic cloud. At the collapse time (last frame at the right of first line) the Bragg pattern is washed out. It then revives at twice the collapse time. Up to five successive collapses and revivals have been observed in this way. Reprinted with permission from [77].

situation, such as a condensate placed in a crystal-like three-dimension lattice. Let us say a few words about this configuration which has been studied extensively theoretically and has recently been investigated in beautiful experiments. They are realized by first preparing a condensate in a magnetic trap, then superposing this trap with an optical lattice made by a combination of three sets of counter propagating light beams creating a three dimensional optical force lattice acting on the atoms. If the wells are shallow enough so that tunneling between them is dominant, the state of the condensate is a big matter wave of the Bloch type, coherent superposition of the ground state wave functions of all the potential wells in the lattice. This state is the multiple well counterpart of the bi-modal states described above. After preparing this initial state, the depth of the lattice is suddenly increased, in a time short compared to the state evolution, and a final lattice configuration is reached in which the tunneling is negligible and the effects of intra-well collisions dominant. These collisions then induce, as in the bimodal case, collapses and revivals of the coherence between any couple of wells in the lattice. Typically, the number of atoms per well is of the order of 2 to 3 and about 10^5 wells are populated in the lattice.

To observe the effect, the optical lattice is suddenly suppressed after having left the collision act during a given time interval. The condensate is then allowed to expand freely for some time, before a picture of the expanded gas is made by absorption of a probe laser beam. When the condensate exhibits inter-well co-

herence, the expanded gas presents interference terms in its density, reminiscent of a Bragg diffraction pattern. When the inter-well coherence has collapsed, the density interferences vanish and the image of the condensate looks like an incoherent diffraction pattern. The experiment is resumed with various time delays between the sudden raise of the inter-well barriers and the condensate release. A periodic change of the image aspect, going in a reversible way from coherent to incoherent scattering-like patterns is observed (see Fig. 27).

There is a strong analogy between this collision induced effect and the Kerr-induced phase spreading of a coherent field in Quantum Optics. The expectation value of the photonic field operator $\langle a \rangle$ then evolves as $\langle a_\beta^\dagger a_\alpha \rangle$ in the boson situation. In the evolution equation, the non-linear Kerr susceptibility γ merely replaces the collision constant g_c and the number of photons plays the role of the boson number. To show in a quantitative way the evolution of the phase in this problem, we have represented in Fig. 28 adapted from [77] the Q function of a coherent field containing on average 3 photons and subjected to a dephasing Kerr effect. The values of the Q function are indicated by a code of shades. The function is plotted at different times following the field initial preparation, up to the first revival time. The pictures clearly show the fast spreading of the field and its sharp refocusing at T_{revival} . It is remarkable to note that this calculation has been performed for a small average particle number, for which the approximations made in the above model (Stirling formula and Gaussian limit) are not valid. Yet, the basic features of the model remain true.

The Q function evolution displays another remarkable feature. At the time $T_{\text{revival}}/2$, the spreading phase of the field refocuses into two components, separated by π (see Fig. 28). This indicates the transient generation of a π -phase cat state induced by the Kerr non-linearity. The appearance of this state is easy to understand by simple arguments based on the parity properties of the phase cat states discussed above (section 1 and 3). At the time $T_{\text{revival}}/2 = \pi/2\gamma$, the $n = 2p$ even Fock states in the coherent state expansion have undergone a shift $\gamma(2p)^2 \times \pi/2\gamma$, equal to 0 (modulo 2π). The $n = 2p + 1$ odd Fock states, on the other hand, have experienced a phase shift $\gamma(2p + 1)^2 \times \pi/2\gamma$, equal to $\pi/2$ (modulo 2π). To make explicit the effect of this parity dependent phase shift, it is convenient to expand the initial coherent state as a sum of even and odd cat components, according to Eq.(3.39), and to multiply the even and odd parts by the corresponding phase factor, equal to 1 for the even part, to $e^{i\pi/2}$ for the odd one. At half the revival time, the field state writes:

$$(1/2)(|\alpha\rangle + |-\alpha\rangle) + (e^{i\pi/2}/2)(|\alpha\rangle - |-\alpha\rangle) \\ = \frac{e^{i\pi/4}}{\sqrt{2}} |\alpha\rangle + \frac{e^{-i\pi/4}}{\sqrt{2}} |-\alpha\rangle . \quad (4.31)$$

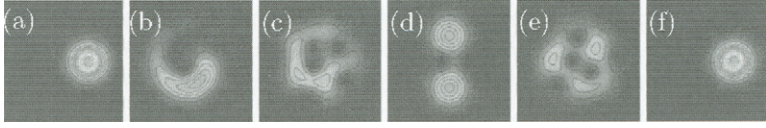


Fig. 28. Evolution of the Q function of an initially coherent field with $\alpha = \sqrt{3}$ in a Kerr non-linear medium. Time for frames (a) to (f) is 0, 0.1, 0.4, 0.5, 0.9 and 1 in units of π/γ . Note the formation of a π phase cat at time $0.5\pi/\gamma$ [frame (d)]. Adapted from [77].

It is a cat state, coherent superposition of two coherent components with opposite phases (although it is not a parity state, since the complex amplitudes of the superposition are not in phase or π out of phase with respect to each other). This process of preparation of cat state has been first described in a paper by Yurke and Stoler [11]. We will show in the next subsection that there is a way to translate this proposal in the condensed boson situation and to use the Kerr-like non-linearity produced by the elastic collisions in the condensate to generate Schrödinger cat states of matter waves.

Let us note, to conclude this subsection, that the collapse and revival phenomenon in photonic or atomic waves presents strong similarities, and also notable differences, with the phenomena bearing the same name in CQED and described in Section 3. Note first that it is not the phase of the field which collapses in the CQED situation, but rather the phase of the Rabi oscillation observed on an atomic signal. Note also that the collapse time of the Rabi oscillation is independent of the photon number for a given vacuum Rabi coupling, whereas it is inversely proportional to the square root of this number in the Kerr collapse. In both cases, the revival occurs after a delay equal to the collapse time multiplied by \sqrt{n} . In both the CQED and the Kerr non-linear optics case, Schrödinger cat states with phase opposite components are produced at half the revival time, but the mechanism of their generation are quite different. In the CQED case, cat states are produced via atom-field entanglement as soon as the collapse has occurred and the dephasing between the cat components evolves continuously, going through a maximum at half the revival time. In the Kerr case, there is only one quantum system (the field) and hence no entanglement. The cat state appears only at specific times, and emerges from a continuous evolution of a phase evolving state. Finally, in the CQED case, only the first revival is clearly marked, while the subsequent ones are smeared out and merged into each other. In a Kerr medium with a pure second order term, the revivals are periodical.

4.3. *Proposal to prepare a Schrödinger cat state in a bi-modal condensate*

The optical Kerr effect analogy suggests that a Schrödinger cat of matter-wave should appear at half the phase revival time $T_{\text{revival}}/2 = \pi/2g$. At this specific

time, the collisional phase appearing in Eq.(4.27) takes the values:

$$g_c(\delta N)^2 T_{\text{revival}}/2\hbar = \frac{\pi}{2} (\delta N)^2 = \begin{cases} 0 & \text{for } \delta N \text{ even} \\ \pi/2 & \text{for } \delta N \text{ odd} \end{cases} \quad (\text{modulo } 2\pi). \quad (4.32)$$

If we express the initial phase state as a sum of a component whose δN 's are even and a component whose δN 's are odd, the evolution produced by the collisions up to time $T_{\text{revival}}/2$ leaves the amplitude of the first component unaltered and phase shifts by $\pi/2$ the amplitude of the second. The separation between even and odd terms in δN is easy to perform analytically, at least when N is even, a situation which we assume fulfilled from now on for simplicity. Inspired by the trick used to write a coherent state as a sum of even and odd π out of phase cats, let us write in the same vein the phase bi-modal state as a superposition of two parity states of the form:

$$\begin{aligned} |\psi^{\text{even}}\rangle &= \frac{1}{2} \frac{1}{2^{N/2}} \left[(a_\alpha^\dagger + e^{-i\bar{\phi}} a_\beta^\dagger)^N |0\rangle + (a_\alpha^\dagger - e^{-i\bar{\phi}} a_\beta^\dagger)^N |0\rangle \right], \\ |\psi^{\text{odd}}\rangle &= \frac{1}{2} \frac{1}{2^{N/2}} \left[(a_\alpha^\dagger + e^{-i\bar{\phi}} a_\beta^\dagger)^N |0\rangle - (a_\alpha^\dagger - e^{-i\bar{\phi}} a_\beta^\dagger)^N |0\rangle \right]. \end{aligned} \quad (4.33)$$

If $N/2$ is an even integer, the first one obviously contains only even powers of δN and the second only odd powers. The δN parity of these states is exchanged if $N/2$ is odd. We have included in the definition of these states the free evolution phase factor (linear in δN) up to the time $T_{\text{revival}}/2$ (phase $\bar{\phi}$ in these expressions). We consider for sake of definiteness the case $N/2$ even and leave the reader to adapt the solution to the $N/2$ odd case. Realizing that the initial state is the sum of the ‘even’ and ‘odd’ states defined above and taking into account the evolution of their phase under the effect of collisions up to the time $T_{\text{revival}}/2$, we find an expression which reminds us of Eq.(4.31):

$$\begin{aligned} |\psi(t = \pi/2g)\rangle &= \frac{1}{2^{N/2}} \frac{e^{-i\pi/4}}{\sqrt{2}} (a_\alpha^\dagger + e^{-i\bar{\phi}} a_\beta^\dagger)^N |0\rangle + \\ &+ \frac{1}{2^{N/2}} \frac{e^{i\pi/4}}{\sqrt{2}} (a_\alpha^\dagger - e^{-i\bar{\phi}} a_\beta^\dagger)^N |0\rangle. \end{aligned} \quad (4.34)$$

The system's state appears now as a superposition of N particles all in the state $\frac{1}{\sqrt{2}}[|\phi_\alpha\rangle + e^{-i\bar{\phi}}|\phi_\beta\rangle]$ with N particles all in the state $\frac{1}{\sqrt{2}}[|\phi_\alpha\rangle - e^{-i\bar{\phi}}|\phi_\beta\rangle]$, obviously a Schrödinger cat situation.

The recipe to prepare such a state could, in principle, follow the stages schematized in Fig. 29, from top to bottom. We realize first a double potential well and start with a condensate with an even number of N bosons prepared in the left well (α), separated from the right well (β) by a high barrier [Fig. 29(a)]. The barrier

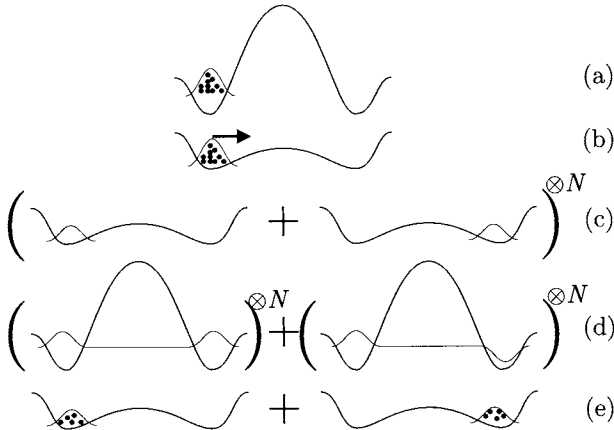


Fig. 29. Creation of a matter Schrödinger cat: the successive stages of the non-local cat preparation are sketched from top to bottom (see text).

is then suddenly lowered at a height such that $J \gg g_c$ [Fig. 29(b)] and we wait a time such that $Jt = \pi/4$: the tunnel effect creates a phase state [Fig. 29(c)]. Note that this is not yet a cat, since all the particles occupy the same quantum state. This is a mere tensor product of N particles in the same wave function, which is expressed by the N exponent at the right of the bracket around the sketch representing this state. The effect of collisions is negligible during this first fast stage. We then suddenly separate the two wells by raising the barrier. The tunnel effect disappears. The collisions become more efficient in each well, due to the extra confinement produced by deepening the wells. Enough time is left for the collisions to achieve the appropriate dephasing. At time $T_{\text{revival}}/2$, a cat state is prepared [Fig. 29(d)]: we have now N atoms, all occupying either one of two orthogonal wave functions. The one particle wave functions are delocalized in both wells, but they are still spatially overlapping. It is possible at this stage to spatially separate the two components of the cat state. To achieve this, the tunnel effect is reestablished by a sudden lowering of the barrier and the system is left to evolve for a quarter period of the coherent oscillation between the two wells (we assume that the collisions have a negligible effect during this time): the N atoms localize at left and at right, in a mesoscopic state superposition [Fig. 29(e)]. The inter-well barrier can then be finally raised, suppressing the tunneling and freezing the non-local cat state. One way to demonstrate the coherence of the cat state generated in this way would be to leave the system alone after the time $T_{\text{revival}}/2$ without raising the inter-well barrier, until the two parts of the cat recombine at time T_{revival} . The recurrence of the bimodal state coherence at this time could be

checked by letting the condensate expand and studying the interference term in the atomic density of the expanded cloud, using a method similar to [77].

We have presented here a very general principle, without discussing the experimental limitations and the causes of decoherence of the system. The loss of a single atom from the condensate during this elaborate succession of operations would be lethal for the cat because the lost atom (or molecule formed by three body recombination) would be in a quantum state entangled with the superposition and its detection would collapse it. As in the CQED photonic case, the method seems to be restricted in practice to the preparation and detection of mesoscopic systems made of a few to a few tens of particles. Their study would nevertheless be of great interest to investigate, on this new system, the quantum-classical boundary.

5. Conclusion: a brief comparison with other mesoscopic state superpositions in quantum optics

We have described various kinds of Schrödinger cat states in quantum or atomic optics. These states are characterized by their extreme fragility and sensitivity to decoherence, which occurs at a rate essentially proportional to the number of particles in the system. This puts severe limits to the size of these cat states. They have to be built within a finite time, to let the processes responsible for the preparation of the superposition to take place. This preparation time must be shorter than the decoherence time of the final cat state and this sets, in practice, an absolute limit to the number of particles in the system. In CQED, the maximum number of photons involved in cat states could not exceed a few hundred, even if the technology of cavities were considerably improved. (A discussion of the maximum size of these CQED cats can be found in [78]). In BEC physics, the atomic cats envisioned in section 4 as well as in other studies [69, 71–73] seem also to be at most of a few tens to a few hundred atoms.

The environment-induced decoherence process we have studied here is of a fundamental quantum nature. In an ideal situation, the system and the environment are both initially, in a pure state. They get entangled together and the coherence of the system is lost when we trace over the environment, expressing in this way our inability to keep track of its complex state. If it were possible to detect all the particles in the environment, the coherence lost in it could be retrieved and cat state interferences restored, in correlation with the recorded state of the environment. This kind of procedure, called quantum erasure, has been demonstrated in some simple cases, but it becomes unpractical for large environments. Other, more realistic methods to preserve the cat state coherence consist in watching the system itself and using this information to correct for decoherence [61]. This

kind of error correction procedure, essential for quantum computing, remains largely to be investigated experimentally. Note also that we must distinguish the decoherence produced by the quantum entanglement of the system with its environment from the more mundane relaxation processes, often called decoherence too, which are induced by a classical noise in the apparatus (e.g. stray fields). This latter form of decoherence is in principle much easier to correct for than the former, since it is of a classical deterministic origin.

The methods we have described to generate these cat states exploit non-linear processes at the single particle level which must be precisely controlled and tuned (interaction of a field with a single atom in CQED or coherent cold atom collisions in BEC). The observation of the cat coherence involves the detection of multiparticle interference effects. Moreover, the experiments generally require low temperature technology (cryogenic atomic beams in the microwave CQED experiments or ultra cold samples of bosons in the BEC proposals). All these experiments are thus extremely difficult, making the exploration in this way of the quantum-classical boundary a very challenging task.

Other experiments investigating entanglement in large atomic samples should be mentioned. They involve two atomic samples at room temperature which get correlated by a light beam propagating through them [79]. The detection of this beam projects the two ensembles into an entangled state, in a process which bears some similarity with the procedure described in section 4.6 where a single atom crossing two cavities was detected, resulting in the collapse of the two cavity field into an entangled state (see P. Zoller Lectures in this Volume). The atomic states in these experiments are conveniently described as large angular momentum states on a sphere (collective Bloch vectors). The length of these vectors is very large since the number of atoms is macroscopic, but the distance on the Bloch sphere of the states involved in the entanglement is relatively small, of the same order as the distance between the cat state components in the experiments discussed in these Notes.

Non-local superpositions of states involving ‘big’ systems at the atomic scale have also been observed in another kind of experiment which appears, at least in its principle, simpler than the ones described in these lectures. Big C_{60} molecules and even biomolecules have been made to interfere in a Young apparatus [80], demonstrating that these objects can exist in state superpositions corresponding to hundreds of nanometers of spatial separation. Since these molecules contain several tens of atoms and that larger molecules can probably be made to interfere in the same way, the question which arises is whether such systems are more ‘macroscopic’ than the cat states described above. In terms of number of elementary particles involved or absolute mass, the answer is yes. But the kind of interferences observed in both cases are very different. In the bosonic or photonic cat states, the particles channeled in the two arms of the interferometer are very

weakly interacting (atoms) or completely independent of each other (photons). To split them collectively in different paths is a delicate multiparticle process, sensitive to all kinds of possible perturbations. In the C_{60} experiments, on the other hand, the atoms are strongly bound together and cannot be split apart by the beam splitter. The molecule essentially behaves as an unbreakable object and, in this sense, must be considered as a single interfering particle, even if its mass is large. The ‘interference of a big molecule with itself’ involves only one relevant parameter of the molecule, the position of its center of mass. This variable is coupled to an ‘internal’ environment (the rotation and vibration states of the molecule), itself interacting with an external environment, the radiation field. The entanglement between the center of mass and these two environments is usually weak. The main cause of decoherence is the radiation of the molecule while it travels across the interferometer, which can result in photons carrying away an information about its path. The photons should have a short enough wavelength, which means that the temperature of the molecule should be very high for this process to be effective. The real difficulty of these experiments is not decoherence, but the shrinking of the molecule de Broglie wavelength which makes interference fringes more and more difficult to observe when the mass is increased.

As shown by this brief discussion, there is a wide variety of effects which can be investigated with the techniques of quantum optics and atomic physics at the boundary between the quantum and the classical worlds. To define the limit between these words in terms of number of particles or mass is not simple and the relevant parameters to consider depend upon the kind of experiment which is performed. The realm of mesoscopic studies becomes even much larger with the possibilities opened by new condensed matter nano-technologies involving superconductors [81] or quantum dots. It would be very interesting to compare, in the context of quantum information science, the kind of cat states realized in quantum optics to those which are made or discussed in solid state physics. This task would have to wait another Les Houches School.

References

- [1] M.A. Nielsen and I.L. Chuang. *Quantum computation and quantum information*. Cambridge University Press, Cambridge, 2000.
- [2] D. Bouwmeester, A. Ekert, and A. Zeilinger. *The physics of quantum information*. Springer, Berlin, 2000.
- [3] W. H. Zurek. Pointer basis of quantum apparatus: Into what mixture does the wave packet collapse? *Phys. Rev. D*, 24(6):1516, 1981.
- [4] A.O. Caldeira and A.J. Leggett. Quantum tunneling in a dissipative system. *Ann. Phys. (N.Y.)*, 149:374, 1983.

- [5] A.O. Caldeira and A.J. Leggett. Influence of damping on quantum interference: An exactly soluble model. *Phys. Rev. A*, 31:1059, 1985.
- [6] E. Joos and H. D. Zeh. The emergence of classical properties through interaction with the environment. *Z. Phys. B*, B59:223, 1985.
- [7] W. H. Zurek. Decoherence, einselection, and the quantum origins of the classical. *Rev. Mod. Phys.*, 75:715, 2003.
- [8] J. A. Wheeler and W. H. Zurek. *Theory of measurement*. Princeton University Press, Princeton, 1983.
- [9] W. H. Zurek. Decoherence and the transition from quantum to classical. *Phys. Today*, 44(10):36, octobre 1991.
- [10] J.P. Paz and W.H. Zurek. Quantum limit of decoherence: environment-induced superselection of energy eigenstates. *Phys. Rev. Lett.*, 82:5181, 1999.
- [11] B. Yurke and D. Stoler. Generating quantum mechanical superpositions of macroscopically distinguishable states via amplitude dispersion. *Phys. Rev. Lett.*, 57:13, 1986.
- [12] B. Yurke, W. Schleich, and D.F. Walls. Quantum superpositions generated by quantum non-demolition measurements. *Phys. Rev. A*42:1703, 1990.
- [13] C.M. Savage, S.L. Braunstein, and D.F. Walls. Macroscopic quantum superpositions by means of single-atom dispersion. *Opt. Lett.*, 15:628, 1990.
- [14] M. Brune, S. Haroche, J.-M. Raimond, L. Davidovich, and N. Zagury. Manipulation of photons in a cavity by dispersive atom-field coupling: Quantum non demolition measurements and generation of Schrödinger cat states. *Phys. Rev. A*, 45:5193, 1992.
- [15] V. Buzek, H. Moya-Cessa, P.L. Knight, and S.D.L. Phoenix. Schrödinger-cat states in the resonant jaynes-cummings model: Collapse and revival of oscillations of the photon-number distribution. *Phys. Rev. A*, 45:8190, 1992.
- [16] M. Brune, E. Hagley, J. Dreyer, X. Maître, A. Maali, C. Wunderlich, J.-M. Raimond, and S. Haroche. Observing the progressive decoherence of the meter in a quantum measurement. *Phys. Rev. Lett.*, 77:4887, 1996.
- [17] C. Monroe, D. M. Meekhof, B. E. King, and D. J. Wineland. A “Schrödinger cat” superposition state of an atom. *Science*, 272:1131, 1996.
- [18] Q.J. Myatt, B.E. King, Q.A. Turchette, C.A. Sackett, D. Kielpinski, W.M. Itano, C. Monroe, and D.J. Wineland. Decoherence of quantum superpositions through coupling to engineered reservoirs. *Nature (London)*, 403:269, 2000.
- [19] A. Auffeves, P. Maioli, T. Meunier, S. Gleyzes, G. Nogues, M. Brune, J.M. Raimond, and S. Haroche. Entanglement of a mesoscopic field with an atom induced by photon graininess in a cavity. *Phys. Rev. Lett.*, 91:230405, 2003.
- [20] R. Loudon. *The Quantum Theory of Light*. Oxford University Press, Oxford, 1983.
- [21] W. Vogel, D.G. Welsch, and S. Wallentowitz. *Quantum optics: an introduction*. Wiley, Berlin, second edition, 2001.
- [22] W.P. Schleich. *Quantum optics in phase space*. Wiley, Berlin, 2001.
- [23] D.F. Walls and G.J. Milburn. *Quantum Optics*. Springer Verlag, New York, 1995.
- [24] S.M. Barnett and P.M. Radmore. *Methods in theoretical quantum optics*. Oxford University Press, Oxford, 1997.
- [25] M.O. Scully and M.S. Zubairy. *Quantum Optics*. Cambridge University Press, Cambridge, 1997.
- [26] C. Cohen-Tannoudji, J. Dupont-Roc, and G. Grynberg. *An Introduction to Quantum Electrodynamics*. Wiley, New York, 1992.

- [27] S. Haroche. Cavity quantum electrodynamics. In J. Dalibard, J.-M. Raimond, and J. Zinn-Justin, editors, *Fundamental Systems in Quantum Optics, Les Houches Summer School, Session LIII*, page 767. North Holland, Amsterdam, 1992.
- [28] S. Haroche and J.-M. Raimond. Manipulation of non-classical field states in a cavity by atom interferometry. In P. Berman, editor, *Advances in Atomic and Molecular Physics, supplement 2*, page 123. Academic Press, New York, 1994.
- [29] P.R. Berman. *Cavity quantum electrodynamics, Advances in atomic, molecular and optical physics, supplement 2*. Academic Press, Boston, 1994.
- [30] J.-M. Raimond, M. Brune, and S. Haroche. Manipulating quantum entanglement with atoms and photons in a cavity. *Rev. Mod. Phys.*, 73:565, 2001.
- [31] R. J. Glauber. Coherent and incoherent states of the radiation field. *Phys. Rev.*, 131(6):2766, 1963.
- [32] U. M. Titulaer and R. J. Glauber. *Phys. Rev.*, 145:1041, 1966.
- [33] E. P. Wigner. On the quantum correction for thermodynamic equilibrium. *Phys. Rev.*, 40:749, 1932.
- [34] C. Cohen-Tannoudji, J. Dupont-Roc, and G. Grynberg. *Photons and Atoms*. Wiley, New York, 1992.
- [35] NV. Weisskopf and E. Wigner. *Z. Phys.*, 63:54, 1930.
- [36] A. Aspect, J. Dalibard, and G. Roger. Experimental test of Bell's inequalities using time-varying analysers. *Phys. Rev. Lett.*, 49(25):1804, 1982.
- [37] R.J. Glauber. Optical coherence and photon statistics. In C. de Witt, A. Blandin, and C. Cohen-Tannoudji, editors, *Quantum Optics and Electronics, Les Houches Summer School*. Gordon and Breach, London, 1965.
- [38] Z.Y. Ou and L. Mandel. Further evidence of nonclassical behavior in optical interference. *Phys. Rev. Lett.*, 62:2941, 1989.
- [39] P. Grangier, G. Roger, and A. Aspect. Experimental evidence for a photon anticorrelation effect on a beam splitter: a new light on single-photon interferences. *Europhys. Lett.*, 1:173, 1986.
- [40] H.J. Kimble. Quantum fluctuations in quantum optics: squeezing and related phenomena. In J. Dalibard, J.-M. Raimond, and J. Zinn-Justin, editors, *Fundamental Systems in Quantum Optics, Les Houches Summer School, Session LIII*, page 545. North Holland, Amsterdam, 1992.
- [41] D. T. Smithey, M. Beck, M. G. Raymer, and A. Faridani. Measurement of the Wigner distribution and the density matrix of a light mode using optical homodyne tomography: Application to squeezed states and the vacuum. *Phys. Rev. Lett.*, 70:1244, 1993.
- [42] G. Breitenbach, S. Schiller, and J. Mlynek. Measurement of the quantum states of squeezed light. *Nature (London)*, 387:471, 1997.
- [43] A.I. Lvovsky, H. Hansen, T. Aichele, O. Benson, J. Mlynek, and S. Schiller. Quantum state reconstruction of the single-photon Fock state. *Phys. Rev. Lett.*, 87:050402, 2001.
- [44] A.I. Lvovsky and J. Mlynek. Quantum-optical catalysis: generating nonclassical states of light by means of linear optics. *Phys. Rev. Lett.*, 88:250401, 2002.
- [45] J.-M. Raimond, M. Brune, and S. Haroche. Reversible decoherence of a mesoscopic superposition of field states. *Phys. Rev. Lett.*, 79:1964, 1997.
- [46] X. Maître, E. Hagley, J. Dreyer, A. Maali, C. Wunderlich, M. Brune, J.-M. Raimond, and S. Haroche. An experimental study of a Schrödinger's cat decoherence with atoms and cavities. *J. Mod. Opt.*, 44:2023, 1997.
- [47] J. Jacobson, G. Björk, I. Chuang, and Y. Yamamoto. Photonic de Broglie waves. *Phys. Rev. Lett.*, 74:4835, 1995.

- [48] D. Leibfried, B. DeMarco, V. Meyer, M. Rowe, A. Ben-Kish, J. Britton, W. M. Itano, B. Jelekovic, C. Langer, T. Rosenband, and D. J. Wineland. Trapped-ion quantum simulator: Experimental application to nonlinear interferometers. *Phys. Rev. Lett.*, 89:247901, 2002.
- [49] D. Leibfried, R. Blatt, C. Monroe, and D. J. Wineland. Quantum dynamics of single trapped ions. *Rev. Mod. Phys.*, 75:281, 2003.
- [50] J.H. Eberly, N.B. Narozhny, and J.J. Sanchez-Mondragon. Periodic spontaneous collapse and revival in a simple quantum model. *Phys. Rev. Lett.*, 44:1323, 1980.
- [51] E. T. Jaynes and F. W. Cummings. Comparison of quantum and semiclassical radiation theories with application to the beam maser. *Proc. IEEE*, page 89, 1963.
- [52] S. Haroche. Rydberg atoms and radiation in a resonant cavity. In G. Grynberg and R. Stora, editors, *New Trends in Atomic Physics, Les Houches Summer School Session XXXVIII*, page 347. North Holland, Amsterdam, 1984.
- [53] J. Gea-Banacloche. Collapse and revival of the state vector in the Jaynes-Cummings model: an example of state preparation by a quantum apparatus. *Phys. Rev. Lett.*, 65:3385, 1990.
- [54] J. Gea-Banacloche. Atom and field evolution in the Jaynes and Cummings model for large initial fields. *Phys. Rev. A*, 44:5913, 1991.
- [55] V. Buzek, H. Moya-Cessa, P.L. Knight, and S.J.D. Phoenix. Schrödinger-cat states in the resonant Jaynes-Cummings model: Collapse and revival of oscillations of the photon-number distribution. *Phys. Rev. A*, 45:8190, 1992.
- [56] M. Brune, F. Schmidt-Kaler, A. Maali, J. Dreyer, E. Hagley, J.-M. Raimond, and S. Haroche. Quantum Rabi oscillation: a direct test of field quantization in a cavity. *Phys. Rev. Lett.*, 76:1800, 1996.
- [57] G. Rempe, H. Walther, and N. Klein. Observation of quantum collapse and revival in a one-atom maser. *Phys. Rev. Lett.*, 58:353, 1987.
- [58] D. M. Meekhof, C. Monroe, B. E. King, W. M. Itano, and D. J. Wineland. Generation of nonclassical motional states of a trapped atom. *Phys. Rev. Lett.*, 76:1796, 1996.
- [59] G. Morigi, E. Solano, B.-G. Englert, and H. Walther. Measuring irreversible dynamics of a quantum harmonic oscillator. *Phys. Rev. A*, 65:040102, 2002.
- [60] J. Dalibard, Y. Castin, and K. M ölmer. Wave-function approach to dissipative processes in quantum optics. *Phys. Rev. Lett.*, 68:580, 1992.
- [61] S. Zippilli, D. Vitali, P. Tombesi, and J.M. Raimond. Scheme for decoherence control in microwave cavities. *Phys. Rev. A*, 67:052101, 2003.
- [62] L. G. Lutterbach and L. Davidovich. Method for direct measurement of the Wigner function in cavity QED and ion traps. *Phys. Rev. Lett.*, 78:2547, 1997.
- [63] P. Bertet, A. Auffeves, P. Maioli, S. Osnaghi, T. Meunier, M. Brune, J.-M. Raimond, and S. Haroche. Direct measurement of the Wigner function of a one-photon Fock state in a cavity. *Phys. Rev. Lett.*, 89:200402, 2002.
- [64] L. Davidovich, A. Maali, M. Brune, J.-M. Raimond, and S. Haroche. Quantum switches and non-local microwave fields. *Phys. Rev. Lett.*, 71:2360, 1993.
- [65] L. Davidovich, M. Brune, J.-M. Raimond, and S. Haroche. Mesoscopic quantum coherences in cavity QED: Preparation and decoherence monitoring schemes. *Phys. Rev. A*, 53:1295, 1996.
- [66] K. Banaszek and K. Wodkiewicz. Testing quantum nonlocality in phase space. *Phys. Rev. Lett.*, 82:2009, 1999.
- [67] P. Meystre. *Atom optics*. Springer, Berlin, 2001.
- [68] E. M. Wright, D. F. Walls, and J. C. Garrison. Collapses and revivals of Bose-Einstein condensates formed in small atomic samples. *Phys. Rev. Lett.*, 77:2158, 1996.

- [69] J. I. Cirac, M. Lewenstein, K. Molmer, and P. Zoller. Quantum superposition states of Bose-Einstein condensates. *Phys. Rev. A*, 57:1208, 1998.
- [70] A. Sinatra and Y. Castin. Phase dynamics of Bose-Einstein condensates: Losses versus revivals. *Eur. Phys. J. D*, 4:247, 1998.
- [71] D. Gordon and C. M. Savage. Creating macroscopic quantum superpositions with Bose-Einstein condensates. *Phys. Rev. A*, 59:4623, 1999.
- [72] D. A. R. Dalvit, J. Dziarmaga, and W. H. Zurek. Decoherence in Bose-Einstein condensates: Towards bigger and better Schrödinger cats. *Phys. Rev. A*, 62:013607, 2000.
- [73] A. Montina and F. T. Arecchi. Bistability and macroscopic quantum coherence in a Bose-Einstein condensate of ^7Li . *Phys. Rev. A*, 66:013605, 2002.
- [74] Y. Castin. Bose-Einstein condensates in atomic gases. In R. Kaiser, C. Westbrook, and F. David, editors, *Coherent atomic matter waves, Les Houches summer school series*, page 1. EDP Sciences, Orsay, 2001.
- [75] S. Inouye, M.R. Andrews, J. Stenger, H.J. Miesner, D.M. Stanper-Kurn, and W. Ketterle. Observation of Feshbach resonances in a Bose-Einstein condensate. *Nature (London)*, 392:151, 1998.
- [76] Y.R. Shen. *The Principles of Non-Linear Optics*. Wiley-interscience, New York, 1984.
- [77] M. Greiner, O. Mandel, T. W. Hänsch, and I. Bloch. Collapse and revival of the matter wave field of a Bose-Einstein condensate. *Nature (London)*, 419:51, 2002.
- [78] S. Haroche. Breeding non-local Schrödinger cats: a thought experiment to explore the quantum-classical boundary. In J.D. Barrow, P.C.W. Davies, and C.L. Harper, editors, *Science and ultimate reality: quantum theory, cosmology and complexity*, page 1. Cambridge University Press, London, 2004.
- [79] B. Julsgaard, A. Kozhekin, and E.S. Polzik. Experimental long-lived entanglement of two macroscopic objects. *Nature (London)*, 413:400, 2001.
- [80] L. Hackermüller, S. Uttenthaler, K. Hornberger, E. Reiger, B. Brezger, A. Zeilinger, and M. Arndt. Wave nature of biomolecules and fluorofullerenes. *Phys. Rev. Lett.*, 91:090408, 2003.
- [81] C.H. van der Wal, A.C.J. ter Haar, F.K. Wilhelm, R.N. Schouten, C.J.P.M. Harmans, T.P. Orlando, S. Lloyd, and J.E. Mooij. Quantum superposition of macroscopic persistent-current states. *Science*, 290:773, 2000.